LINKAGES BETWEEN TROPOPAUSE POLAR VORTICES AND THE DEVELOPMENT OF COLD AIR OUTBREAKS OVER CENTRAL AND EASTERN NORTH AMERICA

by

Kevin A. Biernat

A Thesis

Submitted to the University at Albany, State University of New York

in Partial Fulfillment of

the Requirements for the Degree of

Master of Science

College of Arts & Sciences

Department of Atmospheric and Environmental Sciences

2017

ABSTRACT

Coherent vortices in the vicinity of the tropopause, referred to as tropopause polar vortices (TPVs), may be extracted from high latitudes in conjunction with high-latitude upper-level ridge amplification. Once extracted, TPVs may interact with and strengthen midlatitude jet streams, as well as act as precursor disturbances for the development of intense midlatitude cyclones. Cold pools that may accompany TPVs as they are transported to middle latitudes may lead to widespread cold air outbreaks (CAOs), which may result in significant socioeconomic impacts. The purpose of this study is to investigate 1) the equatorward transport of TPVs and cold pools to middle latitudes and 2) the dynamical linkages between TPVs, cold pools, and CAOs.

To conduct this study, climatologies of TPVs and cold pools were constructed utilizing the ERA-Interim dataset for the period 1979–2015. These climatologies indicate that there are an average of ~678 TPVs and ~227 cold pools transported equatorward to middle latitudes per year and that there are two preferred corridors for their equatorward transport to middle latitudes: 1) central and eastern North America and 2) Siberia and eastern Asia. A similar climatology of CAOs over the central and eastern U.S. was compared to the climatologies of TPVs and cold pools in order to determine which CAOs are linked to cold pools associated with TPVs. Results indicate that ~74–88% of CAOs over northern regions of the central and eastern U.S. are linked to cold pools associated with TPVs.

Case study investigations of two CAOs that are linked to cold pools associated with TPVs were performed. The large spatial overlap and temporal coincidence of the TPV and cold pool in each case suggest that the TPV and cold pool are dynamically linked. Cross sections

transecting the TPV and cold pool in each case show that as the TPV becomes better defined and stronger, the cold pool becomes better defined and stronger as well, illustrating that the TPV and cold pool are dynamically linked. This dynamical linkage demonstrates that the influence of TPVs can extend throughout the depth of the troposphere and cover a widespread geographical area. In each case, CAO development occurs as the TPV and associated cold pool, as well as a strong surface anticyclone, move equatorward into the U.S. The TPV plays a central role in CAO development in each case given that 1) the cold pool associated with the TPV moves in tandem with the TPV into the U.S. during the occurrence of the CAO and 2) the TPV via TPV–jet interaction may help to strengthen the strong surface anticyclone over western North America that helps transport cold air from the cold pool associated with the TPV far away from the core of the cold pool over the U.S.

ACKNOWLEDGEMENTS

I am indebted to my co-advisors, Drs. Lance Bosart and Dan Keyser for their tremendous mentorship, support, and encouragement over the past few years. Their mentorship has significantly fostered my growth as a scientist and as a communicator. For that, I am very grateful. Furthermore, I am incredibly grateful for the opportunities they have provided me to present research at conferences and workshops, which have further helped me to grow as a scientist and as a communicator. Lance and Dan are passionate and exemplary scientists and teachers, and I am thankful for the opportunity I have had to not only work with them, but to be a student in their classes as well.

I would like to also thank the faculty members in the Department of Atmospheric and Environmental Sciences at the University at Albany for the high quality education they provide that has helped me to grow further as a scientist. A special thanks to Barbara Zampella, Annette Audi, and Chaina Porter for their administrative support, and Kevin Tyle and David Knight for their technical support. In addition, I would like to thank my fellow graduate students for their camaraderie, guidance, and programming assistance. I would especially like to thank Philippe Papin, Alicia Bentley, Zach Murphy, Jonny Blufer, Rebecca Steeves, Matt Vaughan, and Kyle Pallozzi for their invaluable support and friendship. In addition, I am indebted to Nicholas Szapiro and Steven Cavallo at the University of Oklahoma for providing their tracking algorithm that made this research possible, as well as for helping me to understand and utilize their tracking algorithm. I am also indebted to Zach Murphy for providing his cold air outbreak climatology that was very important for this research as well.

I would also like to thank past mentors and teachers that have inspired me. I would like to especially thank Dr. Marty Baxter at Central Michigan University. His encouragement and guidance motivated me and helped set me on a pathway that has led me to my graduate career. I am also grateful for the technical and communication skills he instilled in me that helped prepare me for graduate school.

I would especially like to thank my loving family. Their love and unwavering support and encouragement has meant dearly to me throughout my graduate school journey. Their guidance and love have helped me to rise above challenging times and have always kept me motivated.

This research was supported by the American Meteorological Society Graduate Fellowship sponsored by NASA's Earth Science Research Program, and by the National Science Foundation (NSF) grant AGS-1355960, awarded to the University at Albany, SUNY.

Kevin A. Biernat

Albany, New York

November 2017

TABLE OF CONTENTS

LIST OF FIGURES

TPV can be counted more than once if it crosses equatorward of 60°N after returning poleward of 60°N.

Fig. 3.3. Histograms showing (a) the total number of TPVs per season and (b) the total number of TPVs transported to middle latitudes (equatorward of 60°N) per season, normalized to a 91.25 day season, during 1979–2015.

Fig. 3.4. Track density plots showing total number of unique (a) cold pools and (b) cold pools transported to middle latitudes (equatorward of 60°N) within 500 km of each grid point (using a 0.5° grid) during 1979–2015. Also in (b), the 1979–2015 mean DT wind speed (m s^{-1}, black contours).

Fig. 3.5. As in Fig. 3.2, but for cold pools.

Fig. 3.6. Histograms showing (a) the total number of cold pools per season and (b) the total number of cold pools transported to middle latitudes (equatorward of 60°N) per season, normalized to a 91.25-day season, during 1979–2015.

Fig. 3.7. Histograms showing (a) total number of CAOs (blue), number of unique CAOs that are linked to at least one cold pool (gray), and number of unique CAOs that are linked to at least one cold pool associated with TPVs (purple); (b) percentage of unique CAOs that are linked to at least one cold pool (tan); and (c) percentage of unique CAOs that linked to at least one cold pool associated with TPVs (peach) for each NCEI climate region shown in the accompanying map during 1979–2015.

Fig. 4.1. Tracks of TPV (red) from 0600 UTC 15 December 1981 to 0000 UTC 13 January 1982 and cold pool (blue) from 1800 UTC 20 December 1981 to 1800 UTC 13 January 1982 for January 1982 CAO case. Stars denote locations of genesis, crosses denote locations of lysis, and red and blue dots represent 0000 UTC positions of TPV and cold pool, respectively, every 48 h. Numbers pointing toward dots represent dates of the 0000 UTC positions of the TPV and cold pool, such that numbers ≥17 correspond to dates in December 1981 and numbers ≤12 correspond to dates in January 1982.

Fig. 4.2. Time series of minimum DT potential temperature (θ) of TPV (K, red) every 6 h from 0600 UTC 15 December 1981 to 0000 UTC 13 January 1982 and minimum 1000–500-hPa thickness of cold pool (dam, blue) every 6 h from 1800 UTC 20 December 1981 to 1800 UTC 13 January 1982 for January 1982 CAO case.

Fig. 4.3. DT (2-PVU surface) potential temperature (K, shaded), wind speed (black contours every 10 m s^{-1}, beginning at 50 m s^{-1}), and wind (m s^{-1}, flags and barbs) at (a) 0000 UTC 5 January, (c) 0000 UTC 6 January, (e) 0000 UTC 7 January, and (g) 0000 UTC 8 January 1982; 250-hPa wind speed (m s^{-1}, shaded), 1000–500-hPa thickness (dashed red and blue contours every 10 dam, contoured red for values >540 dam and blue otherwise), SLP (black contours every 8 hPa), and precipitable water (mm, shaded) at (b) 0000 UTC 5 January, (d) 0000 UTC 6 January, (f) 0000 UTC 7 January, and (h) 0000 UTC 8 January 1982. Green line and dot

represent track and position of TPV, respectively, and yellow line and dot represent track and position of cold pool, respectively.

Fig. 4.4. Precipitable water (mm, shaded), 600–400-hPa ascent (red contours every 2.5×10^{-3} hPa s^{-1}), and 300–200-hPa PV (PVU, gray), irrotational wind (vectors, starting at 3 m s^{-1}), and negative PV advection by the irrotational wind (PVU day^{-1}, shaded) at (a) 0000 UTC 6 January and (b) 0000 UTC 7 January 1982.

Fig. 4.5. DT (2-PVU surface) potential temperature (K, shaded), wind speed (black contours every 10 m s^{-1}, beginning at 50 m s^{-1}), and wind (m s^{-1}, flags and barbs) at (a) 0000 UTC 8 January, (c) 0000 UTC 9 January, (e) 0000 UTC 10 January, and (g) 0000 UTC 11 January 1982; 250-hPa wind speed (m s^{-1}, shaded), 1000–500-hPa thickness (dashed red and blue contours every 10 dam, contoured red for values >540 dam and blue otherwise), SLP (black contours every 8 hPa), and precipitable water (mm, shaded) at (b) 0000 UTC 8 January, (d) 0000 UTC 9 January, (f) 0000 UTC 10 January, and (h) 0000 UTC 11 January 1982. Green line and dot represent track and position of TPV, respectively, and yellow line and dot represent track and position of cold pool, respectively.

Fig. 4.6. Precipitable water (mm, shaded), 600–400-hPa ascent (red contours every 2.5×10^{-3} hPa s^{-1}), and 300–200-hPa PV (PVU, gray), irrotational wind (vectors, starting at 3 m s^{-1}), and negative PV advection by the irrotational wind (PVU day^{-1}, shaded) at (a) 0000 UTC 10 January and (b) 0000 UTC 11 January 1982.

Fig. 4.7. (a) Cross section along line AA' of PV (PVU, shading), potential temperature (K, black), and wind speed (dashed white contours every 10 m s^{-1}, beginning at 50 m s^{-1}); (b) DT (2-PVU surface) potential temperature (K, shaded), wind speed (black contours every 10 m s^{-1}, beginning at 50 m s^{-1}), and wind (m s^{-1}, flags and barbs); and (c) 1000–500-hPa thickness (dam, shading) at 1200 UTC 16 December 1981. Green line in (b) and (c) represents transect of cross section AA'. Label "TPV" represents location of TPV.

Fig. 4.8. As in Fig. 4.7, but for cross section along line BB' at 1200 UTC 2 January 1982. Label "CP" represents location of cold pool.

Fig. 4.9. As in Figs. 4.7 and 4.8, but for cross section along line CC' at 0000 UTC 10 January 1982.

Fig. 4.10. In all panels are SLP (thick blue contours every 5 hPa, beginning at 1040 hPa), and 600–400-hPa geopotential height (dark gray contours every 10 dam) and potential temperature (dashed red contours every 5°C). Also, 600–400-hPa wind speed (m s^{-1}, shaded) at (a) 1200 UTC 8 January, (d) 0000 UTC 9 January, (g) 1200 UTC 9 January, and (j) 0000 UTC 10 January 1982; 600–400-hPa $\mathbf{Q}_n$ (K m^{-1} s^{-1}, vectors) and $\mathbf{Q}_n$ forcing for vertical motion (10^{-17} Pa^{-1} s^{-3}, shaded) at (b) 1200 UTC 8 January, (e) 0000 UTC 9 January, (h) 1200 UTC 9 January, and (k) 0000 UTC 10 January 1982; and 600–400-hPa $\mathbf{Q}_s$ (K m^{-1} s^{-1}, vectors) and $\mathbf{Q}_s$ forcing for vertical motion (10^{-17} Pa^{-1} s^{-3}, shaded) at (c) 1200 UTC 8 January, (f) 0000 UTC 9 January, (i) 1200 UTC 9 January, and (l) 0000 UTC 10 January 1982. Green line and dot represent track and position of TPV, respectively.

Fig. 4.11. Tracks of TPV (red) from 1800 UTC 16 January to 1200 UTC 2 February 1985 and cold pool (blue) from 1800 UTC 11 January to 0600 UTC 28 January 1985 for January 1985 CAO case. Stars denote locations of genesis, crosses denote locations of lysis, and red and blue dots represent 0000 UTC positions of TPV and cold pool, respectively, every 48 h. Numbers pointing toward dots represent dates of the 0000 UTC positions of the TPV and cold pool, such that numbers ≥13 correspond to dates in January 1985 and the number "2" corresponds to 2 February 1985.

Fig. 4.12. Time series of minimum DT potential temperature (θ) of TPV (K, red) every 6 h from 1800 UTC 16 January to 1200 UTC 2 February 1985 and minimum 1000–500-hPa thickness of cold pool (dam, blue) every 6 h from 1800 UTC 11 January to 0600 UTC 28 January 1985 for January 1985 CAO case.

Fig. 4.13. DT (2-PVU surface) potential temperature (K, shaded), wind speed (black contours every 10 m s^{-1}, beginning at 50 m s^{-1}), and wind (m s^{-1}, flags and barbs) at (a) 0000 UTC 14 January, (c) 0000 UTC 15 January, (e) 0000 UTC 16 January, and (g) 0000 UTC 17 January 1985; 250-hPa wind speed (m s^{-1}, shaded), 1000–500-hPa thickness (dashed red and blue contours every 10 dam, contoured red for values >540 dam and blue otherwise), SLP (black contours every 8 hPa), and precipitable water (mm, shaded) at (b) 0000 UTC 14 January, (d) 0000 UTC 15 January, (f) 0000 UTC 16 January, and (h) 0000 UTC 17 January 1985. Green line and dot represent track and position of TPV, respectively, and yellow line and dot represent track and position of cold pool, respectively.

Fig. 4.14. Precipitable water (mm, shaded), 600–400-hPa ascent (red contours every 2.5×10^{-3} hPa s^{-1}), and 300–200-hPa PV (PVU, gray), irrotational wind (vectors, starting at 3 m s^{-1}), and negative PV advection by the irrotational wind (PVU day^{-1}, shaded) at (a) 0000 UTC 15 January and (b) 0000 UTC 16 January 1985.

Fig. 4.15. DT (2-PVU surface) potential temperature (K, shaded), wind speed (black contours every 10 m s^{-1}, beginning at 50 m s^{-1}), and wind (m s^{-1}, flags and barbs) at (a) 0000 UTC 18 January, (c) 0000 UTC 19 January, (e) 0000 UTC 20 January, and (g) 0000 UTC 21 January 1985; 250-hPa wind speed (m s^{-1}, shaded), 1000–500-hPa thickness (dashed red and blue contours every 10 dam, contoured red for values >540 dam and blue otherwise), SLP (black contours every 8 hPa), and precipitable water (mm, shaded) at (b) 0000 UTC 18 January, (d) 0000 UTC 19 January, (f) 0000 UTC 20 January, and (h) 0000 UTC 21 January 1985. Green line and dot represent track and position of TPV, respectively, and yellow line and dot represent track and position of cold pool, respectively.

Fig. 4.16. Precipitable water (mm, shaded), 600–400-hPa ascent (red contours every 2.5×10^{-3} hPa s^{-1}), and 300–200-hPa PV (PVU, gray), irrotational wind (vectors, starting at 3 m s^{-1}), and negative PV advection by the irrotational wind (PVU day^{-1}, shaded) at (a) 0000 UTC 21 January and (b) 0000 UTC 22 January 1985.

Fig. 4.17. As in Fig. 4.7, but for cross section along line DD' at 0000 UTC 13 January 1985.

Fig. 4.18. As in Fig. 4.7, but for cross section along line EE' at 0000 UTC 17 January 1985.

Fig. 4.19. As in Fig. 4.7, but for cross section along line FF' at 0000 UTC 20 January 1985.

Fig. 4.20. In all panels are SLP (thick blue contours every 5 hPa, beginning at 1030 hPa), and 600–400-hPa geopotential height (dark gray contours every 10 dam) and potential temperature (dashed red contours every 5°C). Also, 600–400-hPa wind speed (m s^{-1}, shaded) at (a) 1200 UTC 18 January, (d) 0000 UTC 19 January, (g) 1200 UTC 19 January, and (j) 0000 UTC 20 January 1985; 600–400-hPa $\mathbf{Q}_n$ (K m^{-1} s^{-1}, vectors) and $\mathbf{Q}_n$ forcing for vertical motion (10^{-17} Pa^{-1} s^{-3}, shaded) at (b) 1200 UTC 18 January, (e) 0000 UTC 19 January, (h) 1200 UTC 19 January, and (k) 0000 UTC 20 January 1985; and 600–400-hPa $\mathbf{Q}_s$ (K m^{-1} s^{-1}, vectors) and $\mathbf{Q}_s$ forcing for vertical motion (10^{-17} Pa^{-1} s^{-3}, shaded) at (c) 1200 UTC 18 January, (f) 0000 UTC 19 January, (i) 1200 UTC 19 January, and (l) 0000 UTC 20 January 1985. Green line and dot represent track and position of TPV, respectively.

1. Introduction

1.1 Motivation

Tropopause polar vortices (TPVs) are coherent tropopause-based cyclonic vortices that spend at least a portion of their lifetimes in the high latitudes (e.g., Cavallo and Hakim 2009, 2010). TPVs are tropopause-based material features, characterized by a local minimum of potential temperature on the dynamic tropopause (DT) and by a local maximum of pressure on the DT. TPVs represent a subset of coherent tropopause disturbances (CTDs; e.g., Pyle et al. 2004), which are also tropopause-based material features, but are not required to spend at least a portion of their lifetimes in the high latitudes. TPVs are subsynoptic and mesoscale features that may last from days to months (e.g., Hakim and Canavan 2005; Cavallo and Hakim 2012). Also, TPVs often spend much of their lifetimes in the high latitudes, where they may be maintained and intensified via radiative processes (Cavallo and Hakim 2009, 2010, 2012, 2013).

Although TPVs often spend much of their lifetimes in the high latitudes, some TPVs may be extracted from high latitudes in conjunction with high-latitude upper-level ridge amplification (e.g., Hakim et al. 1995, 1996). Once extracted, TPVs may interact with and strengthen midlatitude jet streams (e.g., Pyle et al. 2004), as well as act as precursors to the development of strong extratropical cyclones (ECs; e.g., Hakim et al. 1995, 1996; Bosart et al. 1996). Strong ECs may lead to extreme weather events (EWEs) associated with heavy precipitation and strong winds that can pose significant hazards to life and property. In addition, lower-tropospheric cold pools (hereafter referred to as cold pools) may accompany TPVs as they are transported to middle latitudes and may lead to widespread cold air outbreaks (CAOs; e.g., Shapiro et al. 1987).

CAOs are EWEs themselves, posing a hazard to life, infrastructure, and agriculture [e.g., Florida citrus freezes (Rogers and Rohli 1991)].

In view of the hazards CAOs associated with TPVs may pose, the opportunity to improve understanding of the equatorward transport of TPVs to middle latitudes and the role of TPVs in the development of CAOs motivates this research. Although past studies have examined the equatorward transport of TPVs to middle latitudes from a case study perspective (e.g., Hakim et al. 1995, 1996), a climatological analysis of the equatorward transport of TPVs to middle latitudes is lacking. In addition, although past studies have shown that cold pools leading to CAOs may accompany TPVs as they are transported to middle latitudes (e.g., Shapiro et al. 1987), the linkages between TPVs, cold pools, and CAOs have not been explicitly explored. Therefore, the goal of this research is to improve understanding of the equatorward transport of TPVs to middle latitudes and the linkages between TPVs, cold pools, and CAOs.

1.2 Literature Review

1.2.1 Structure of TPVs

Coherent tropopause-based vortices know as TPVs that are transported to middle latitudes may contribute to the development of EWEs. In order to understand how TPVs contribute to the development of EWEs, it is important to understand the structure of TPVs. Hoskins et al. (1985, section 3) were among the first to conceptualize coherent tropopause-based vortices from a potential vorticity (PV) perspective as upper-level cyclonic PV anomalies (Fig. 1.1). The upper-level cyclonic PV anomaly shown in Fig. 1.1 is associated with anomalously high static stability and cyclonic absolute vorticity relative to its surroundings, and a downward

displacement of the tropopause. Furthermore, upward bowing of isentropes in the troposphere beneath the upper-level cyclonic PV anomaly illustrates that upper-level cyclonic PV anomalies are cold core and associated with anomalously cold air within the troposphere beneath them.

Later studies of coherent tropopause-based vortices have referred to these features as CTDs (e.g., Pyle et al. 2004) and TPVs (e.g., Cavallo and Hakim 2009, 2010). CTDs and TPVs are characterized by closed material contours on the DT, such that under adiabatic and frictionless flow, air parcels are trapped within CTDs and TPVs. However, unlike CTDs, TPVs are required to spend at least a portion of their lifetimes in the high latitudes (Cavallo and Hakim 2009, 2010). An example of a CTD studied by Pyle et al. (2004) qualifying as a TPV is shown in Fig 1.2. This TPV, which formed in the Arctic and lasted 17.5 days during November–December 1991 (not shown), is characterized by a local minimum of DT potential temperature (Fig. 1.2a), local maximum of DT pressure (Fig. 1.2b), and local maximum of PV (Fig. 1.2d). In addition, this TPV was located on the edge of a broader cyclonic circulation at 300 hPa (Fig. 1.2c), illustrating that TPVs are subsynoptic scale and mesoscale structures within the broader tropospheric polar vortex, the edge of which is typically located at the core of upper-tropospheric westerly winds (Waugh et al. 2017).

Cavallo and Hakim (2010) composited TPVs located in the Canadian Arctic and created composite west-to-east cross-TPV sections (Fig. 1.3). Anomalies shown in Fig. 1.3 were computed with respect to a west-to-east "background" cross section located over northern Canada near several radiosonde stations. The composite structure of TPVs is similar to the structure of the upper-level cyclonic PV anomaly shown in Hoskins et al. (1985, section 3; Fig. 1.1 in this thesis). Anomalously cold air is located within the TPV and throughout the troposphere beneath the TPV (Fig. 1.3a), anomalously cyclonic flow is located around the TPV

(Fig. 1.3b), and anomalously positive PV is located within and above the TPV (Fig. 1.3c). Furthermore, anomalously low relative humidity (RH) air within and above the TPV associated with dry stratospheric air is located above anomalously high RH air beneath the TPV (Fig. 1.3d). Idealized numerical modeling experiments by Cavallo and Hakim (2013) have shown that longwave radiative cooling associated with large-magnitude vertical gradients in water vapor concentration near the tropopause implied by Fig. 1.3d is important for TPV maintenance and intensification.

Cavallo and Hakim (2010) also discussed that a sloping dipole in vertical motion is located about the composite TPV core, with upward vertical motion located downshear of the composite TPV core and downward vertical motion located upshear and partially within the composite TPV core (not shown). Downward vertical motion within the TPV core is suggestive of the production of relative vorticity within the TPV core via vortex stretching. As stated by Cavallo and Hakim (2010), the dipole of vertical motion can be qualitatively explained by geostrophic vorticity advection by the thermal wind. Similar results were found by Hakim (2000) in his zonal composite cross section of "extreme" 500-hPa relative vorticity maxima occurring during the winter of 1988–89.

1.2.2 Climatologies of TPVs

Hakim and Canavan (2005) tracked cyclonic tropopause-based vortices (i.e., CTDs, represented as minima in DT potential temperature) for the 1948–99 period using the 2.5° NCEP–NCAR reanalysis dataset (Kalnay et al. 1996). Kravitz (2007) created a global climatology of CTDs by tracking DT pressure maxima using the NCEP GFS 1.0° final analysis

for the 2000–04 period. Figure 1.4 shows the geographical distribution of CTDs tracked by Hakim and Canavan (2005). Regions of high CTD occurrence are located over the Canadian Archipelago, extending southeastward to Hudson Bay and Labrador; over portions of Siberia and northeastern Asia; and on the poleward side of the North Pacific and North Atlantic jet streams. In addition, regions of low CTD occurrence are found over high terrain features including the Rocky Mountains and the Tibetan Plateau. Most of these regions of high and low CTD occurrence are similar to those found by Kravitz (2007, chapter 3, section 3.2.1.1).

Cavallo and Hakim (2012) created TPV climatologies using the Weather Research and Forecasting (WRF) model and NCEP–NCAR reanalysis for winter (December–February) and summer (June–August) for 1990–99. These climatologies indicate that the number of TPVs identified is sensitive to grid resolution, with the higher resolution WRF winter climatology containing 7426 TPVs, but the lower-resolution NCEP–NCAR winter climatology containing only 442 TPVs. The NCEP–NCAR TPV climatologies show that large TPV track densities are located within climatological troughs over northeastern Canada and northern Siberia, which are also regions of high CTD occurrence identified by Hakim and Canavan (2005; Fig. 1.4 in this thesis) and Kravitz (2007, chapter 3, section 3.2.1.1). In addition, a 1948–99 NNRP climatology of TPVs created by Cavallo and Hakim (2009) shows that regions of TPV genesis and lysis are in close proximity, suggesting that TPVs spend the majority of their lifetimes in the same region of the high latitudes.

1.2.3 Equatorward Transport of TPVs and Arctic Air to Middle Latitudes

Although TPVs are most often found in the high latitudes (e.g., Cavallo and Hakim 2009), case study evidence has indicated that TPVs can be transported to middle latitudes, where they may participate in the development of EWEs (e.g., Hakim et al. 1995, 1996; Bosart et al. 1996). Furthermore, case study evidence from Hakim et al. (1995, 1996) and Bosart et al. (1996) has shown that high latitude upper-level ridge amplification can play an important role in the equatorward transport of TPVs. For example, Bosart et al. (1996) showed that the strengthening of the positive Pacific–North American (PNA) pattern (Wallace and Gutzler 1981) during March 1993, associated with ridge amplification over western North America, facilitated the equatorward transport of a high-latitude coherent tropopause-based disturbance (i.e., a TPV) over North America that played an important role in the development of the 1993 Superstorm. Kravitz (2007, chapter 4, section 4.2.1) examined changes in CTD distribution with respect to positive PNA transitions, representing ridge amplification over the eastern North Pacific and western North America. A positive PNA transition was defined as a period in which the PNA increases by at least a +2.0 standard deviation anomaly over seven days. During days 4–7 of the positive PNA transition, regions of anomalously positive CTD frequency extend from northern Canada, Alaska, and the adjacent Arctic to the middle latitudes of eastern North America, suggesting that ridge amplification may play an important role in the equatorward transport of CTDs (i.e., TPVs) from high latitudes to middle latitudes. Although studies such as Bosart et al. (1996) and Kravitz (2007, chapter 4, section 4.2.1) provide evidence of the equatorward transport of TPVs from high latitudes to middle latitudes, a detailed climatological analysis of the equatorward transport of TPVs to middle latitudes is lacking in the literature. Since TPVs transported to middle latitudes

may play important roles in the development of EWEs, there is a need for a climatological analysis of the equatorward transport of TPVs to middle latitudes.

High-latitude upper-level ridge amplification is also important for the equatorward transport of arctic air and CAO development. Waugh et al. (2017) noted that large displacements of the tropospheric polar vortex edge, accompanying high-amplitude large-scale waves, are often related to the development of CAOs. They suggest that synoptic-scale disturbances moving equatorward along the tropospheric polar vortex edge may allow for the equatorward transport of cold air. Since TPVs are embedded within the tropospheric polar vortex, these synoptic-scale disturbances moving equatorward along the tropospheric polar vortex edge may include TPVs, suggesting that the equatorward transport of TPVs may be related to the equatorward transport of cold air and the development of CAOs.

As discussed by Namias (1978) for the winter of 1976–77, precursor disturbances over the North Pacific may contribute to the development of highly amplified flow patterns over North America supportive of equatorward surges of arctic air leading to CAO development. Namias explained that anomalous west-to-east SST gradients and associated strengthened baroclinicity over the eastern North Pacific facilitated cyclogenesis and the concomitant development of anomalous southerly flow over the eastern North Pacific. This anomalous southerly flow supported the development of a highly amplified ridge over western North America and highly amplified trough over eastern North America. This highly amplified flow pattern allowed arctic air to be transported equatorward deep into eastern North America, leading to the development of CAOs. Enhanced thermal contrast between arctic air moving off the East Coast of North America and the warm Gulf Stream provided favorable condition for rapidly deepening ECs off the East Coast of North America. These ECs not only helped to reinforce the

highly amplified trough over eastern North America, but also helped to create and maintain a persistent 700-hPa cyclone over southeastern Canada. Warm air advection and redistribution of vorticity north and east of this persistent 700-hPa cyclone was believed to force upper-level ridging over the high latitudes, supporting the creation and maintenance of persistent high-latitude blocking. Furthermore, the high-latitude blocking likely reinforced the highly amplified flow pattern and supported recurrent CAOs over eastern North America.

Many studies have also discussed the importance of strong surface anticyclogenesis on the downstream side of amplified ridges for the equatorward transport of arctic air (Dallavalle and Bosart 1975; Colucci and Davenport 1987; Colle and Mass 1995; Jones and Cohen 2011). Jones and Cohen (2011) composited strong surface anticyclones occurring over northwestern North America and showed that a ridge becomes highly amplified over Alaska in the two days prior to the time of maximum sea level pressure (SLP) of the composite surface anticyclone. Jones and Cohen explained that the composite surface anticyclone over northwestern North America rapidly develops in a region of Q-vector forcing for descent and in a region of strong tropospheric subsidence associated with cold air advection and anticyclonic vorticity advection downstream of the ridge. As the composite surface anticyclone strengthens, strengthening cold air advection transports cold air equatorward over North America.

1.2.4 Role of TPVs in the Development of EWEs

1.2.4.1 Role of TPVs in the Development of ECs and Jet Streaks

Hoskins et al. (1985, section 6e) illustrated the dynamical importance of upper-level cyclonic PV anomalies, which may be considered to represent TPVs, on the development of ECs

(Fig. 1.5). They showed that when an upper-level cyclonic PV anomaly approaches a lower-tropospheric baroclinic zone, the upper-level cyclonic PV anomaly may induce cyclonic flow in the lower troposphere, which could act to produce a lower-level cyclonic PV anomaly and thus a surface cyclone via warm air advection (Figs. 1.5a,b). The lower-level cyclonic PV anomaly can induce a cyclonic circulation in the upper troposphere that may slow down the propagation of and/or strengthen the upper-level cyclonic PV anomaly via positive PV advection (Fig. 1.5b). The PV anomalies can thus become phased-locked and mutually amplify one another. In addition, if cold tropospheric air associated with the upper-level cyclonic PV anomaly moves over relatively warm lower-level air, static stability may be reduced, supporting enhanced upward vertical motions on the downshear side of the upper-level cyclonic PV anomaly. If sufficient moisture is present, clouds and precipitation may develop within the region of upward vertical motion. Associated latent heat release in the lower to middle troposphere may strengthen the lower-level cyclonic PV anomaly, resulting in a PV tower, which can more readily interact with the upper-level cyclonic PV anomaly than a cyclonic lower-level PV anomaly in a dry atmosphere. Thus, there may be stronger interaction and mutual amplification of the upper-level and lower-level cyclonic PV anomalies and consequently more robust surface cyclogenesis in the presence of moisture and latent heat release compared to in a dry atmosphere.

Takayabu (1991) illustrated via an idealized numerical study that the interaction between upper-level and lower-level cyclonic PV anomalies can lead to the rapid development of surface cyclones. In this idealized numerical study, an initial upper-level cyclonic PV anomaly was placed to the north of an upper-level jet and an initial lower-level cyclonic PV anomaly was placed to the southeast of the upper-level cyclonic PV anomaly. As the upper-level cyclonic PV anomaly interacted with the jet, a jet streak formed. The transverse ageostropic circulation in the

entrance region of the jet streak caused the upper-level cyclonic PV anomaly to penetrate downward beneath the jet streak into the lower troposphere. This upper-level cyclonic PV anomaly led to lower-level warm air advection, yielding upward vertical motion and concomitantly the production of cyclonic relative vorticity via vortex stretching at the northern edge of the lower-level cyclonic PV anomaly. The production of cyclonic relative vorticity at the northern edge of the lower-level cyclonic PV anomaly allowed the lower-level cyclonic PV anomaly to move northward and strengthen. As the PV anomalies merged along sloping isentropes, upward vertical motion further intensified, resulting in greater vortex stretching and concomitantly greater production of cyclonic relative vorticity, aiding in the rapid development of the lower-level cyclonic PV anomaly and thus surface cyclone.

Uccellini et al. (1985) diagnosed the role of a polar jet–trough system corresponding to a CTD on the development of the Presidents' Day Storm of 1979. As the CTD progressed from the Dakotas to off the U.S. East Coast from 18 to 20 February 1979 and interacted with a subtropical jet, rapid cyclogenesis ensued off the U.S. East Coast between 19 and 20 February 1979. Uccellini et al. (1985) found that geostrophic deformation forced subsidence near the polar jet, leading to tropopause folding associated with the CTD. Vertical stretching of stratospheric air that extruded downward within the tropopause fold toward 800 hPa contributed to an increase in absolute vorticity and concomitant rapid surface cyclogenesis near the U.S. East Coast.

Subsequent studies have also documented the important role of CTDs and TPVs on the development of strong ECs. Hakim et al. (1995, 1996) and Bosart et al. (1996) both showed that the interaction of a high-latitude coherent tropopause-based disturbance (i.e., a TPV) with a midlatitude coherent tropopause-based disturbance (i.e., a CTD) was important in the development of the 1978 Cleveland Superbomb and the 1993 Superstorm, respectively. In both

cases, confluent flow over western and central North America was important in drawing the TPV and CTD together. Advection of the TPV and CTD by the confluent flow was found to be critical in leading to the explosive development of the 1978 Cleveland Superbomb (Hakim et al. 1996). Bosart et al. (1996) and Dickinson et al. (1997) showed that during the development of the 1993 Superstorm, the approach of the CTD over warm and moist low-level air over the northwestern Gulf of Mexico helped to trigger widespread deep convection. Vertical gradients in diabatic heating in the lower troposphere associated with the deep convection likely led to the production of lower-level PV that aided in the rapid development of the 1993 Superstorm.

In addition, past studies have shown that CTDs and TPVs that interact with the jet stream may lead to the formation and intensification of jet streaks (Cunningham and Keyser 2000; Donnadille et al. 2001a,b; Pyle et al. 2004). Figure 1.6 shows the evolution of the TPV examined by Pyle et al. (2004) that was briefly discussed in section 1.2.1. Between 0000 UTC 30 November and 0000 UTC 1 December 1991, the TPV approached and interacted with a jet stream located on the periphery of an amplifying ridge over western North America, resulting in the intensification of the DT potential temperature gradient and the concomitant formation of a northerly flow jet streak (Figs. 1.6a,b). As the TPV moved southeastward and approached and interacted with a jet streak extending from the southwestern U.S to southeastern Canada between 0000 UTC 1 December and 1200 UTC 2 December 1991, the jet streak strengthened (Figs. 1.6b,c), before weakening by 0000 UTC 4 December 1991 as the TPV weakened and moved downstream over the North Atlantic (Fig. 1.6d). Vertical motion patterns that are part of ageostrophic circulations associated with jet streaks and tropopause folds resulting from ageostrophic circulations associated with jet streaks may play important roles in the development of ECs associated with EWEs (e.g., Uccellini et al. 1985; Uccellini and Kocin 1987; Lackmann

et al. 1997). Thus, stronger jet streaks resulting from TPV–jet interactions may supports stronger ageostrophic circulations that may provide enhanced forcing for the development of ECs associated with EWEs.

ECs resulting from TPV–jet interactions also may lead to downstream flow amplification via downstream baroclinic development (e.g., Orlanski and Chang 1993; Chang and Orlanski 1993; Orlanski and Sheldon 1995; Nielsen-Gammon and Lefevre 1996), potentially creating favorable conditions for the development of EWEs. For example, Bosart et al. (2017) found that interactions of polar coherent tropopause-based disturbances (i.e., TPVs) with midlatitude and tropical disturbances and with the North Pacific jet stream led to flow amplification over the North Pacific and subsequent flow amplification over North America via downstream baroclinic development during October 2007. The associated large-scale flow reconfiguration over the North Pacific and North America was important for the development of multiple EWEs over North America during October 2007.

1.2.4.2 Role of TPVs in the Development of CAOs

The composite west-to-east cross-TPV section from Cavallo and Hakim (2010) showed that anomalously cold air is located throughout the depth of the troposphere within and beneath the TPV (Fig. 1.3a), suggesting that TPVs may be associated with cold pools. Defant and Taba (1957) showed that the tropopause height is lowered above “cold polar vortices” and “cold polar outbreaks” when discussing an analysis of tropopause height for 1 January 1956. This analysis, along with the composite west-to-east cross-TPV section, suggests that regions of lowered tropopause associated with TPVs may coincide with cold pools and regions experiencing CAOs.

Shapiro et al. (1987) examined the connection between a "polar vortex" transported equatorward from high latitudes to the U.S. and a widespread CAO over central and eastern North America during January 1985. A cross section transecting this "polar vortex" at 0000 UTC 20 January 1985 (Fig. 1.7) indicates that it is associated with a downward displacement of the tropopause, and thus may be a TPV. In addition, a pool of very cold air is evident within and beneath the "polar vortex," as illustrated by the widespread region of very low 500-hPa temperatures (Fig. 1.7a) and 850-hPa temperatures (not shown), and significant upward bowing of isentropes (Fig. 1.7b). The cold pool overspread much of the central and eastern U.S., leading to a severe CAO associated with significant socioeconomic impacts including devastation to agriculture over central and southern Florida. The positioning of the cold pool beneath the possible TPV in the Shapiro et al. (1987) study suggests that TPVs may be associated with cold pools that can play important roles in CAO development.

Other studies also point to possible linkages between TPVs, cold pools, and CAOs. Hakim et al. (1995) illustrated that the tracks of the TPV and CTD linked to the development of the 1978 Cleveland Superbomb are similar to the tracks of 1000–500-hPa thickness minima. In addition, as the TPV and associated thickness minimum moved equatorward into the U.S., surface-based arctic air overspread much of the central and eastern U.S. Walsh et al. (2001) performed a backward trajectory analysis to determine the origin of cold air associated with several CAOs impacting different regions of the central and eastern U.S. Trajectories were released 50 hPa above the surface at the location of greatest negative temperature anomaly during the center date of a CAO. These trajectories indicate that the cold air originates mainly over high-latitude regions (Figs. 1.8a–f). These trajectories resemble those of TPVs moving equatorward from regions of high TPV track density over high latitudes (e.g., Cavallo and

Hakim 2009). Furthermore, Walsh et al. (2001) pointed out that many of the trajectories may be moving slowly over northwestern Canada, where efficient longwave radiative cooling may diabatically cool the low-level cold air and strengthen the TPVs (e.g., Cavallo and Hakim 2012, 2013). Although the foregoing studies discussed in this section of the thesis together allude to possible linkages between TPVs, cold pools, and CAOs, none of these studies has explicitly examined these linkages, suggesting an opportunity to better understand these linkages.

Cold pools associated with TPVs may also be important from an EC perspective. Sanders and Gyakum (1980) showed that explosively deepening surface cyclones tend to occur in and around the strongest SST gradients associated with the Gulf Stream and Kuroshio currents over the western North Atlantic and western North Pacific, respectively. They noted that cold continental air masses moving over the strong SST gradients associated with the Gulf Stream and Kuroshio currents may allow for strong sensible and latent heat exchange and a resulting reduction of static stability. The reduction of static stability in addition to strong lower-tropospheric baroclinicity associated with strong SST gradients may provide favorable conditions for rapid surface cyclogenesis. Konrad and Colucci (1989) studied 17 strong CAOs over North America and found that rapid surface cyclogenesis tends to follow the strongest CAOs, including the January 1985 CAO studied by Shapiro et al. (1987). Since the January 1985 CAO may be linked to a cold pool associated with a TPV, cold pools associated with TPVs may play important roles in EC development.

1.3 Research Goals and Thesis Structure

TPVs transported from high latitudes to middle latitudes may play important roles in the development of CAOs. This research expands upon previous work on TPVs and CTDs by focusing on TPVs transported from high latitudes to middle latitudes and that play a role in the development of CAOs. This research especially focuses on examining the linkages between TPVs, cold pools, and CAOs, as these linkages have not been addressed explicitly in previous studies. Therefore, the goals of this research are to improve understanding of: 1) the transport of TPVs and cold pools from high latitudes to middle latitudes by constructing climatologies of TPVs and cold pools transported from high latitudes to middle latitudes; and 2) dynamical linkages between TPVs, cold pools, and CAOs by constructing a climatology of CAOs over the central and eastern U.S. that are linked to cold pools associated with TPVs and by performing case studies of these CAOs.

The organization of the remainder of this thesis is as follows. Data and methodology are described in chapter 2. Climatologies of TPVs, cold pools, and CAOs that are linked to cold pools associated with TPVs are discussed in chapter 3. Case studies of CAOs that are linked to cold pools associated with TPVs are discussed in chapter 4. Research results, conclusions, and suggestions for future work are discussed in chapter 5.

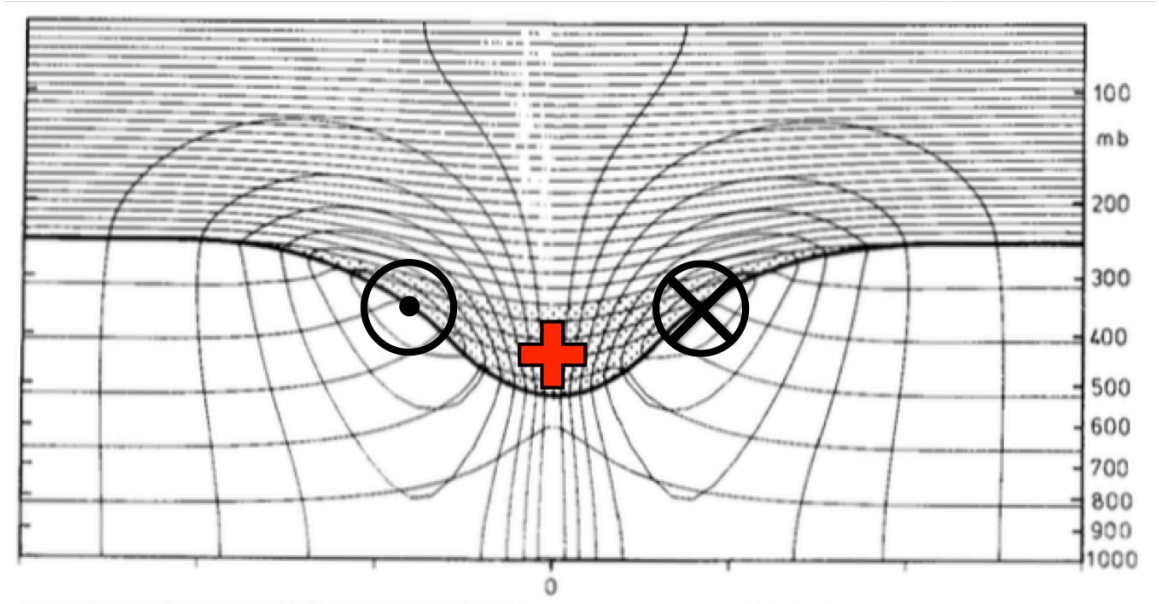

Fig. 1.1. Cross section of circularly symmetric cyclonic flow induced by simple isolated upper-level cyclonic PV anomaly (stippled region and red plus symbol). The thick line represents the tropopause and the solid contours represent potential temperature (every 5 K) and azimuthal wind velocity (every 3 m s^{-1}). Cross symbol represents azimuthal wind velocity directed into cross section and dot symbol represents azimuthal wind velocity directed out of cross section. [Figure 15 and caption adapted from Hoskins et al. (1985, section 3).]

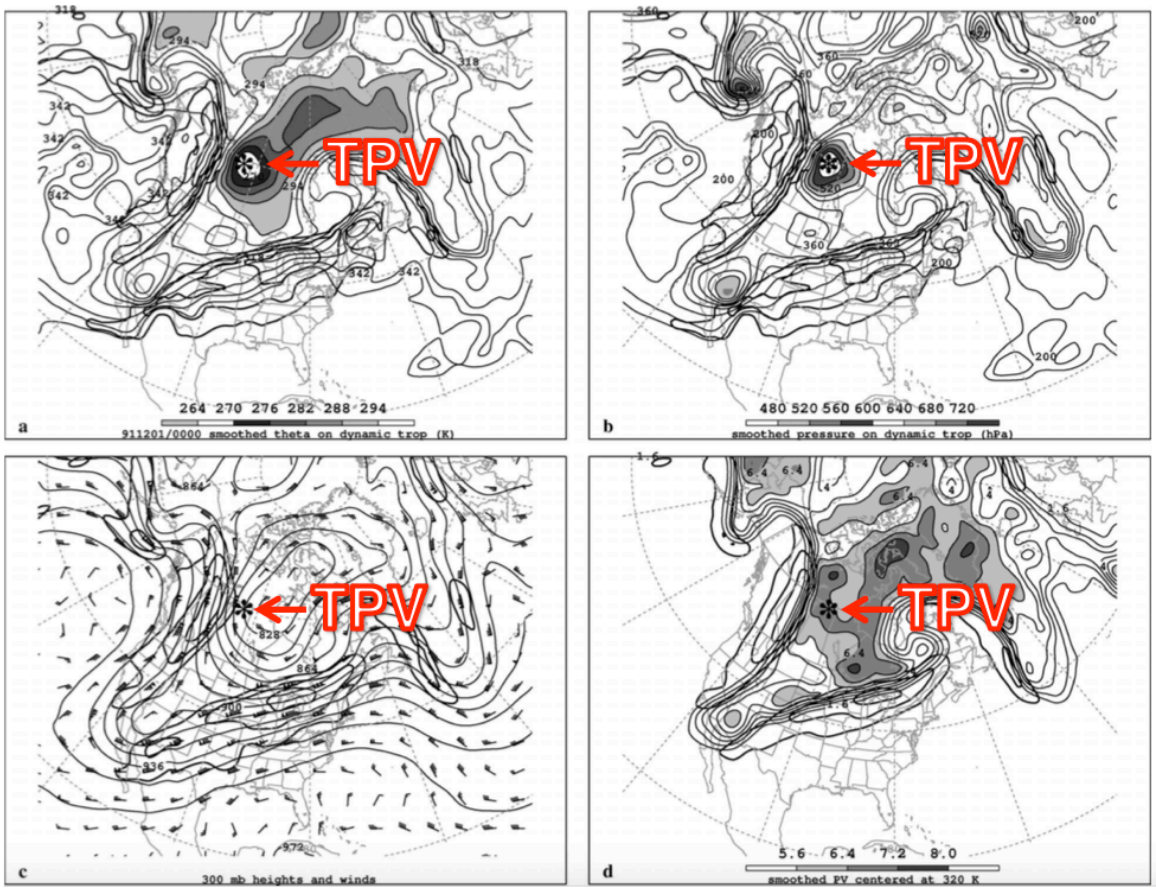

Fig. 1.2. Analyses for 0000 UTC 1 December 1991: (a) DT (1.5-PVU) potential temperature (thin solid; values at and below 342 K contoured at a 6-K interval; shaded as indicated for values below 294 K) and wind speed (thick solid; contoured at a 15 m s^{-1} interval, starting at 50 m s^{-1}); (b) DT pressure (thin solid; contoured at a 40 hPa interval; shaded as indicated for values greater than 480 hPa) and wind speed [contoured as in (a)]; (c) 300-hPa geopotential height (thin solid; contoured at a 12 dam interval), wind speed [contoured as in (a)], and wind (plotted using standard convention: pennant, full barb, and half barb denote 25, 5, and 2.5 m s^{-1}, respectively); and (d) PV calculated over the 316–324-K layer (thin solid; contoured at a 0.8 PVU interval for values greater than 1.6 PVU; shaded as indicated for values greater than 5.6 PVU) and wind speed at 320 K [contoured as in (a)]. The position of the DT pressure maximum associated with the TPV of interest is marked with an asterisk in each panel. Label "TPV" and arrow point to position of TPV. [Figure 11 and caption adapted from Pyle et al. (2004).]

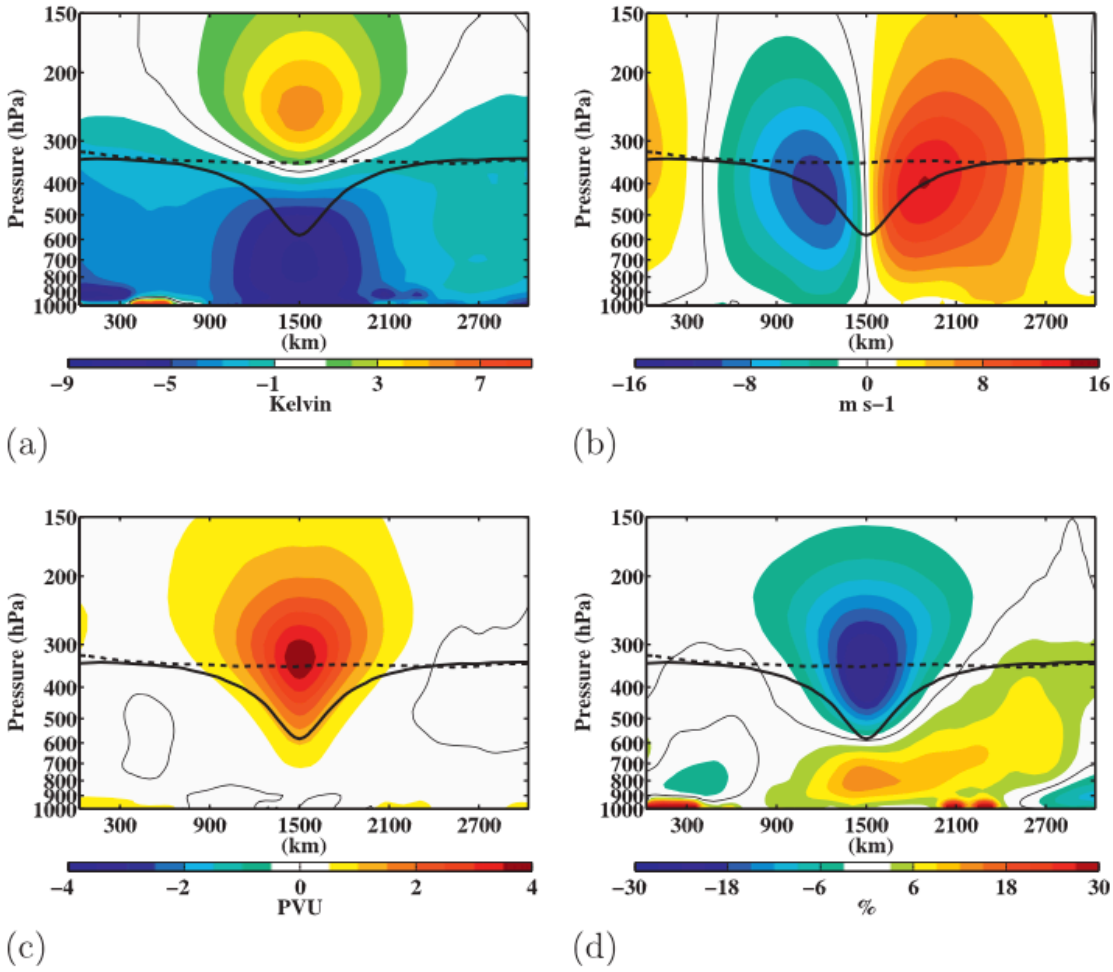

Fig. 1.3. Composite west-to-east cross-TPV section of anomalous (a) temperature (K), (b) v-wind component (m s^{-1}), (c) Ertel PV (PVU), and (d) relative humidity (%). Thick solid black contour is the composite tropopause, thick dashed black contour is the background tropopause, and thin solid contour is the 0 contour. [Figure 9 and adapted caption from Cavallo and Hakim (2010).]

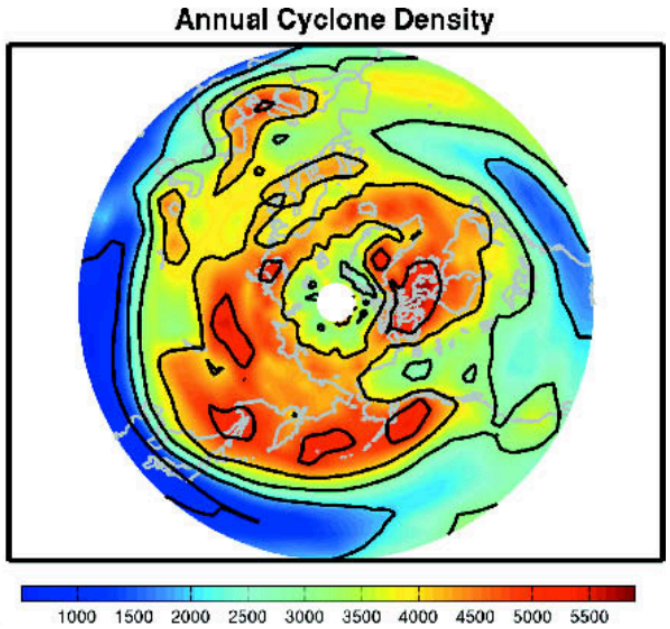

Fig. 1.4. Total number of cyclonic tropopause-based vortex events occurring in a 2.5°–10° latitude–longitude box centered at a point, with a cosine-latitude normalization applied for equal-area weighting [Figure 2 and adapted caption from Hakim and Canavan (2005).]

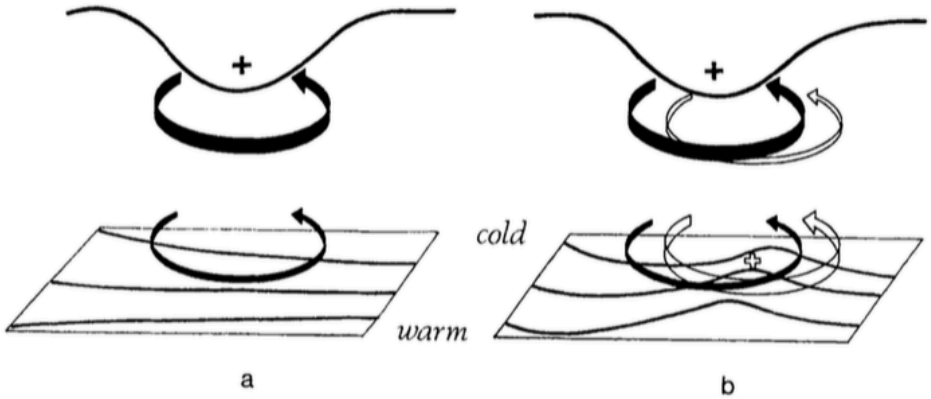

Fig. 1.5. A schematic picture of cyclogenesis associated with the arrival of an upper-level cyclonic PV anomaly over a low-level baroclinic region. In both (a) and (b) solid plus sign indicates location of the upper-level cyclonic PV anomaly, solid black contour at the top represents the tropopause, black contours at the bottom represent isentropes at the ground, thick solid arrow represents the cyclonic circulation induced by the upper-level cyclonic PV anomaly at upper levels, and thin solid arrow represents the cyclonic circulation induced by the upper-level cyclonic PV anomaly at lower levels. In (b), open plus sign represents location of the lower-level cyclonic PV anomaly, thick open arrow represents the cyclonic circulation induced by the lower-level cyclonic PV anomaly at lower levels, and the thin open arrow represents the cyclonic circulation induced by the lower-level cyclonic PV anomaly at upper levels. [Figure 21 and adapted caption from Hoskins et al. (1985, section 6e).]

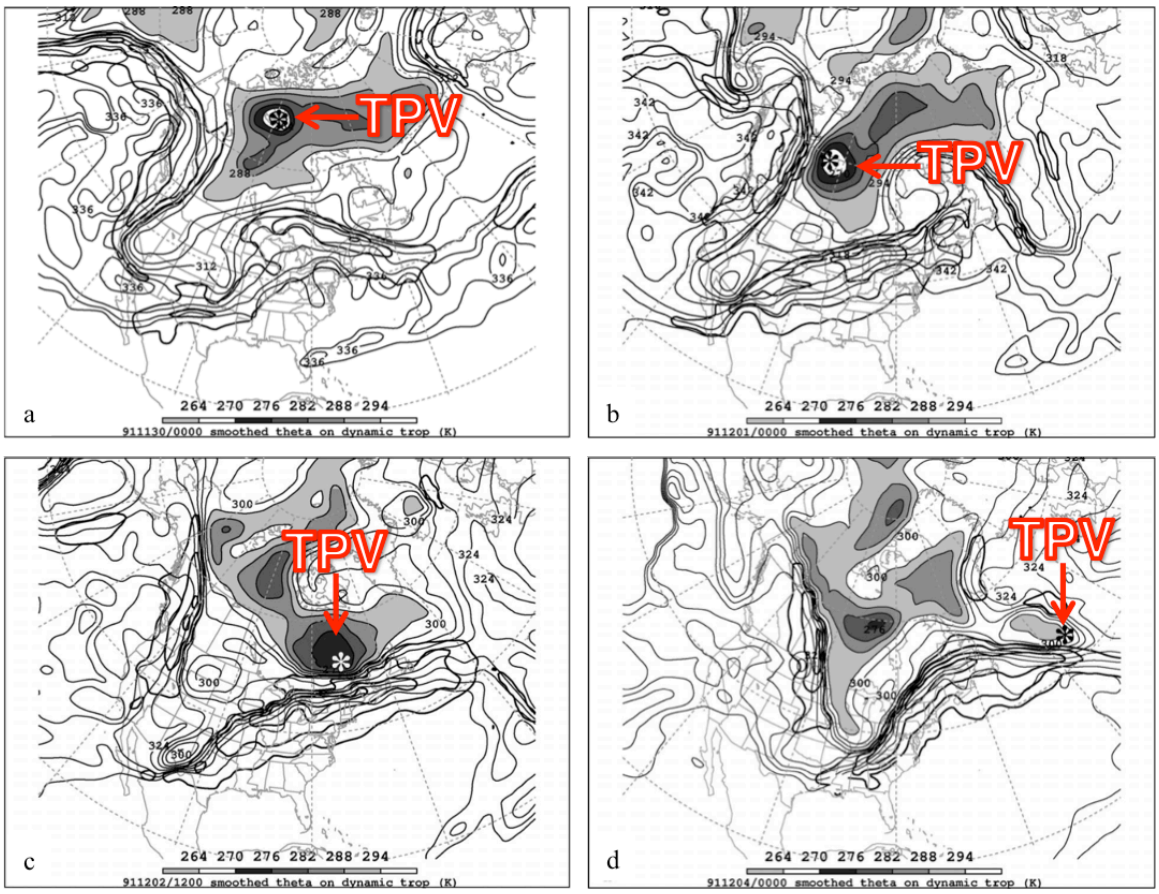

Fig. 1.6. DT (1.5-PVU) potential temperature (thin solid; values at and below 342 K contoured at a 6-K interval; shaded as indicated for values below 294 K) and wind speed (thick solid; contoured at a 15 m s^{-1} interval, starting at 50 m s^{-1}) valid (a) 0000 UTC 30 November, (b) 0000 UTC 1 December, (c) 1200 UTC 2 December, and (d) 0000 UTC 4 December 1991. The position of the DT pressure maximum associated with the TPV of interest is marked with an asterisk in each panel. Label "TPV" and arrow point to position of TPV. [Figures 10–13 and captions adapted from Pyle et al. (2004).]

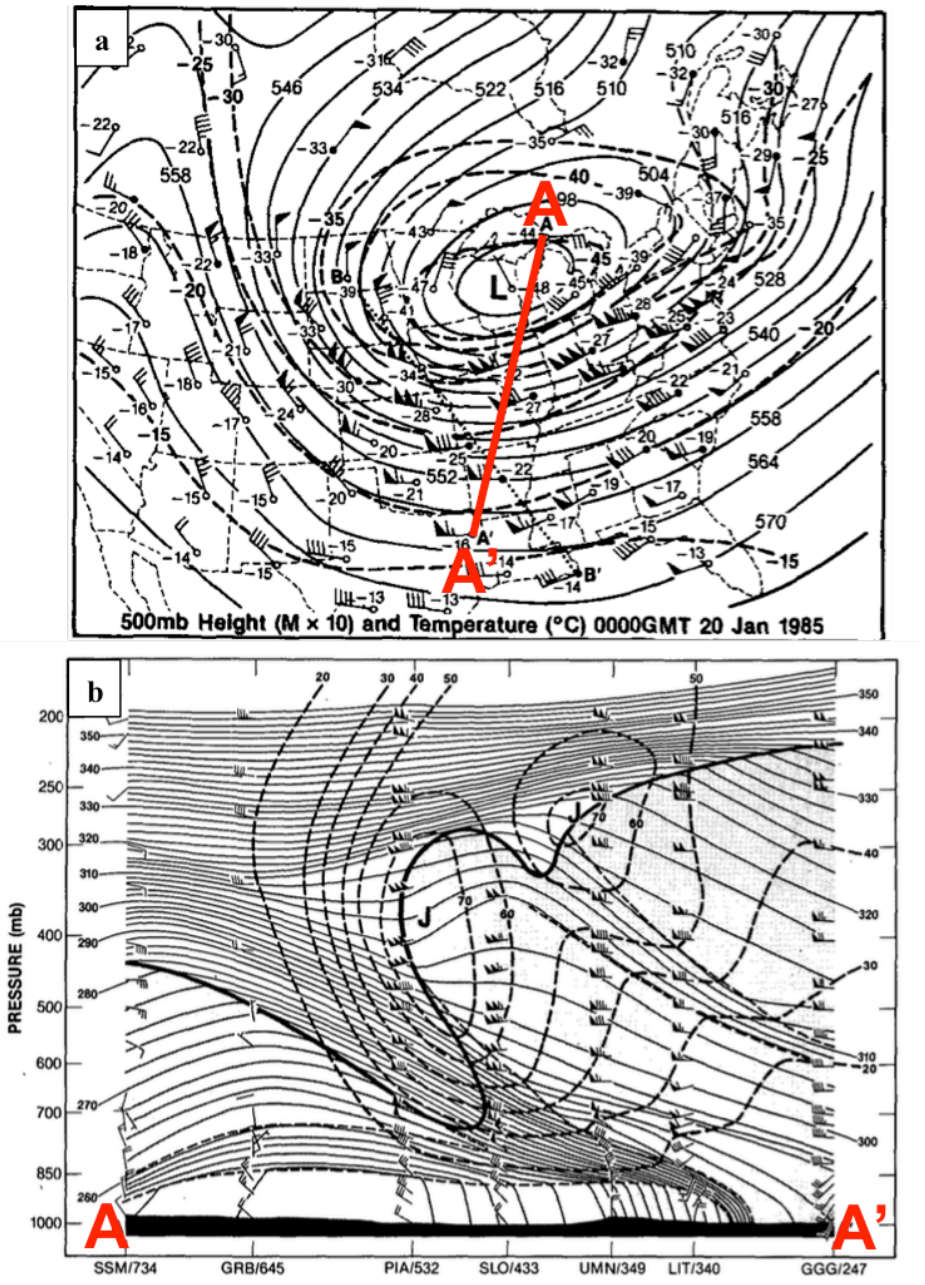

Fig. 1.7. (a) Isopleths showing 500-hPa geopotential height (dam; solid contours) and temperature (°C; dashed contours), and stations showing 500-hPa temperature (°C) and wind (flags and barbs, where flag denotes 25 m s^{-1}, full barb denotes 10 m s^{-1}, and half barb denotes 2.5 m s^{-1}) at 0000 UTC 20 January 1985. Projection line for cross section AA' is shown by bold red line. (b) Cross section of potential temperature (K, thin solid lines) and wind speed (m s^{-1}, heavy dashed lines) between Sault Sainte Marie, MI and Longview, TX, along the projection line AA' shown in (a). Heavy solid line is tropopause (10^{-7} K s^{-1} hPa^{-1} isopleth of PV) and light dashed lines indicate tropospheric frontal and stable layer boundaries. Soundings for stations (labeled at bottom) show wind [units and symbols same as for winds shown in (a)]. Jet cores are marked by "J." [Figures 8–9 and captions adapted from Shapiro et al. (1987).]

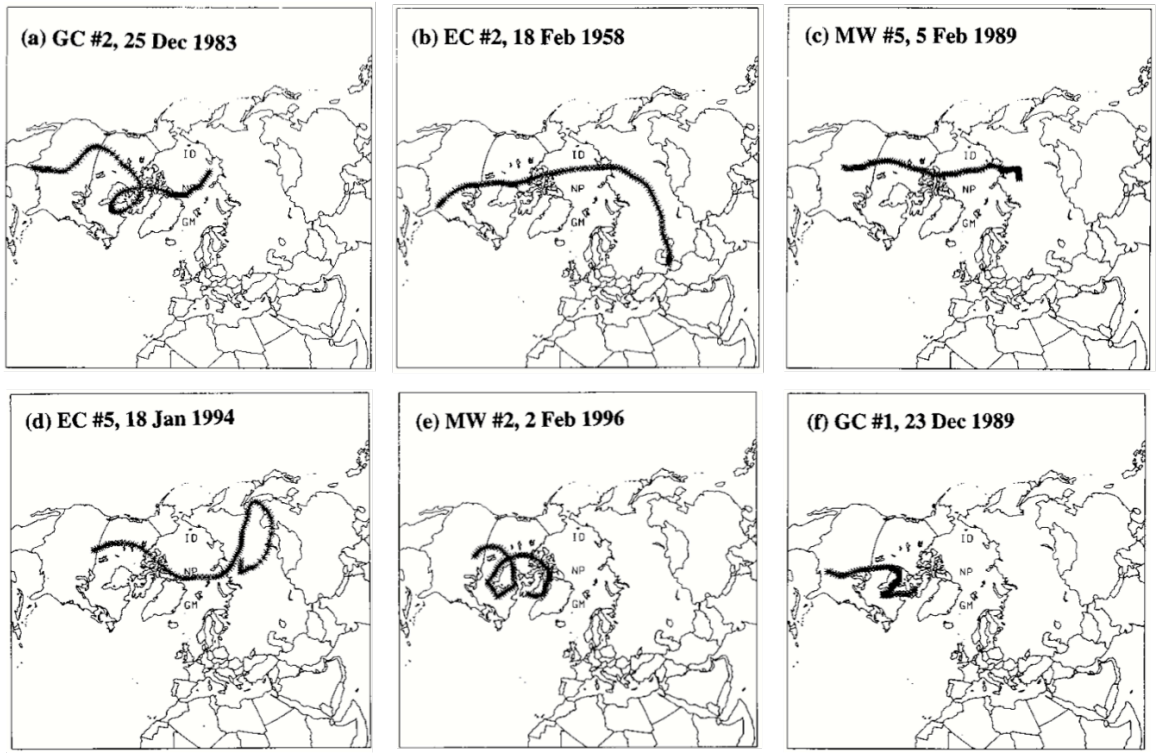

Fig. 1.8. Trajectories of air parcels reaching a point 50 hPa above the surface on center dates of the following major North American cold events from Table 1c of Walsh et al. (2001; not shown): (a) Gulf Coast (GC) #2, 25 December 1983; (b) East Coast (EC) #2, 18 February 1958; (c) Midwest (MW) #5, 5 February 1989; (d) EC #5, 18 January 1994; (e) MW #2, 2 February 1996; (f) GC #1, 23 December 1989. [Figure 5 and caption adapted from Walsh et al. (2001).]

2. Data and Methodology

2.1 TPV and Cold Pool Tracking

The ERA-Interim (ERA-I) reanalysis dataset (Dee et al. 2011) is utilized for this study. The ERA-I fields, which have a native horizontal resolution of ~0.7°, were regridded to a horizontal resolution of 0.5°. TPVs were identified and tracked for the 1979–2015 period poleward of 30°N by utilizing a TPV tracking algorithm developed by Nicholas Szapiro and Steven Cavallo at the University of Oklahoma (https://github.com/nickszap/tpvTrack). This tracking algorithm uses potential temperature, zonal wind, meridional wind, and the vertical component of relative vorticity on the DT (2-PVU surface) as input variables. At each time stamp (6 h interval), the potential temperature field on the DT is segmented into regions associated with potential temperature minima and maxima on the DT with use of the sign of the vertical component of relative vorticity, such that grid cells in regions associated with potential temperature minima and maxima on the DT possess positive and negative values of the vertical component of relative vorticity on the DT, respectively. Although both regions associated with potential temperature minima and maxima on the DT are identified as part of the segmentation process, only regions associated with potential temperature minima on the DT are then tracked spatially and temporally with use of the zonal and meridional winds on the DT to create TPV tracks. The location or center of a TPV is defined as the location of the potential temperature minimum on the DT of the TPV. For more detailed information about how TPVs are identified and tracked in the TPV tracking algorithm, see the above link for the TPV tracking algorithm.

As discussed in section 1.2.1, the composite west-to-east cross-TPV section from Cavallo and Hakim (2010) shows that anomalously cold air is located throughout the depth of the

troposphere within and beneath the TPV (Fig. 1.3a). Accordingly, 1000–500-hPa thickness minima are considered to be representative of cold pools that may be associated with TPVs. Cold pools were identified and tracked for the 1979–2015 period poleward of 30°N by using the same TPV tracking algorithm discussed above, but with different input variables. Instead of using potential temperature on the DT, the 1000–500-hPa thickness is used. Instead of using zonal and meridional winds on the DT, the 700-hPa zonal and meridional winds are used. Finally, instead of using the vertical component of relative vorticity on the DT, the 1000–500-hPa thermal vorticity, calculated by subtracting the 1000-hPa vertical component of relative vorticity from the 500-hPa vertical component of relativity vorticity, is used. At each time stamp (6 h interval), the 1000–500-hPa thickness field is segmented into regions associated with 1000–500-hPa thickness minima and maxima with use of the sign of the 1000–500-hPa thermal vorticity, such that grid cells in regions associated with 1000–500-hPa thickness minima and maxima possess positive and negative values of 1000–500-hPa thermal vorticity, respectively. Although both regions associated with 1000–500-hPa thickness minima and maxima are identified as part of the segmentation process, only regions associated with 1000–500-hPa thickness minima are then tracked spatially and temporally with use of the 700-hPa zonal and meridional winds to create cold pool tracks. The location or center of a cold pool is defined as the location of the 1000–500-hPa thickness minimum of the cold pool.

2.2 TPV and Cold Pool Filtering

Cavallo and Hakim (2009) required that TPVs spend at least 60% of their lifetimes poleward of 65°N. In this study, TPVs are required to spend at least 6 h poleward of 60°N.

Cavallo and Hakim imposed a stricter latitude criterion to isolate TPVs from the polar jet stream in order to understand the basic dynamics of TPVs themselves. A less strict latitude criterion is imposed here because the primary interest of this study is on TPVs transported from high latitudes (>60°N) to middle latitudes (30°N–60°N). It is anticipated that TPVs that spend little time in high latitudes and TPVs that spend a majority of their lifetimes in high latitudes may both result in the development of CAOs in middle latitudes. Thus, the use of a less strict latitude criterion allows for the identification of more TPVs that may play an important role in the development of CAOs. Cold pools are also required to spend at least 6 h poleward of 60°N for consistency with the latitude criterion imposed for TPVs. TPVs and cold pools are both required to last at least two days for consistency with the longevity criterion used by Cavallo and Hakim (2009) for TPVs. In addition, since this study focuses on TPVs and cold pools transported from high latitudes to middle latitudes, the focus will be on TPVs and cold pools that move equatorward of 60°N after being located in high latitudes.

2.3 CAO Identification

A regional CAO climatology created by Murphy (2017) was utilized for this study. Murphy (2017) used daily minimum temperature data extracted from stations within the National Centers for Environmental Information (NCEI) Global Historical Climatology Network-Daily dataset (Menne et al. 2012). Murphy (2017) extracted daily minimum temperature data from 53 stations evenly distributed throughout the continental U.S., as well as throughout nine climate regions defined by NCEI (Fig. 2.1) for 1948–2015. According to Murphy (2017), a regional CAO is defined to occur within a climate region whenever two or more stations within the

climate region experience three or more consecutive days where daily minimum temperatures are less than or equal to the 31-day centered moving average of the 5th percentile minimum temperature for those days and share at least one overlapping day. For this study, only regional CAOs (hereafter referred to as CAOs) occurring in the six climate regions encompassing the central and eastern U.S., i.e., the climate regions east of the black line and labeled in the black box shown in Fig. 2.1, during 1979–2015 are considered.

2.4 Identification of CAOs that are Linked to Cold Pools Associated with TPVs

One of the goals of this study is to determine the linkages between TPVs, cold pools, and CAOs. For this portion of this study, only TPVs and cold pools transported from high latitudes to middle latitudes as described in section 2.2 are considered. In order to investigate the linkages between TPVs, cold pools, and CAOs, CAOs that are linked to cold pools were first determined for each climate region in the central and eastern U.S. for the 1979–2015 period. CAOs that are linked to cold pools were determined for each climate region by requiring that a circle of radius 1500 km surrounding the center of a cold pool must overlap at least one grid point (using a 0.5° grid) of the climate region for at least one time stamp (6 h interval) during a CAO. Figure 2.2a shows a circle of radius 1500 km surrounding the center of a cold pool at 1200 UTC 20 January 1985, a time during which the CAO studied by Shapiro et al. (1987), which was briefly discussed in Section 1.2.4.2, impacted the central and eastern U.S. This CAO was identified to occur in the Central, Northeast, South, and Southeast climate regions during the 19–24 January 1985 period. Also, the cold pool circle intersects at least one grid point in the Central, Northeast, South, and Southeast climate regions at 1200 UTC 20 January 1985 (Fig. 2.2b), so, based on this time stamp

alone, all of these climate regions are identified as experiencing a CAO that is linked to a cold pool.

The same cold pool circle radius threshold of 1500 km is used for all cold pools for simplicity and consistency. The choice of a 1500-km radius threshold for the cold pool circle was subjectively chosen based on its general representation of the size of the cold pool shown in Fig. 2.2a as well as other cold pools examined (not shown). Other cold pool circle radius thresholds were tested, including 1250 km and 1750 km, and the sensitivity of the number and percentage of CAOs that are linked to cold pools for each climate region to the cold pool circle radius threshold will be briefly discussed in chapter 3. There may be situations in which surface-based Arctic air associated with a cold pool spreads beyond the cold pool circle edge. Thus, a larger cold pool circle radius threshold may help avoid a "miss" scenario in which a climate region experiencing a CAO is not identified as experiencing a CAO that is linked to a cold pool because the cold pool circle does not intersect the climate region, but the surface-based Arctic air associated with the cold pool actually impacts the climate region. However, there also may be situations in which the surface-based Arctic air associated with a cold pool does not spread far from the cold pool center and/or the cold pool is located too far away from a climate region experiencing a CAO such that the surface-based Arctic air associated with the cold pool does not reach the climate region. Thus, a smaller cold pool circle radius threshold may help avoid a "false alarm" scenario in which a climate region is identified as experiencing a CAO that is linked to a cold pool because the cold pool circle intersects the climate region, but the cold pool actually has no impact on the climate region and another feature, e.g., a trough, is causing the CAO in the climate region. An intermediate cold pool circle radius threshold value of 1500 km was thought to be a good compromise, although stricter criteria could be enforced to more

precisely determine climate regions experiencing CAOs that are linked to cold pools in different situations.

Once the CAOs that are linked to cold pools were identified for each climate region, cold pools that are associated with TPVs were determined for the 1979–2015 period. In order to determine which cold pools are associated with TPVs, the centers of the cold pools and TPVs were required to be located within a 750-km distance of one another for at least two consecutive days. Requiring that the centers of the cold pools and TPVs be located within a 750-km distance of one another for at least two consecutive days helps ensure that there is both spatial and temporal overlap between the cold pools and TPVs, and thus helps ensure that the cold pools and TPVs are associated with one another. Once it was determined which cold pools are associated with TPVs, a 1979–2015 climatology of CAOs that are linked to cold pools associated with TPVs was determined for each climate region in the central and eastern U.S. Figure 2.3 illustrates that the cold pool linked to the 19–24 January 1985 CAO is also associated with a TPV. At 1200 UTC 20 January 1985, a circle of radius 750 km surrounding the TPV center (TPV shown in Fig. 2.3a) encapsulates the cold pool center (cold pool shown in Fig. 2.3b). In addition, the cold pool center was identified to be located within a 750-km radius circle surrounding the TPV center for at least two consecutive days (not shown). As discussed earlier for this cold pool, the Central, Northeast, South, and Southeast climate regions are identified as experiencing a CAO that is linked to a cold pool. Given, that this cold pool is associated with a TPV, the Central, Northeast, South, and Southeast climate regions are also identified as experiencing a CAO that is linked to a cold pool associated with a TPV.

Other distance thresholds between the centers of the TPVs and cold pools, such as 500 km and 1000 km, were tested, and the sensitivity of the number and percentage of CAOs that are

linked to cold pools associated with TPVs for each climate region to these distance thresholds will be discussed briefly in chapter 3. Too strict of a distance threshold may result in a "miss" scenario in which a cold pool that generally overlaps spatially and temporally with a TPV is not identified to be associated with the TPV because, for example, the cold pool and TPV are temporarily spaced too far away from one another at some intermediate time or times. Too relaxed of a distance threshold may result in a "false alarm" scenario in which a cold pool is identified to be associated with a TPV that does not overlap with the cold pool. For example, there may be situations in which there are multiple cold pools and TPVs located near one another, so too relaxed of a distance threshold may falsely associate a cold pool with nearby TPVs that do not overlap with the cold pool.

2.5 Case Studies

Illustrative CAOs that are clearly linked to well-defined cold pools associated with TPVs were chosen as case studies to illustrate important linkages between TPVs, cold pools, and CAOs. These illustrative CAOs are the 9–14 January 1982 CAO and the 19–24 January 1985 CAO. Both CAOs led to significant socioeconomic impacts over the central and eastern U.S.

In addition, TPV–jet interaction is hypothesized to play a role in the development of the CAO in each case. In order to help diagnose the role of TPV–jet interaction on the development of the CAO in each case, the across-isentrope ($\mathbf{Q}_n$) and along-isentrope ($\mathbf{Q}_s$) components of the Q vector and their associated forcing for vertical motion during TPV–jet interaction are examined. The Q vector is calculated in pressure coordinates using the following equation from Hoskins and Pedder (1980):

$$\boldsymbol{Q} = -\left(\frac{\partial \boldsymbol{V}_g}{\partial x} \cdot \nabla_p \theta\right) \boldsymbol{i} - \left(\frac{\partial \boldsymbol{V}_g}{\partial y} \cdot \nabla_p \theta\right) \boldsymbol{j}\,, \tag{1}$$

where $\boldsymbol{V}_g$ is the geostrophic wind, θ is the potential temperature, and ∇_p is the horizontal gradient operator along a constant pressure surface. Q vectors are separated into $\mathbf{Q}_n$ and $\mathbf{Q}_s$ following Keyser et al. (1992) as follows:

$$\boldsymbol{Q}_n = \left[\boldsymbol{Q} \cdot \left(-\frac{\nabla\theta}{|\nabla\theta|}\right)\right]\left(-\frac{\nabla\theta}{|\nabla\theta|}\right) \tag{2}$$

$$\boldsymbol{Q}_s = \left(\frac{\boldsymbol{Q}\cdot(\boldsymbol{k}\times\nabla\theta)}{|\nabla\theta|}\right)\left(\frac{\boldsymbol{k}\times\nabla\theta}{|\nabla\theta|}\right). \tag{3}$$

$\mathbf{Q}_n$ and $\mathbf{Q}_s$ describe the rate of change of the magnitude and direction of $\nabla\theta$, respectively (Keyser et al. 1992). Q vector forcing for vertical motion associated with $\mathbf{Q}_n$ and $\mathbf{Q}_s$ are calculated using the right-hand side of the Q vector form of the QG omega equation in pressure coordinates from Hoskins and Pedder (1980), given by

$$\left(\sigma\nabla_p^2 + f_0^2\frac{\partial^2}{\partial p^2}\right)\omega = -2h\left(\nabla_p \cdot \boldsymbol{Q}\right), \tag{4}$$

with $\mathbf{Q}$ replaced by $\mathbf{Q}_n$ and $\mathbf{Q}_s$ respectively. In (4), $h = (\rho\,\theta)^{-1}$, where ρ is the density, or equivalently, $h = \frac{R}{p_o}\left(\frac{p_0}{p}\right)^{c_v/c_p}$, where R is the gas constant for dry air, p is the pressure, p_0 is 1000 hPa, c_v is the specific heat of dry air at constant volume, and c_p is the specific heat of dry air at constant pressure. Also in (4), f_0 is a constant reference value of the Coriolis parameter, ω is the vertical velocity in pressure coordinates, and $\sigma = -h\frac{d\Theta}{dp}$, where $\frac{d\Theta}{dp}$ is the vertical derivative of reference potential temperature with respect to pressure, is the static stability parameter. The Q vector components and their associated forcing for vertical motion are calculated every 100 hPa over a layer representative of the TPV in each case.

As discussed in section 1.2.3, surface anticyclones can play an important role in the equatorward transport of Arctic air and thus CAO development. Surface anticyclones may be

found in and/or near the left entrance region of the jet (e.g., Jones and Cohen 2011), and so it is anticipated that TPV–jet interaction may influence the strength of these surface anticyclones. It is hypothesized that TPV–jet interaction will result in a strengthening of the thermal gradient accompanying the jet, supporting stronger ageostrophic circulations associated with the jet. Thus, $\mathbf{Q}_n$ and its associated forcing for vertical motion are used to infer changes in the strength of the thermal gradient accompanying the jet and concomitant changes in the structure and magnitude of vertical motion patterns that are part of the ageostrophic circulations associated with the jet during TPV–jet interaction. It is anticipated that there will be $\mathbf{Q}_n$ forcing for descent in and/or near the left entrance region of the jet associated with the intensification of the thermal gradient accompanying the jet during TPV–jet interaction. In addition, because TPVs are cyclonic vortices that may be accompanied by large curvature in the geostrophic flow, TPVs may alter the orientation of the thermal gradient during TPV–jet interaction. Thus, $\mathbf{Q}_s$ and its associated forcing for vertical motion are used to infer changes in the direction of the thermal gradient and concomitant changes in the structure and magnitude vertical motion patterns during TPV–jet interaction. Lang and Martin (2010) showed that $\mathbf{Q}_s$ divergence and thus $\mathbf{Q}_s$ forcing for descent is expected to be located upshear of an isolated vertical vorticity maximum. It is anticipated that there will also be $\mathbf{Q}_s$ forcing for descent upshear of the TPV in and/or near the left entrance region of the jet during TPV–jet interaction. The anticipated forcing for descent associated with $\mathbf{Q}_n$ and $\mathbf{Q}_s$ in and/or near the left entrance region of the jet during TPV–jet interaction may provide forcing to strengthen a surface anticyclone that may be located in and/or near the left entrance region of the jet. Therefore, the strengthening of a surface anticyclone associated with TPV–jet interaction may play a role in the development of the CAO in each case.

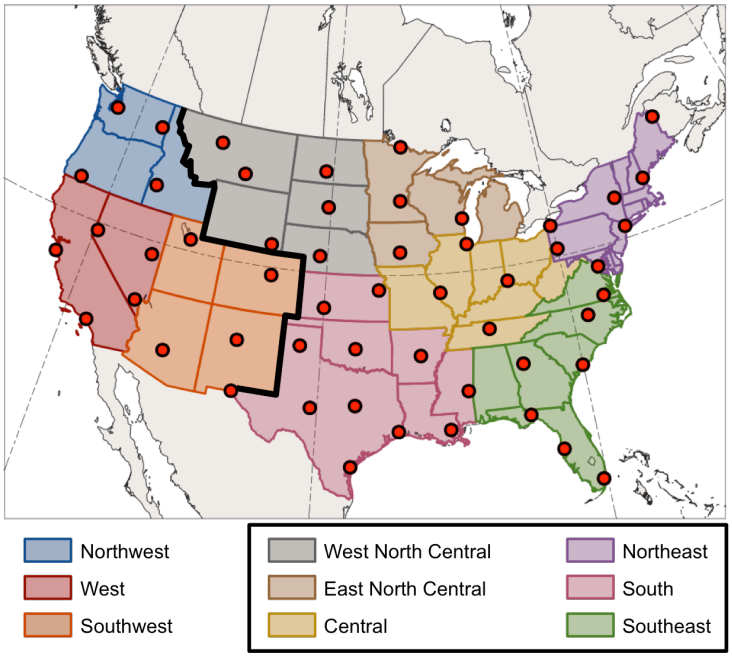

Fig. 2.1. Climate regions and stations (red dots) used in the Murphy (2017) CAO study. Climate regions east of the black line and labeled in the black box are considered for this study.

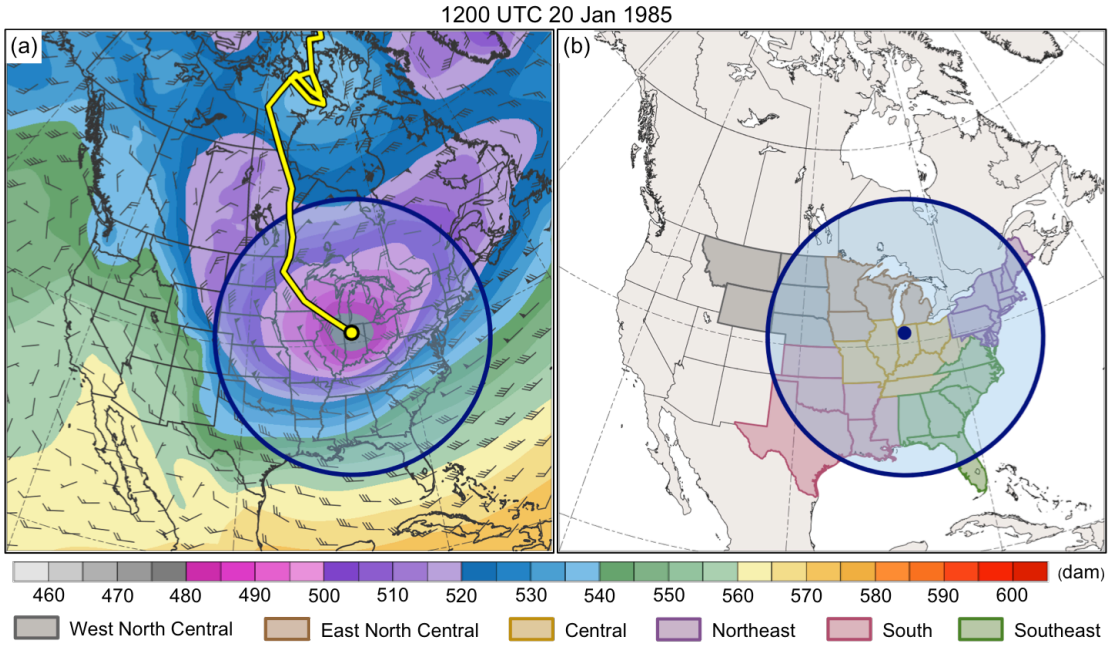

Fig. 2.2. (a) 1000–500-hPa thickness (dam, shading), 700-hPa wind (m s^{-1}, flags and barbs), cold pool track (yellow line), and circle of radius 1500 km (blue circle and shading) surrounding cold pool center (yellow dot) at 1200 UTC 20 January 1985. (b) Climate regions used in this study (colored shaded regions) and same circle as in (a) surrounding cold pool center (blue dot) at 1200 UTC 20 January 1985.

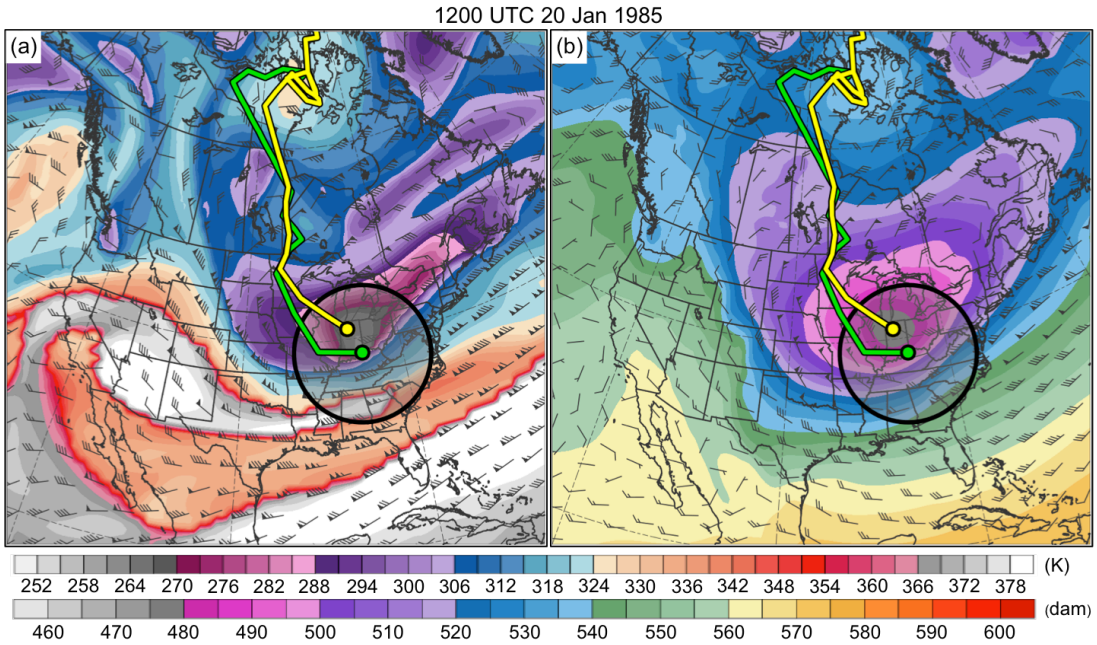

Fig. 2.3. (a) DT (2-PVU surface) potential temperature (K, shaded) and wind (m s^{-1}, flags and barbs), TPV and cold pool tracks (green and yellow lines, respectively), position of TPV center and cold pool center (green and yellow dots, respectively), and circle of radius 750 km (black circle and shading) surrounding TPV center at 1200 UTC 20 January 1985. (b) Same as in (a) except 1000–500-hPa thickness (dam, shading) and 700-hPa wind at 1200 UTC 20 January 1985.

3. Climatologies

3.1 Climatology of TPVs

There are a total of 58,563 TPVs during 1979–2015, for an average of ~1,583 TPVs per year. Figure 3.1a shows a track density plot of all TPVs. Regions of high TPV track density are found over northern Canada, the Canadian Archipelago, the Norwegian Seas, and northern Scandinavia extending eastward into northern Siberia and the adjacent Arctic Ocean. A local maximum of TPV track density is also evident over western Alaska and the adjacent Bering Sea. The regions of high TPV track density over the Canadian Archipelago and northern Siberia were also shown in Hakim and Canavan (2005; Fig. 1.4 in this thesis) and Kravitz (2007; their Fig. 3.2) for CTDs and Cavallo and Hakim (2009, 2012) for TPVs. Furthermore, regions of high TPV track density extend equatorward from high latitudes into middle latitudes over central and eastern North America and Siberia and eastern Asia, suggesting that these regions are preferred corridors for the equatorward transport of TPVs. Regions of relatively low TPV track density are found over regions of high terrain, including the Rocky Mountains and the Tibetan Plateau, in agreement with the results of Hakim and Canavan (2005) and Kravitz (2007) for CTDs.

There are a total of 25,085 TPVs transported to middle latitudes (equatorward of 60°N), ~42.8% of all TPVs, during 1979–2015, for an average of ~678 TPVs per year. Figure 3.1b shows a track density plot of TPVs transported to middle latitudes. Well-defined maxima of track density of TPVs transported to middle latitude are located over central Canada and Siberia, with regions of high track density of TPVs transported to middle latitudes extending equatorward over central and eastern North America and Siberia and eastern Asia, again indicating that central and eastern North America and Siberia and eastern Asia are preferred corridors for the

equatorward transport of TPVs. To get a better sense of the preferred corridors for the equatorward transport of TPVs, Fig. 3.2 shows the number of instances in which TPVs cross equatorward of 60°N per 10° longitude bin globally. It is clear from Fig. 3.2 that there is a distinct maximum in the number of instances in which TPVs cross equatorward of 60°N over central and eastern North America and a broader maximum in the number of instances in which TPVs cross equatorward of 60°N across much of Siberia and especially eastern Asia, providing further evidence that these regions are indeed preferred corridors for the equatorward transport of TPVs. In addition, Fig. 3.1b suggests that TPVs frequently track near the entrance regions and along the poleward sides of the North Atlantic and North Pacific jet streams, which are also regions of high CTD track density shown by Hakim and Canavan (2005; Fig. 1.4 in this thesis). Fig. 3.1b also shows that regions of relatively low track density of TPVs transported to middle latitudes are found over western North America, and Fig. 3.2 shows that there is a distinct minimum in the number of instances in which TPVs cross equatorward of 60°N over the eastern North Pacific and western North America, likely related to upper-level ridging that often occurs in this region.

Figures 3.3a and 3.3b show the number of TPVs and TPVs transported to middle latitudes (equatorward of 60°N), respectively, per season, normalized to a 91.25-day season. The highest number of TPVs is found during the winter [December, January, and February (DJF)], while the lowest number of TPVs is found during the summer [June, July, and August (JJA)], in agreement with the results of Cavallo and Hakim (2012). There are fairly similar numbers of TPVs during the spring [March, April, and May (MAM)] and autumn [September, October, and November (SON)]. Similar to all TPVs, the highest and lowest number of TPVs transported to middle latitudes is found during the winter and summer, respectively. There is an intermediate

number of TPVs transported to middle latitudes during the spring and autumn. Although not shown here, if the number of TPVs transported to middle latitudes per season is divided by the total number of TPVs per season, there is also a slightly higher percentage of TPVs transported to middle latitudes during the winter compared to the summer, suggesting that TPVs are more likely to be transported to middle latitudes during the winter compared to the summer.

3.2 Climatology of Cold Pools

There are a total of 23,045 cold pools during 1979–2015, for an average of ~623 cold pools per year. Figure 3.4a shows a track density plot of all cold pools. Similar to the regions of high TPV track density, there are regions of high cold pool track density over northern Canada, the Canadian Archipelago, and northern Siberia and the adjacent Arctic Ocean. High cold pool track density is also found over northern Greenland and the central Arctic Ocean (Fig. 3.4a), but there is a relative minimum of TPV track density in these same regions compared to surrounding locations like the Canadian Archipelago and northern Siberia (Fig. 3.1a). Similar to regions of high TPV track density, regions of high cold pool track density extend equatorward from high latitudes to middle latitudes over central and eastern North America and Siberia and eastern Asia (Fig. 3.4a), suggesting that these regions are preferred corridors for the equatorward transport of cold pools. Also, similar to regions of relatively low TPV track density, regions of relatively low cold pool track density are located over high terrain features like the Rocky Mountains and the Tibetan Plateau.

There are a total of 8,395 cold pools transported to middle latitudes (equatorward of 60°N), ~36.4% of all cold pools, during 1979–2015, for an average of ~227 cold pools per year.

Figure 3.4b shows that there are well-defined maxima of track density of cold pools transported to middle latitude over central and eastern Canada and Siberia and eastern Asia, similar to those of TPVs. However, comparing Fig. 3.4b with Fig. 3.1b shows that these well-defined maxima of track density of cold pools are shifted somewhat eastward from those of TPVs. In addition, there is a distinct maximum in the number of instances in which cold pools cross equatorward of 60°N (Fig. 3.5) over central and eastern North America, similar to that for TPVs (Fig. 3.2), though this maximum for cold pools is shifted somewhat eastward from that for TPVs. There is also a broad maximum in the number of instances in which cold pools cross equatorward of 60°N over much of Siberia (Fig. 3.5), similar to that of TPVs (Fig. 3.2). However, the maximum in the number of instances in which cold pools cross equatorward of 60°N over eastern Asia (Fig. 3.5) is a bit more distinct than that for TPVs (Fig. 3.2), and this maximum for cold pools is also shifted somewhat eastward from that for TPVs over eastern Asia.

The reason for the somewhat eastward shift of the maximum of track density of cold pools transported to middle latitudes over central and eastern Canada and eastern Asia from that of TPVs is not currently clear. It is possible that sometimes there may be a tilted baroclinic structure in the middle-to-upper troposphere such that some upper-level troughs and embedded TPVs may be located somewhat farther west than cold pools. Regardless, as will be illustrated in chapter 4, TPVs and cold pools that are linked can often be vertically aligned or nearly so, suggesting that not all TPVs may be located farther west than cold pools. In addition, like TPVs transported to middle latitudes, Fig. 3.4b suggests that cold pools transported to middle latitudes often track near the entrance regions and along the poleward sides of the North Atlantic and North Pacific jet streams. As cold pools move eastward toward the east coasts of North America and Asia, surface radiative cooling over land may possibly allow the centers of cold pools to

remain over land before eventually moving off the coast, where surface heat fluxes over the ocean may weaken cold pools. TPVs moving eastward toward the east coasts of North America and Asia may move more quickly off the east coasts of North America and Asia compared to cold pools as the TPVs interact with the North Atlantic and North Pacific jet streams, respectively. Thus for TPVs and cold pools moving eastward toward the east coasts of North America and Asia, cold pools may possibly remain over land over eastern Canada and eastern Asia longer than TPVs. Thus, a given cold pool may possibly impact more land areas of eastern Canada and eastern Asia compared to a given TPV, possibly contributing to the somewhat eastward shift in the maximum of track density of cold pools transported to middle latitudes over central and eastern Canada and eastern Asia from that of TPVs.

Figure 3.4b also shows that as for TPVs, there is a relative minimum in track density of cold pools transported to middle latitudes over western North America, and Fig. 3.5 shows that as for TPVs, there is a distinct minimum in the number of instances in which cold pools cross equatorward of 60°N over the eastern North Pacific and western North America, likely again related to upper-level ridging that often occurs in this region.

Figures 3.6a and 3.6b show the number of cold pools and cold pools transported to middle latitudes (equatorward of 60°N), respectively, per season, normalized to a 91.25-day season. Perhaps unexpected and contrary to the results for TPVs, the highest numbers of cold pools and cold pools transported to middle latitudes are found during the summer, while the lowest numbers of cold pools and cold pools transported to middle latitudes are found during the winter. However, if considering cold pools transported deep into the middle latitudes (equatorward of 45°N), the highest and lowest numbers of cold pools transported deep into the middle latitudes are found during the winter and summer, respectively (not shown). One possible

reason for the higher number of cold pools during the summer compared to the winter is that 1000–500-hPa thickness minima associated with cold pools may be more distinct from the surrounding 1000–500-hPa thickness field during the summer compared to the winter, and thus cold pools may be more identifiable and trackable during the summer compared to the winter. Furthermore, cold pools may be embedded in stronger horizontal thickness gradients during the winter than the summer. Since cold pools that are embedded in strong horizontal thickness gradients may be less identifiable than if they are embedded in weak horizontal thickness gradients, there may be less cold pools identified during the winter than the summer. When considering all cold pools transported equatorward of 60°N, given the higher number of cold pools during the summer compared to the winter, there is also a higher number of cold pools transported equatorward of 60°N during the summer compared to the winter. However, because the polar jet stream is located farther equatorward during the winter compared to the summer (not shown), there are still more cold pools transported deep into the middle latitudes, equatorward of 45°N, during the winter compared to the summer (not shown), regardless of there being a lower total number of cold pools during the winter compared to the summer.

The relatively similar track density patterns of TPVs and cold pools in Fig. 3.1 and Fig 3.4, respectively, and similar longitudinal corridors of maxima in the number of instances in which TPVs and cold pools cross equatorward of 60°N in Fig. 3.2 and Fig. 3.5, respectively, suggest that there are likely linkages between TPVs and cold pools. Given the high track density of TPVs and cold pools transported to middle latitudes and the maximum in the number of instances in which TPVs and cold pools cross equatorward of 60°N over central and eastern North America, a region prone to troughing and CAOs, the linkages between TPVs, cold pools, and CAOs over this region will be examined in detail.

3.3 Climatology of CAOs that are Linked to Cold Pools Associated with TPVs

The results in this section will only apply to cold pools and TPVs transported to middle latitudes (equatorward of 60°N). The total number of CAOs for each region over the central and eastern U.S during 1979–2015 is shown in Fig. 3.7a. There is regional variability in the number of CAOs, with the lowest number of CAOs over the East North Central (ENC) region (41) and the highest number of CAOs over the South region (162). Part of this regional variability in the number of CAOs may be due to the methodology used to define CAOs. Because the South region is larger and contains more stations compared to, for example, the ENC region, there may be more opportunity for a CAO to be identified in the South region compared to the ENC region. There also may be additional features, aside from cold pools transported from high latitudes to middle latitudes, that may lead to CAOs in the South region. For example, a midlatitude cutoff low may be associated with sufficiently cold air to lead to a CAO in the South region, but not sufficiently cold air to lead to a CAO in regions to the north.

Figure 3.7a also shows the total number of unique CAOs that are linked to at least one cold pool for each region over the central and eastern U.S during 1979–2015. It is evident that there is a larger number of unique CAOs that are linked to at least one cold pool over the northern regions of the U.S., such as the West North Central (WNC; 84) and Northeast (58) regions, compared to the southern regions of the U.S., such as the South (46) and Southeast (33) regions. Figure 3.7b shows the percentage of unique CAOs that are linked to at least one cold pool for each region over the central and eastern U.S during 1979–2015. It is clear that there is a much higher percentage of unique CAOs that are linked to at least one cold pool in northern regions of the U.S., comprising the WNC (84.8%), ENC (90.2%), and Northeast (86.6%) regions

compared to the southern regions of the U.S., comprising the South (28.4%) and Southeast (36.3%) regions. As shown in the track density plot of cold pools transported to middle latitudes (Fig. 3.4b), there is a large meridional gradient in track density of cold pools over southern Canada and the northern U.S., indicating that there are more cold pools that track over and near the northern regions of the U.S. compared to the southern regions of the U.S. Thus, CAOs are more likely to be linked to cold pools over the northern regions of the U.S. compared to the southern regions of the U.S. Although the South region does have more unique CAOs that are linked to at least one cold pool (46) compared to the ENC region (37), the South region has a much lower percentage of unique CAOs that are linked to at least one cold pool (28.4%) compared to the ENC region (90.2%). The higher number of unique CAOs that are linked to at least one cold pool in the South region compared to the ENC region may be related to the South region having a much higher number of CAOs (162) compared to the ENC region (41). Furthermore, cold pools may not need to be associated with as extreme cold air to lead to a CAO in the South region compared to cold pools leading to CAOs in the ENC region.

As discussed in chapter 2, a cold pool circle radius threshold of 1500 km was utilized to determine the number and percentage of unique CAOs that are linked to at least one cold pool. Other cold pool circle radius thresholds, including 1250 km and 1750 km, were tested, and it was found that the sensitivity of the number and percentage of unique CAOs that are linked to at least one cold pool to changes of the cold pool circle radius threshold varies by region. For example, for the ENC region, a 1250-km, 1500-km, and 1750-km cold pool circle radius threshold results in the identification of 34, 37, and 37 unique CAOs that are linked to at least one cold pool, respectively, or 82.9%, 90.2%, and 90.2% of CAOs, respectively. For the South region, a 1250-km, 1500-km, and 1750-km cold pool circle radius threshold results in the identification of 35,

46, and 62 unique CAOs that are linked to at least one cold pool, respectively, or 21.6%, 28.4%, and 38.3% of CAOs, respectively. Thus, the number and percentage of unique CAOs that are linked to at least one cold pool is more sensitive to changes of the cold pool circle radius threshold for the South region compared to the ENC region. Overall, there is greater sensitivity of the number and percentage of unique CAOs that are linked to at least one cold pool to a change in the cold pool circle radius threshold from 1500 km to 1750 km for the southern regions, comprising the South and Southeast regions, compared to the northern regions, comprising the WNC, ENC, and Northeast regions. This greater sensitivity for the southern regions compared to the northern regions may result from the large meridional gradient in the track density of cold pools transported to middle latitudes over southern Canada and the northern U.S. (Fig. 3.4b), such that by increasing the cold pool circle radius threshold from 1500 km to 1750 km, there is a larger increase in the number of CAOs that are identified as linked to cold pools for southern regions compared to northern regions.

Now that the unique CAOs that are linked to at least one cold pool have been determined for each region, the cold pools that are associated with TPVs are identified. It has been found that 6,288 out of the total 8,395 cold pools transported to middle latitudes, or 74.9%, match with at least one TPV transported to middle latitudes. It has also been found that 6,510 out of the total 25,085 TPVs transported to middle latitudes, or 26.0%, match with at least one cold pool transported to middle latitudes. Overall, a large percentage of cold pools transported middle latitudes (74.9%) can be said to be associated with TPVs. A large percentage of TPVs transported to middle latitudes (74%) are not associated with cold pools. A few possible reasons why TPVs may not be associated with cold pools may include TPVs being too small or too weak to be associated with trackable cold pools, TPVs being associated with 1000–500-hPa thickness

troughs that are not trackable, and TPVs being associated with cold pools that do not meet the latitude criterion imposed in chapter 2. Now, CAOs that are linked to at least one cold pool associated with TPVs can be determined.

The total number of unique CAOs that are linked to at least one cold pool associated with TPVs for each region over the central and eastern U.S during 1979–2015 is shown in Fig. 3.7a. For all regions, by comparing the total number of unique CAOs that are linked to at least one cold pool to the total number of unique CAOs that are linked to at least one cold pool associated with TPVs in Fig. 3.7a, it evident that a large percentage of the unique CAOs that are linked to at least one cold pool consists of CAOs that are linked to at least one cold pool associated with TPVs. Figure 3.7c shows the percentage of unique CAOs that are linked to at least one cold pool associated with TPVs for each region over the central and eastern U.S during 1979–2015. Similar to unique CAOs that are linked to at least one cold pool, there is a much higher percentage of unique CAOs that are linked to at least one cold pool associated with TPVs over the northern regions of the U.S., comprising the WNC (73.7%), ENC (87.8%), and Northeast (79.1%) regions, compared to the southern regions of the U.S., comprising the South (24.7%) and Southeast (27.5%) regions. As shown in Fig. 3.1b and Fig. 3.4b, there is a large meridional gradient in track density of both TPVs and cold pools transported to middle latitudes, respectively, over southern Canada and the northern U.S., indicating that there are more TPVs and cold pools that track over and near the northern regions of the U.S. compared to the southern regions of the U.S. Thus, CAOs are more likely to be linked to cold pools associated with TPVs over northern regions of the U.S. compared to southern regions of the U.S. Overall, given the high percentage of unique CAOs that are linked to cold pools associated with TPVs over

northern regions of the U.S., it is clear that TPVs can play important roles in the development of CAOs.

As discussed in chapter 2, a 750-km distance threshold between the centers of TPVs and cold pools was used to help determine which cold pools are associated with TPVs and thus which CAOs are linked to at least one cold pool associated with TPVs. Other distance thresholds including 500 km and 1000 km were tested, and the sensitivity of the number and percentage of unique CAOs that are linked to at least one cold pool associated with TPVs to changes of the distance threshold was examined. For the ENC region, a 500-km, 750-km, and 1000-km distance threshold results in the identification of 35, 36, and 36 unique CAOs that are linked to at least one cold pool associated with TPVs, respectively, or 85.4%, 87.8%, and 87.8% of CAOs, respectively. For the South region, a 500-km, 750-km, and 1000-km distance threshold results in the identification of 38, 40, and 41 unique CAOs that are linked to at least one cold pool associated with TPVs, respectively, or 23.5%, 24.7%, and 25.3% of CAOs, respectively. For the WNC region, a 500-km, 750-km, and 1000-km distance threshold results in the identification of 64, 73, and 74 unique CAOs that are linked to at least one cold pool associated with TPVs, respectively, or 64.6%, 73.7%, and 74.7% of CAOs, respectively. Thus in the WNC region, there is notable sensitivity of the number and percentage of CAOs that are linked to at least one cold pool associated with TPVs to a change of the distance threshold from 500 km to 750 km, but like the ENC and South regions as well as all other regions (not discussed), there is small sensitivity to a change of the distance threshold from 750 km to 1000 km. Overall, there is a large percentage of unique CAOs that are linked to at least one cold pool associated with TPVs over northern regions of the U.S., regardless of the exact distance threshold utilized. Thus, again it is clear that TPVs can play important roles in the development of CAOs.

(a) **All TPVs**

(N = 58,563; avg. of ~1,583 per yr)

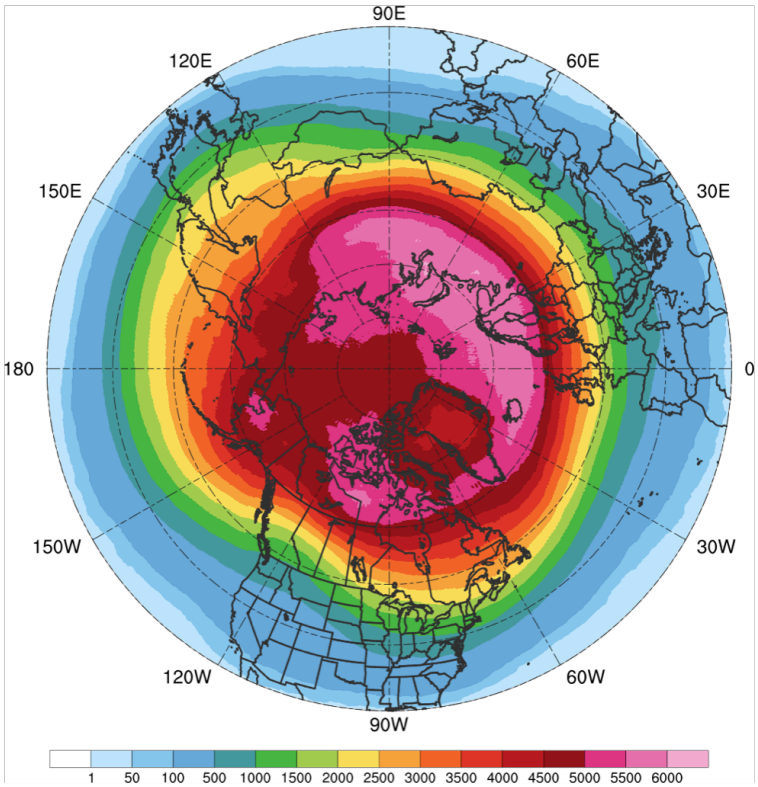

(b) **TPVs Transported to Middle Latitudes**

(N = 25,085; avg. of ~678 per yr)

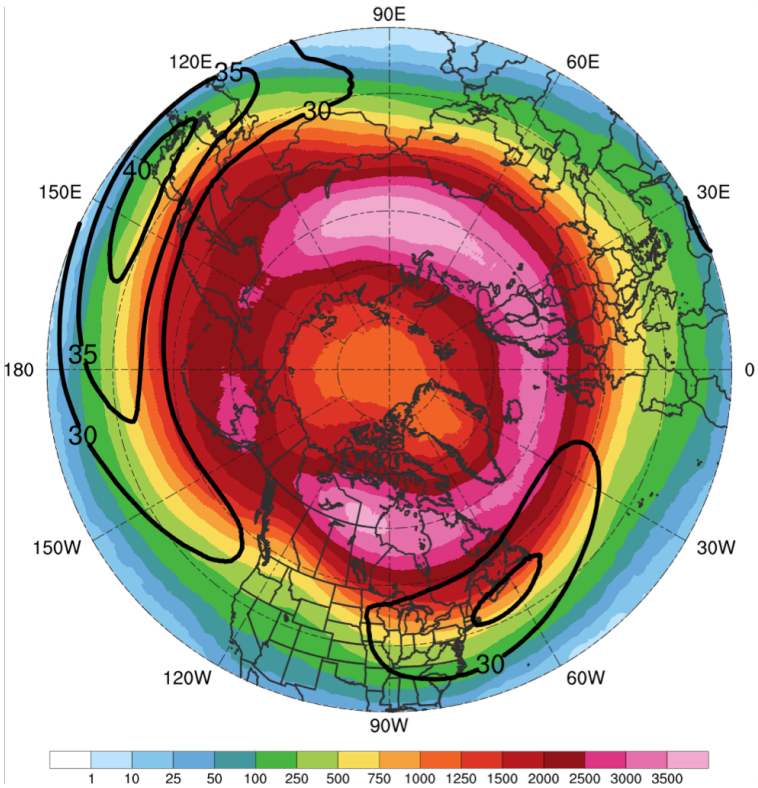

Fig. 3.1. Track density plots showing total number of unique (a) TPVs and (b) TPVs transported to middle latitudes (equatorward of 60°N) within 500 km of each grid point (using a 0.5° grid) during 1979–2015. Also in (b), the 1979–2015 mean DT wind speed (m s^{-1}, black contours).

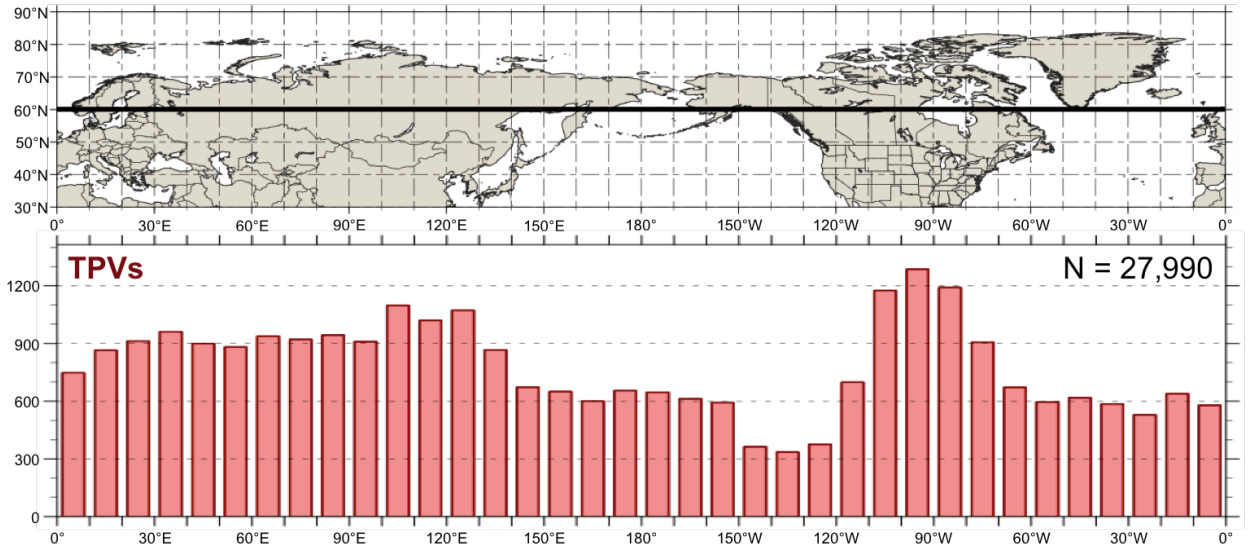

Fig. 3.2. Histogram showing total number of instances in which TPVs cross equatorward of 60°N (black line on map) for each 10° longitude bin globally during 1979–2015. An individual TPV can be counted more than once if it crosses equatorward of 60°N after returning poleward of 60°N.

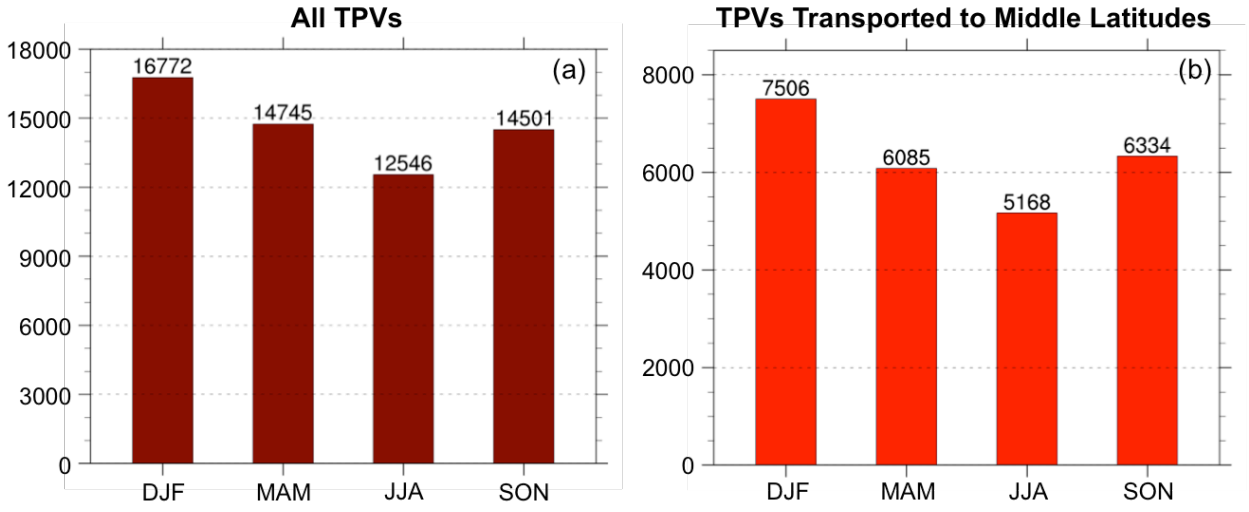

Fig. 3.3. Histograms showing (a) the total number of TPVs per season and (b) the total number of TPVs transported to middle latitudes (equatorward of 60°N) per season, normalized to a 91.25 day season, during 1979–2015.

(a) **All Cold Pools**
(N = 23,045; avg. of ~623 per yr)

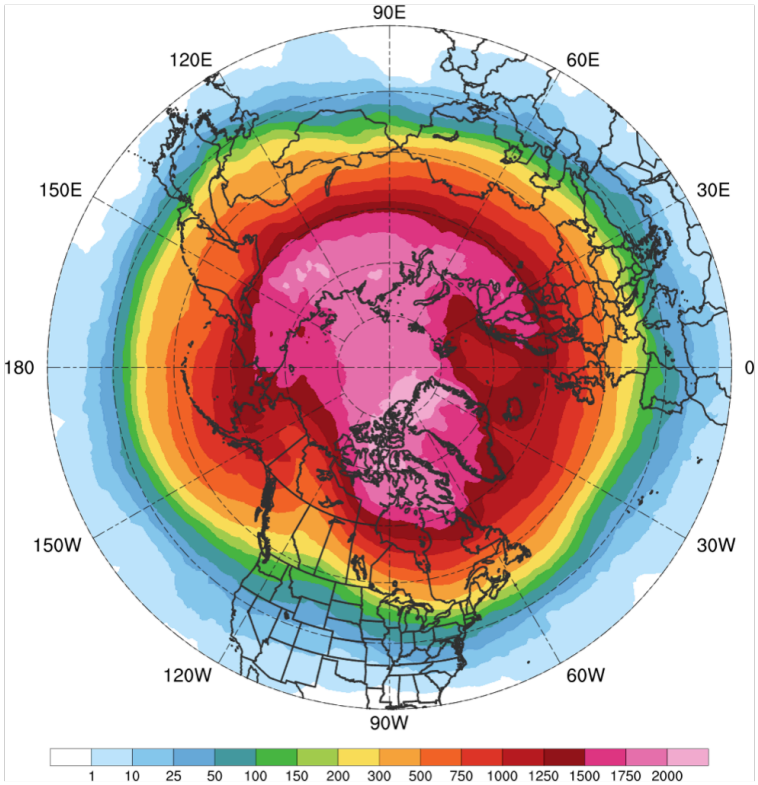

(b) **Cold Pools Transported to Middle Latitudes**
(N = 8,395; avg. of ~227 per yr)

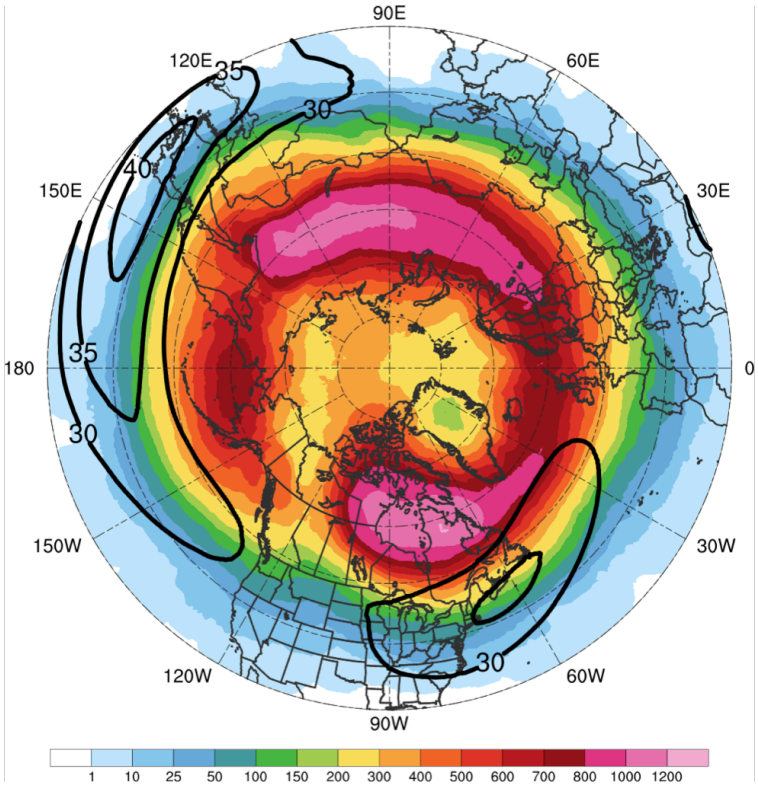

Fig. 3.4. Track density plots showing total number of unique (a) cold pools and (b) cold pools transported to middle latitudes (equatorward of 60°N) within 500 km of each grid point (using a 0.5° grid) during 1979–2015. Also in (b), the 1979–2015 mean DT wind speed (m s^{-1}, black contours).

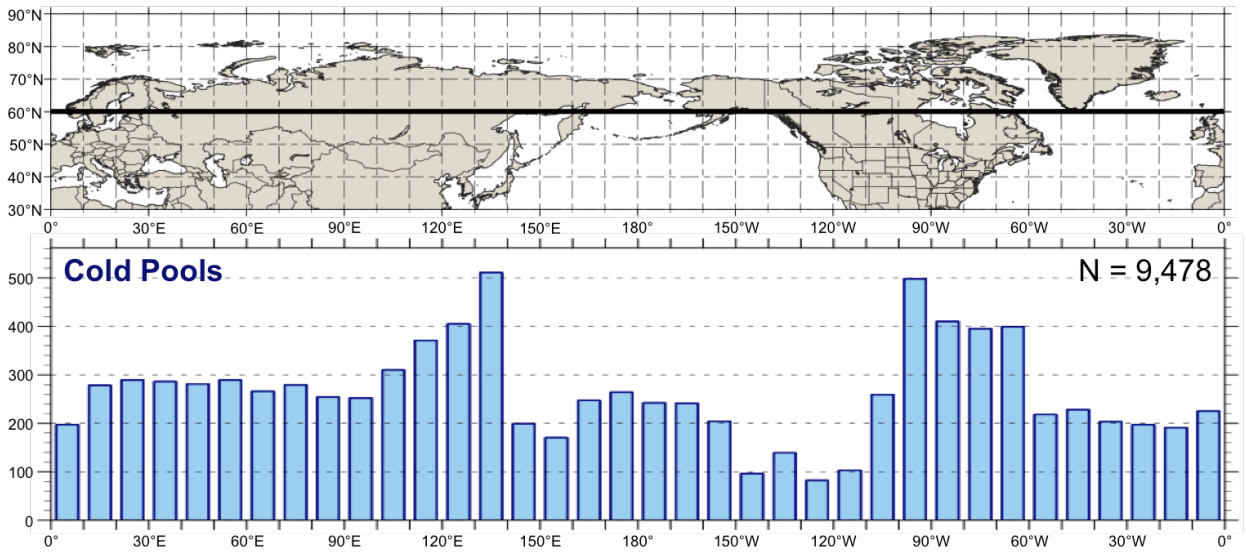

Fig. 3.5. As in Fig. 3.2, but for cold pools.

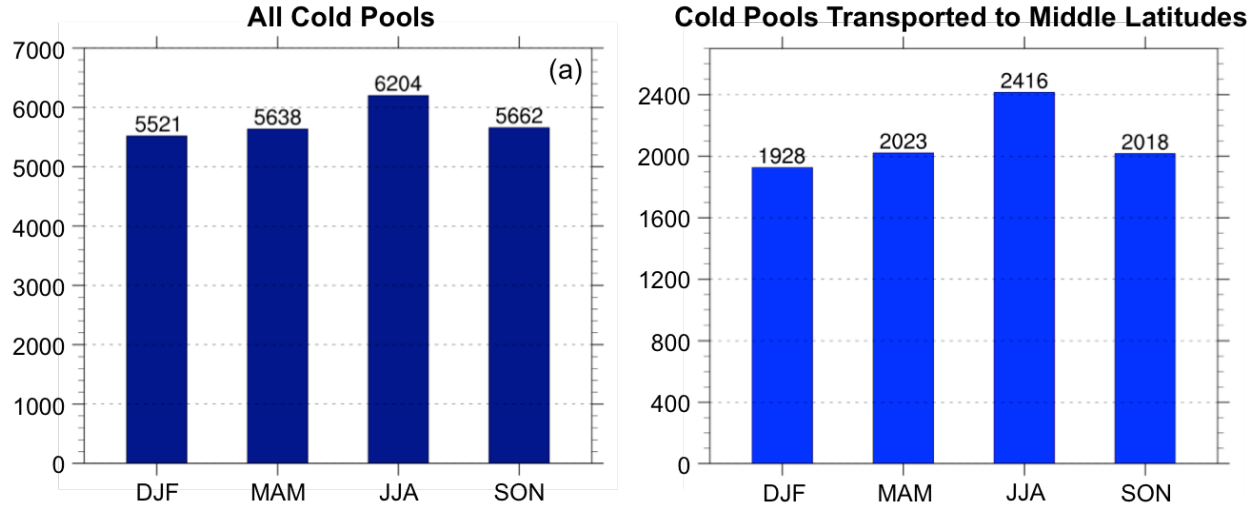

Fig. 3.6. Histograms showing (a) the total number of cold pools per season and (b) the total number of cold pools transported to middle latitudes (equatorward of 60°N) per season, normalized to a 91.25-day season, during 1979–2015.

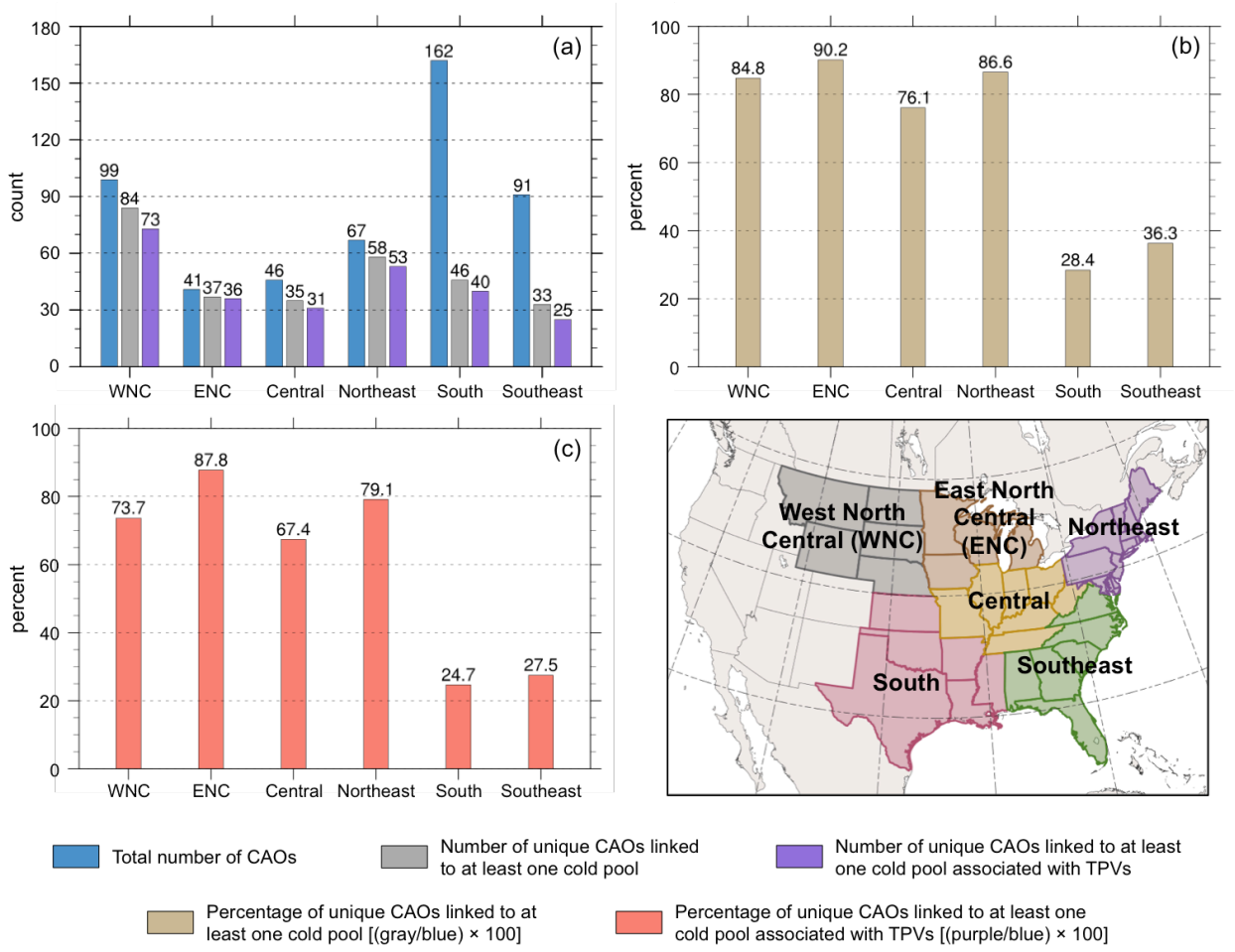

Fig. 3.7. Histograms showing (a) total number of CAOs (blue), number of unique CAOs that are linked to at least one cold pool (gray), and number of unique CAOs that are linked to at least one cold pool associated with TPVs (purple); (b) percentage of unique CAOs that are linked to at least one cold pool (tan); and (c) percentage of unique CAOs that linked to at least one cold pool associated with TPVs (peach) for each NCEI climate region shown in the accompanying map during 1979–2015.

4. Case Studies

4.1 9–14 January 1982 CAO

4.1.1 Case Overview

During 9–14 January 1982, a CAO impacted a widespread area of central and eastern North America, leading to significant socioeconomic impacts. According to NOAA NCEI, during 10–16 January 1982, a cold wave, which includes the 9–14 January 1982 CAO (hereafter referred to as the January 1982 CAO), and a winter storm in the U.S. contributed to an estimated cost of 1.7 billion dollars, after 2017 consumer price index adjustment, and 85 deaths (https://www.ncdc.noaa.gov/billions/). The January 1982 CAO led to widespread record low surface temperatures across the central and eastern U.S., with all-time record low temperatures of −32.2°C (−26°F) and −17.2°C (1°F) recorded in Chicago, IL and Augusta, GA on 10 and 11 January 1982, respectively (Wagner 1982). The January 1982 CAO qualifies as a CAO for the Northeast, Central, South, and Southeast regions (see Fig. 2.1 for map of regions) and a CAO that is linked to a cold pool associated with a TPV for all of these regions as well. Given 1) the well-defined structure and longevity of the TPV and cold pool involved in the January 1982 CAO, as will be shown, and 2) the extremely cold air and significant socioeconomic impacts associated with the January 1982 CAO, this CAO will be examined in detail.

4.1.2 TPV and Cold Pool Track and Intensity

Figure 4.1 shows the tracks of the TPV and cold pool of interest for the January 1982 CAO. The TPV forms over Baffin Bay at 0600 UTC 15 December 1981. The TPV moves over

Greenland between 17 and 21 December 1981 and then spends much of its lifetime meandering over northern and central Canada during late December 1981 and early January 1982. The TPV moves equatorward into the U.S. and then eastward across the U.S. during 8–11 January 1982, before moving quickly northeastward toward southern Greenland through 12 January 1982. The TPV undergoes lysis off the southeast coast of Greenland at 0000 UTC 13 January 1982. Overall, the TPV has a lifetime of ~29 days. The cold pool forms over the northern coast of Greenland at 1800 UTC 20 December 1981, several days after the TPV forms (Fig. 4.1). The cold pool has a similar track to the TPV throughout much of its lifetime, spending much of its lifetime meandering over northern and central Canada before moving equatorward into the U.S. between 8 and 10 January 1982. However, unlike the TPV, the cold pool meanders over eastern North America during 11–12 January 1982 before finally moving off the east coast of North America. The cold pool undergoes lysis at 1800 UTC 13 January 1982 east of Newfoundland. Overall, the cold pool has a lifetime of ~24 days. The large spatial overlap and temporal coincidence of the TPV and cold pool tracks suggest that the TPV and cold pool are dynamically linked. Furthermore, the movement of the TPV and cold pool over and near the U.S. during 9–11 January 1982, when the January 1982 CAO is occurring, suggests that these features play an important role in the development of the January 1982 CAO.

To understand the evolution of the intensity of the TPV and cold pool during their lifetimes, Fig. 4.2 shows a time series of the minimum DT potential temperature of the TPV and the minimum 1000–500-hPa thickness of the cold pool. In general, ignoring rapid fluctuations of TPV intensity as evident by large spikes in the time series of the minimum DT potential temperature of the TPV (e.g., during 29 December 1981), which may be numerical artifacts, the TPV gradually intensifies during late December 1981, with the minimum DT potential

temperature of the TPV decreasing from ~290 K on 15 December 1981 to close to 260 K on 28 December 1981. During early January 1982, the minimum DT potential temperature of the TPV is low (~255 K) and decreases to ~249 K on 9 January 1982. However, during 10–12 January 1982, the TPV rapidly weakens, with the minimum DT potential temperature of the TPV increasing to ~284 K by 13 January 1982. The overall gradual intensification of the TPV suggests that longwave radiative cooling likely contributes importantly to the intensification of the TPV, especially given that Cavallo and Hakim (2009, 2010, 2012, 2013) have shown that longwave radiative cooling can play a critical role in the intensification of TPVs. The weakening of the TPV during 10–12 January 1982 may be related to latent heat release associated with an extratropical cyclone (EC) that undergoes rapid cyclogenesis off the east coast of North America during 10–11 January 1982, which will be shown in section 4.1.3. Latent heat release may contribute to weakening of the TPV by leading to PV destruction aloft that may erode the TPV.

About two days after the cold pool forms, similarly as the TPV, the cold pool gradually intensifies during late December 1981 and early January 1982, with the minimum 1000–500-hPa thickness of the cold pool decreasing from ~488 dam on 20 December 1981 to ~463 dam on 7 January 1982 (Fig. 4.2). Between 7 and 9 January 1982, the cold pool slowly weakens as it moves toward southern Canada and into the U.S., but similarly as the TPV, rapidly weakens during 10–13 January 1982. Longwave radiative cooling (e.g., Curry 1983; Emanuel 2008) may contribute to the gradual intensification of the cold pool during late December 1981 and early January 1982. Some of the weakening of the cold pool during 9–12 January 1982 may be related to sensible heat fluxes from the surface as the cold pool moves over the relatively warmer land of the U.S compared to that of Canada, especially considering that there is a thinner snowpack over portions of the eastern U.S. the cold pool moves over compared to over Canada during this

period (not shown). Sensible heat fluxes from the relatively warm waters of the North Atlantic may contribute to the weakening of the cold pool on 13 January 1982. Latent heat release and warm air advection associated with the aforementioned EC may also contribute to the weakening of the cold pool during 10–13 January 1982. Latent heat release may contribute to weakening the cold pool by warming the upper portion of the cold pool in the 1000–500-hPa layer. The similar patterns in intensity changes for the TPV and cold pool also suggest that the TPV and cold pool may be dynamically linked.

4.1.3 Synoptic Evolution of TPV, Cold Pool, and CAO

Ridge amplification over the eastern North Pacific and western North America likely plays an important role in the equatorward transport of the TPV and cold pool. At 0000 UTC 5 January 1982, an EC is intensifying over the central North Pacific in the left exit region of the North Pacific jet stream, downstream of a short-wave trough (Figs. 4.3a,b). Afterward, through 0000 UTC 8 January 1982, the EC moves northeastward toward the Gulf of Alaska and the aforementioned trough over the central North Pacific moves eastward and becomes negatively tilted, with a corridor of precipitable water values in excess of 25 mm becoming established from the subtropics poleward toward the Gulf of Alaska (Figs. 4.3c–h). Warm air advection, as implied by the nearly perpendicular orientation of the SLP contours to the 1000–500-hPa thickness contours downstream of the EC during 5–8 January 1982 (Figs. 4.3b,d,f,h), likely supports the ridge amplification that occurs downstream of the EC over the eastern North Pacific and into western North America (Figs. 4.3a,c,e,g). In addition, Figs. 4.4a,b show that at 0000 UTC 6 January and 0000 UTC 7 January 1982, associated with the EC over the central North

Pacific and with the corridor of precipitable water values in excess of 25 mm is a widespread region of midlevel ascent. The concomitant diabatically driven upper-tropospheric divergent outflow and associated negative PV advection by the irrotational wind shown in Figs. 4.4a,b likely also support the aforementioned ridge amplification. Furthermore, as the ridge comes into closer proximity with the TPV and associated cold pool located over western North America, the thermal gradient over the Gulf of Alaska and southwestern Canada strengthens, supporting the development and intensification of a jet streak over this region during 7–8 January 1982 (Figs. 4.3e–h).

Between 0000 UTC 8 January and 0000 UTC 9 January 1982, as the ridge continues to build eastward and comes into closer proximity with the TPV and associated cold pool, the jet streak between the ridge and TPV strengthens as TPV–jet interaction begins to occur (Figs. 4.5a–d). Between 0000 UTC 9 January and 0000 UTC 10 January 1982, as TPV–jet interaction occurs, the TPV and associated cold pool move equatorward into the U.S., and a strong surface anticyclone in the left entrance region of the jet streak rapidly strengthens and expands equatorward over western North America into the central U.S., just east of the Rocky Mountains (Figs. 4.5c–f). Strong cold air advection over the Great Plains, as suggested in Fig. 4.5f, along with an expected terrain-tied northerly component of low-level motion on the eastern side of the Rocky Mountains (e.g., Colle and Mass 1995) likely help allow the cold air from the cold pool associated with the TPV to spread far away from the core of the cold pool. Thus, the cold pool associated with the TPV has a geographically widespread impact. The development of the strong surface anticyclone over western North America in association with the CAO has been similarly shown in past studies, including Boyle and Bosart (1983), Colucci and Davenport (1987), Konrad and Colucci (1989), Colle and Mass (1995), and Walsh et al. (2001).

By 0000 UTC 11 January 1982, the TPV and cold pool have moved eastward toward the U.S east coast, and cold air associated with the cold pool has overspread the entire eastern U.S. (Figs. 4.5g,h). As discussed in section 4.1.2, the TPV and cold pool rapidly weaken during 10–12 January 1982. Between 0000 UTC 10 January and 0000 UTC 11 January 1982, TPV–jet interaction occurs, with the TPV located on the cyclonic shear side of the jet streak. As TPV–jet interaction occurs, the TPV becomes deformed as suggested by the TPV becoming more anisotropic (Figs. 4.5e,g). Horizontal shear on the cyclonic shear side of the jet streak in combination with confluent flow in the entrance region of the jet streak and diffluent flow in the exit region of the jet streak, as suggested in Figs. 4.5e,g, may contribute to the deformation of the TPV, which may contribute to the weakening of the TPV. In addition, rapid cyclogenesis of an EC occurs off the east coast of North America, in the left exit region of the jet streak between 0000 UTC 10 January and 0000 UTC 11 January 1982 (Figs. 4.5f,h). Latent heat release associated with widespread ascent in the vicinity of the EC during 0000 UTC 10 January and 0000 UTC 11 January 1982 (Figs. 4.6a,b) may also contribute to the weakening of the TPV and cold pool. As discussed in section 4.1.2, latent heat release may lead to the destruction of upper-level PV, which may weaken the TPV, and latent heat release may warm the upper portion of the cold pool, which may weaken the cold pool. In addition, warm air advection that is implied over Labrador and eastern Quebec at 0000 UTC 11 January 1982 (Fig. 4.5h) may further contribute to the weakening of the cold pool.

The fact that the TPV and cold pool move in tandem into the U.S. during the time of the January 1982 CAO suggests that the TPV and cold pool are dynamically linked, as discussed at the end of section 4.1.2, and that the TPV and cold pool play an important role in the development of the January 1982 CAO. In section 4.1.4, the evolution of the three-dimensional

structure of the TPV and cold pool will be examined to gain more insight on how these features evolve together over time. In addition, the relationship between TPV–jet interaction and the development of the strong surface anticyclone important for the evolution of the CAO will be explored further in section 4.1.5.

4.1.4 Three-dimensional Structure of TPV and Cold Pool

Figure 4.7 shows a meridional cross section (AA') transecting the TPV early in its life cycle at 1200 UTC 16 December 1981, when the TPV is relatively weak and located over Baffin Bay, and when the cold pool has not yet formed. Using the position of the 2-PVU contour in the cross section as a proxy for the position of the DT, the TPV extends downward to ~450 hPa, which is not too far beneath the position of the background DT (Fig. 4.7a). The TPV is a mesoscale feature embedded in a broad region of lowered DT (Fig. 4.7a) and relatively low DT potential temperature air (Fig. 4.7b). Although the cold pool has not yet formed, there is a broad region of cold air characterized by 1000–500-hPa thickness values below 500 dam where the TPV and broad region of relatively low DT potential temperature air is located (Figs. 4.7b,c), suggesting that the TPV is still associated with cold air beneath it throughout the troposphere. Also, the cross section shows an upward bowing of isentropes beneath the TPV, with potential temperature values less than 268 K in the lower troposphere beneath the TPV (Fig. 4.7a).

As shown in Fig. 4.2, the TPV strengthens throughout late December 1981 and is intense during early January 1982. Also, the cold pool intensifies during late December 1981 and early January 1982. Figure 4.8 shows a meridional cross section (BB') transecting the TPV and cold pool at 1200 UTC 2 January 1982. Compared to early in its life cycle, at 1200 UTC 16

December 1981 (Fig. 4.7a), the cross section in Fig. 4.8a at 1200 UTC 2 January 1982 shows that the TPV has become a much better defined, larger, and deeper feature, with the TPV now extending downward to ~650 hPa. Furthermore, the TPV (Fig. 4.8b) and cold pool (Fig. 4.8c) are intense, isotropic, and vertically aligned at 1200 UTC 2 January 1982. The substantial upward bowing of the isentropes within and beneath the TPV throughout the depth of the troposphere (Fig. 4.8a) is indicative of the well-defined cold pool (Fig. 4.8c) that is collocated with the TPV (Fig. 4.8b) and the tropospheric-deep influence of the TPV. Also, potential temperature values are less than 240 K near the surface beneath the TPV (Fig. 4.8a), indicative of the very cold air associated with the cold pool. As the TPV has become better defined and deeper, there has become a more pronounced upward bowing of the isentropes beneath the TPV and concomitantly a better defined and intense cold pool, illustrating that the TPV and cold pool are likely dynamically linked. It is also evident in the cross section that near the surface, isentropes spread outward, far away from the center of the TPV and cold pool (Fig. 4.8a), indicative of surface-based Arctic air spreading far from the center of the TPV and cold pool. In fact, especially to the south and north of the TPV, there is a very strong near-surface vertical potential temperature gradient, with near-surface PV values in excess of 4 PVU north of the TPV and between 2 and 4 PVU south of the TPV (Fig. 4.8a). As shown by Emanuel (2008), Arctic air can be characterized by relatively high values of PV. The strong near-surface vertical potential temperature gradient also suggests that a steep temperature inversion is in place, which is likely related to longwave radiative cooling (e.g., Curry 1983).

Figure 4.9 shows a meridional cross section (CC') transecting the TPV and cold pool at 0000 UTC 10 January 1982, when both features have moved into the northern U.S. and are contributing to CAO development. Compared to at 1200 UTC 2 January 1982 (Fig. 4.8a), the

TPV is even deeper at 0000 UTC 10 January 1982, now extending downward to ~750 hPa (Fig. 4.9a). The TPV is interacting with a jet streak at this time (Fig. 4.9b) and a PV wall associated with a large horizontal PV gradient is evident throughout much of the troposphere between the TPV and warm air to its south, coincident with the jet streak (Fig. 4.9a). Furthermore, the cross section illustrates a classic tropopause fold structure (e.g., Reed and Danielsen 1959; Danielsen 1968; Keyser and Shapiro 1986) associated with the TPV as the TPV interacts with the jet streak (Fig. 4.9a). There continues to be a very notable upward bowing of isentropes throughout the troposphere within and beneath the TPV (Fig. 4.9a), illustrative of the cold pool (Fig. 4.9c) associated with the TPV (Fig. 4.9b). The surface-based Arctic air continues to spread far away from the center of the TPV and cold pool, with the leading edge of the Arctic air associated with the Arctic front located south of 40°N where there is a strong surface horizontal potential temperature gradient (Fig. 4.9a). Furthermore, within the Arctic air, the boundary layer appears well mixed given the nearly vertical orientation of the isentropes within the boundary layer. A well-mixed boundary layer was also shown by Shapiro et al. (1987; Fig. 1.7 in this thesis) in a cross section transecting the January 1985 "polar vortex" feature (or TPV as will be discussed in section 4.2), and they suggest that this well-mixed boundary layer may result from diabatic heating induced by the flow of Arctic air over the relatively warm land surface. Overall, the cross sections, in particular those in Figs. 4.8a and 4.9a, illustrate that the influence of the TPV extends throughout the depth of the troposphere and over a widespread geographical area, and also illustrate that the TPV and associated cold pool plays a crucial role in CAO development.

4.1.5 Q-vector Diagnosis

The concomitant occurrence of the interaction of the TPV with a jet streak over western North America and the rapid strengthening and southeastward expansion of the strong surface anticyclone over western North America in the left entrance region of the jet streak during 8–10 January 1982 (Figs. 4.5a–f) suggests that TPV–jet interaction may play an important role in the rapid strengthening and expansion of the strong surface anticyclone. Figure 4.10 shows plots of 600–400-hPa wind speed, as well as $\mathbf{Q}_n$ and $\mathbf{Q}_s$ and their associated forcings for vertical motion from 1200 UTC 8 January to 0000 UTC 10 January 1982. At 1200 UTC 8 January 1982, between the ridge and the TPV, and in the left entrance region of a broad jet streak over western North America, there is a region of divergence of $\mathbf{Q}_n$ and $\mathbf{Q}_n$ forcing for descent collocated with and to the south and east of the ~1047 hPa surface anticyclone (Figs. 4.10a,b). The orientation of the Q_n vectors from cold to warm air suggests that the geostrophic flow may be contributing to upper-level frontogenesis, which may support a strengthening of the jet streak. In addition, there is a small region of $\mathbf{Q}_s$ forcing for descent over northern Alberta, to the south and east of the surface anticyclone (Fig. 4.10c). The $\mathbf{Q}_n$ and $\mathbf{Q}_s$ forcing for descent over and to the south and east of the surface anticyclone may provide forcing for anticyclogenesis, suggesting that the surface anticyclone may strengthen and expand southeastward.

By 0000 UTC 9 January 1982, the maximum SLP of the surface anticyclone remains ~1047 hPa, but the surface anticyclone has expanded southeastward over the previous 12 h (compare Figs. 4.10a,d). In addition, the jet streak has intensified, likely related to TPV–jet interaction beginning to occur as the TPV has come into closer proximity with the jet streak (compare Figs. 4.10a,d). Concomitantly, the magnitude of $\mathbf{Q}_n$ and $\mathbf{Q}_n$ forcing for descent have

increased in the left entrance region of the jet streak, over and to the south and east of the surface anticyclone (compare Figs. 4.10d,e to Figs. 4.10a,b). The orientation of the Q_n vectors from cold to warm air in the entrance region of the jet streak (Figs. 4.10d,e) continues to suggest that the geostrophic flow may be contributing to upper-level frontogenesis. Furthermore, by comparing Figs. 4.10c,f, the region of $\mathbf{Q}_s$ forcing for descent has increased in size and magnitude between 1200 UTC 8 January and 0000 UTC 9 January 1982. At 0000 UTC 9 January 1982, the region of $\mathbf{Q}_s$ forcing for descent is located upstream of the TPV, in the left entrance region of the jet streak, over and to the south and east of the surface anticyclone (Figs. 4.10d,f). This region of $\mathbf{Q}_s$ forcing for descent may be related a short-wave trough over northern Saskatchewan that is associated with the TPV (Fig. 4.10f). The location of the maximum of $\mathbf{Q}_s$ forcing for descent upstream of the short-wave trough is anticipated from Sanders and Hoskins (1990). The position of the regions of $\mathbf{Q}_n$ and $\mathbf{Q}_s$ forcing for descent over and to the south and east of the surface anticyclone suggests that the surface anticyclone may strengthen and build southeastward.

Between 0000 UTC and 1200 UTC 9 January 1982, the surface anticyclone rapidly strengthens from ~1047 hPa to ~1054 hPa**,** or by ~7 hPa in 12 h, and builds southward and eastward in the left entrance region of the jet streak, which continues to intensify as TPV–jet interaction continues to occur (compare Figs. 4.10d,g). Furthermore, the magnitude of the 600–400-hPa potential temperature gradient associated with the jet streak has strengthened during the same time period (not shown), indicating that upper-level frontogenesis may be occurring as previously suggested. Also, accompanying the intensification of the jet streak is increased confluence in the entrance region of the jet streak as indicated by an increase in the along-stream variation in the 600–400-hPa wind speed in the entrance region of the jet streak (compare Figs. 4.10d,g). The increased confluence in the entrance region of the jet streak suggests that the

thermally direct ageostrophic circulation in the entrance region of the jet streak may have strengthened, which would support increased forcing for descent in the left entrance region of the jet streak. Concomitantly, the magnitude of $\mathbf{Q}_n$ and $\mathbf{Q}_n$ forcing for descent has increased upstream of the TPV, in the left entrance region of the jet streak, over and to the south and east of the surface anticyclone (compare Figs. 4.10g,h to Figs. 4.10d,e). In addition, as the short-wave trough associated with the TPV has sharpened, there has been a concomitant increase in $\mathbf{Q}_s$ and $\mathbf{Q}_s$ forcing for decent upstream of the TPV, in the left entrance region of the jet streak, over and to the south and east of the surface anticyclone (compare Figs. 4.10g,i to Figs. 4.10d,f). The location of the maximum of both $\mathbf{Q}_n$ and $\mathbf{Q}_s$ forcing over and to the south and east of the surface anticyclone (Figs. 4.10h,i) suggests that the surface anticyclone may strengthen further and build southeastward.

As anticipated, between 1200 UTC 9 January and 0000 UTC 10 January 1982, the surface anticyclone strengthens from ~1054 hPa to ~1060 hPa, or by ~6 hPa in 12 h, and builds southeastward in the left entrance region of the jet streak, which strengthens further as TPV–jet interaction continues (compare Figs. 4.10g,j). There continues to be similar patterns of $\mathbf{Q}_n$ and $\mathbf{Q}_s$ and their associated forcings for descent at 0000 UTC 10 January 1982 as 12 h earlier (compare Figs. 4.10k,l to Figs. 4.10h,i). In general, as the jet streak strengthens during TPV–jet interaction, there is an increase in $\mathbf{Q}_n$ and $\mathbf{Q}_s$ and their associated forcings for descent in the left entrance region of the jet streak. The concomitant rapid strengthening and expansion of the surface anticyclone in the left entrance region of the jet streak, corresponding to the region of $\mathbf{Q}_n$ and $\mathbf{Q}_s$ forcing for descent, suggests that TPV–jet interaction may play an important role in the rapid strengthening and expansion of the surface anticyclone. Given the important role that this surface

anticyclone plays in the development of the January 1982 CAO, TPV–jet interaction may play an important role in CAO development.

4.2 19–24 January 1985 CAO

4.2.1 Case Overview

During 19–24 January 1985, a CAO impacted a widespread area of central and eastern North America, leading to significant socioeconomic impacts. According to NOAA NCEI, extremely cold air associated with the 19–24 January 1985 CAO (hereafter referred to as the January 1985 CAO) and winter storms over the U.S. contributed to an estimated cost of 1.9 billion dollars, after 2017 consumer price index adjustment, and contributed to 150 deaths (https://www.ncdc.noaa.gov/billions/). Also, according to NOAA NCEI, there was an additional cost of 2.8 billion dollars, after 2017 consumer price index adjustment, due to a severe freeze associated with the January 1985 CAO over Florida that led to citrus crop damages. Furthermore, minimum surface temperatures below −17.8°C (0°F) were observed over a widespread area of the central and eastern U.S. (Shapiro et al. 1987). The January 1985 CAO qualifies as a CAO for the Northeast, Central, South, and Southeast regions (see Fig. 2.1 for map of regions) and a CAO that is linked to a cold pool associated with a TPV for all of these regions as well. Given the significant socioeconomic impacts and extremely cold air associated with the January 1985 CAO, this CAO will be examined in detail. In addition, examination of the January 1985 CAO will serve to complement and extend the work of Shapiro et al. (1987) by illustrating that the "polar vortex" feature shown to play an important role in the development of the January 1985 CAO corresponds to a TPV.

4.2.2 TPV and Cold Pool Track and Intensity

Figure 4.11 shows the tracks of the cold pool and TPV of interest for the January 1985 CAO. The cold pool is identified to form over the northeastern coast of Baffin Island at 1800 UTC 11 January 1985. The cold pool meanders for several days over northern Canada before being transported equatorward from northern Canada into the U.S. during 17–20 January 1985. The cold pool then moves northeastward toward Labrador during 21–22 January 1985 and meanders over and near Labrador during 22–27 January 1985, before undergoing lysis over Quebec at 0600 UTC 28 January 1985. In total, the cold pool has a lifetime of ~17 days. The TPV forms at 1800 UTC 16 January 1985 over north central Canada, several days after the cold pool is identified to form (Fig. 4.11). The TPV moves generally westward over the next day before being quickly transported equatorward into southern Canada and then into the central U.S. between 18 and 20 January 1985 together with the cold pool. Similarly to the cold pool, the TPV is quickly transported northeastward toward Labrador during 21–22 January 1985, and then meanders over and near Labrador during 22–27 January 1985. Unlike the cold pool, the TPV then moves over the northwestern North Atlantic, where it meanders for ~5 days before undergoing lysis at 1200 UTC 2 February 1985. In total, the TPV has a lifetime of 17 days. In general, the large spatial overlap and temporal coincidence of the TPV and cold pool tracks over North America suggest that the these features are dynamically linked. Furthermore, the movement of the TPV and cold pool over and near the U.S. during 19–21 January 1985, when the January 1985 CAO is occurring, suggests that these features play an important role in the development of the January 1985 CAO.

Figure 4.12 shows a time series of the minimum DT potential temperature of the TPV and the minimum 1000–500-hPa thickness of the cold pool. At the beginning of its life cycle, the cold pool is characterized by a 1000–500-hPa thickness value of ~478 dam. Although the cold pool is objectively identified to form on 11 January 1985, subjectively, the cold pool appears to form several days earlier, when it was weaker (not shown). There may have been separate 1000–500-hPa thickness minima embedded within the cold pool that may have contributed to multiple cold pool tracks. In general, the cold pool strengthens during 11–19 January 1985, with the cold pool reaching a minimum 1000–500-hPa thickness value of ~468 dam on 19 January 1985 (Fig. 4.12) over southern Canada (Fig. 4.11). The cold pool then weakens as it moves across the U.S. and then northeastward toward Labrador during 19–22 January 1985. The cold pool then generally intensifies as is meanders over and near Labrador until 27 January 1985, before weakening again. When the TPV forms, it is characterized by a minimum DT potential temperature value of ~269 K. As will be shown in section 4.2.3, the TPV forms from a preexisting broad area of relative low DT potential temperature air. In general, the TPV intensifies until 20 January 1985 as the cold pool intensifies, though the TPV reaches a minimum DT potential temperature value of ~259 K on 20 January 1985, when the cold pool is already weakening. Afterward, during 21–29 January 1985, the patterns of intensity change of the TPV are similar to that of the cold pool.

The periods of strengthening of the cold pool and TPV may be related to longwave radiative cooling, as in the January 1982 CAO case. Weakening of the cold pool and TPV during 21–22 January 1985 may be related to latent heat release in association with a strong EC that rapidly intensifies during 21–22 January 1985 over the east coast of North America, as will be discussed in section 4.2.3. As in the January 1982 CAO case, latent heat release may contribute

to weakening of the TPV by leading to PV destruction aloft that may erode the TPV, and latent heat release may contribute to weakening of the cold pool by warming the upper portion of the cold pool in the 1000–500-hPa layer. Also, weakening of the cold pool as it moves across the U.S. during 19–22 January 1985 may be related to sensible heat fluxes from the surface as the cold pool moves over the relatively warmer land of the U.S compared to that of Canada, considering that there is a thinner snowpack over the U.S. compared to over Canada during this period (not shown).

4.2.3 Synoptic Evolution of TPV, Cold Pool, and CAO

The equatorward transport of the TPV and cold pool is likely tied to flow amplification over the North Pacific and North Atlantic. Poleward fluxes of warm, moist air associated with a strengthening EC in the left exit region of a strong North Pacific jet stream over the central North Pacific and with an EC moving poleward off the coast of Labrador likely support ridge amplification over the eastern North Pacific and over Greenland, respectively, between 0000 UTC 14 January and 0000 UTC 15 January 1985 (Figs. 4.13a–d). Meanwhile, during this same time period, the cold pool over northeastern North America moves southward on the western side of the ridge over Greenland. Collocated with the cold pool is a broad region of relatively low DT potential temperature air that will evolve into the TPV. The EC over the North Pacific moves northeastward to the Gulf of Alaska between 0000 UTC 15 January and 0000 UTC 17 January 1985, while the ridge over the eastern North Pacific concomitantly amplifies into western North America (Figs. 4.13c–h). During the same time period, a new EC rapidly develops and then occludes as it moves from the northeastern U.S. to southeastern Canada, contributing to

ridge amplification over the northwestern North Atlantic (Figs. 4.13c–h). Both ECs are associated with a narrow corridor of relatively high precipitable water values extending from the subtropics toward the high latitudes (e.g., Fig. 4.13f). Figures 4.14a,b show that at 0000 UTC 15 January and 0000 UTC 16 January 1985, associated with the aforementioned ECs and narrow corridors of relatively high precipitable water values are widespread regions of midlevel ascent. The concomitant diabatically driven upper-tropospheric divergent outflow and associated negative PV advection by the irrotational wind shown in Figs. 4.14a,b likely also contribute to the ridge amplification over western North America and the northwestern North Atlantic. Also, at 0000 UTC 17 January 1985, the broad region of relatively low DT potential temperature air has consolidated into a single TPV that is now tracked (Fig. 4.13g). Although the consolidation of the broad region of relatively low DT potential temperature air into the TPV has not been examined closely, it may be related to the close approach and merger of separate midlevel vorticity maxima (not shown).

The combination of ridging over western North America and over Greenland and Baffin Bay force the TPV and cold pool to move equatorward over Canada between 0000 UTC 18 January and 0000 UTC 19 January 1985 (Figs. 4.15a–d). A jet streak strengthens between the TPV and the ridge over western North America as the TPV moves equatorward and interacts with the jet streak. In addition, a strong surface anticyclone over the Arctic and extending southward into northern Canada strengthens and builds southeastward over western Canada in the left entrance region of the jet streak. As the TPV and cold pool move equatorward into the northern U.S. through 0000 UTC 20 January 1985, the strong surface anticyclone strengthens in the left entrance region of the jet streak and rapidly builds southeastward into the central U.S (Figs. 4.15e,f). Similar to the January 1982 CAO case, strong cold air advection over the central

U.S., as suggested in Fig. 4.15f, along with an expected terrain-tied northerly component of low-level motion on the eastern side of the Rocky Mountains (e.g., Colle and Mass 1995), likely help allow the cold air from the cold pool associated with the TPV to spread far away from the core of the cold pool. Thus, the cold pool associated with the TPV has a geographically widespread impact.

As the TPV and cold pool move eastward over the U.S. through 0000 UTC 21 January 1985 (Figs. 4.15g,h), the cold air associated with the cold pool overspreads the entire eastern U.S. Also, as the TPV interacts with a jet streak to its south and east between 0000 UTC 20 January and 0000 UTC 21 January 1985, the TPV becomes deformed and weakens (Figs. 4.15e,g), suggesting that the deformation of the TPV may contribute to the weakening of the TPV. In addition, an EC forms over southeastern Canada at 0000 UTC 21 January 1985, in the left exit region of the aforementioned jet streak (Fig. 4.15h), and this EC rapidly deepens over the next day (not shown). Latent heat release associated with widespread ascent found in the vicinity of the EC at 0000 UTC 21 January and 0000 UTC 22 January 1985 (Figs. 4.16a,b) may contribute to the weakening of the TPV and cold pool during 21–22 January 1985 shown in Fig. 4.12. As discussed at the end of section 4.2.2, latent heat release may lead to the destruction of upper-level PV, which may contribute to the weakening of the TPV, and latent heat release may warm the upper portion of the cold pool, which may contribute to the weakening of the cold pool.

As in the January 1982 CAO case, the fact that the TPV and cold pool in the January 1985 CAO case move in tandem into the U.S. during the time of the January 1985 CAO suggests that the TPV and cold pool are dynamically linked and that the TPV and cold pool play an important role in the development of the January 1985 CAO. To get a better sense of the

evolution of the three-dimensional structure of the TPV and cold pool in this case, cross sections of these features will be examined in section 4.2.4. In addition, the relationship between TPV–jet interaction and the development of the strong surface anticyclone important for the evolution of the January 1985 CAO will be explored further in section 4.2.5.

4.2.4 Three-dimensional Structure of TPV and Cold Pool

Figure 4.17 shows a meridional cross section (DD') transecting the cold pool early in its life cycle at 0000 UTC 13 January 1985, prior to the formation of the TPV. At this time, the cross section shows a broad region of depressed DT extending downward below 400 hPa, with embedded mesoscale undulations of the DT (Fig. 4.17a). This broad region of depressed DT corresponds to a broad region of relatively low DT potential temperature air with embedded DT potential temperature minima (Fig. 4.17b) that is collocated with the broad cold pool (Fig. 4.17c). There is a broad region of upward bowing of isentropes in the cross section beneath the broad region of lowered DT, indicative of the broad cold pool, with potential temperature values near the surface as low as 240 K illustrating the very cold air associated with the cold pool (Fig. 4.17a).

Figure 4.18 shows a meridional cross section (EE') transecting the TPV and cold pool at 0000 UTC 17 January 1985, shortly after the TPV has been first identified. The region of lowered DT in the cross section in Fig. 4.18a corresponding to the TPV (Fig. 4.18b) at 0000 UTC 17 January 1985 is more focused and extends farther downward compared to the region of lowered DT in the cross section in Fig. 4.17a corresponding to the broad region of relatively low DT potential temperature air (Fig. 4.17b) at 0000 UTC 13 January 1985. There is also a more

pronounced upward bowing of the isentropes beneath the TPV in the cross section in Fig. 4.18a at 0000 UTC 17 January 1985 compared to beneath the broad region of relatively low DT potential temperature air in the cross section in Fig. 4.17a at 0000 UTC 13 January 1985. The more pronounced upward bowing of isentropes at 0000 UTC 17 January 1985 compared to at 0000 UTC 13 January 1985 corresponds to a more intense cold pool at 0000 UTC 17 January 1985 (Fig. 4.18c) compared to at 0000 UTC 13 January 1985 (Fig. 4.17c).

Figure 4.19 shows a meridional cross section (FF') transecting the TPV and cold pool at 0000 UTC 20 January 1985, when both features have moved into the northern U.S. and are contributing to CAO development. The TPV has deepened since 0000 UTC 17 January 1985 (compare Figs. 4.19a and 4.18a), extending downward to ~750 hPa at 0000 UTC 20 January 1985 (Fig. 4.19a), as the TPV has intensified (compare Figs. 4.19b and 4.18b). The robust upward bowing of the isentropes within and beneath the TPV (Fig. 4.19a) illustrates the impressive cold pool (Fig. 4.19c) collocated with the TPV (Fig. 4.19b). In addition, the TPV is interacting with a jet streak to its south (Fig. 4.19b), and a PV wall similar to that in the cross section in Fig. 4.9a for the January 1982 CAO case extends throughout much of the troposphere between the TPV and warm air to the south, coincident with the jet streak (Fig. 4.19a). Furthermore, the cross section shows a classic tropopause fold structure (e.g., Reed and Danielsen 1959; Danielsen 1968; Keyser and Shapiro 1986) associated with the TPV similar to that in the cross section in Fig. 4.9a for the January 1982 CAO case as the TPV interacts with the jet streak (Fig. 4.19a). Near the surface, the isentropes spread horizontally outward, far away from the core of the TPV and cold pool, with the Arctic front associated with the leading edge of Arctic air located south of 37.5°N where there is a strong surface horizontal potential temperature gradient (Fig. 4.19a). As discussed by Shapiro et al. (1987) for a cross section

transecting the same TPV and cold pool (Fig. 1.7 in this thesis), the cross section in Fig. 4.19a shows that within the Arctic air, the boundary layer appears well mixed, which, as suggested by Shapiro et al. (1987), may result from diabatic heating induced by the flow of Arctic air over the relatively warm land surface. Overall, the cross section in Fig. 4.19a illustrates that the TPV has a tropospheric-deep influence, impacts a widespread geographical area, and plays an important role in the development of the January 1985 CAO.

4.2.5 Q-vector Diagnosis

The concomitant occurrence of the interaction of the TPV with a jet streak over western North America and the strengthening and southeastward expansion of the strong surface anticyclone over western North America in the left entrance region of the jet streak during 18–20 January 1985 (Figs. 4.15a–f) suggests that TPV–jet interaction may play an important role in the strengthening and expansion of the strong surface anticyclone. Figure 4.20 shows plots of 600–400-hPa wind speed, as well as $\mathbf{Q}_n$ and $\mathbf{Q}_s$ and their associated forcings for vertical motion from 1200 UTC 18 January to 0000 UTC 20 January 1985. At 1200 UTC 18 January 1985, the jet streak is located between the ridge and TPV over western North America, with a region of $\mathbf{Q}_n$ forcing for descent in the left entrance region of the jet streak, over and to the southeast of the surface anticyclone (Figs. 4.20a,b). Over the same region, Q_s vectors are small in magnitude and there is not an organized region of $\mathbf{Q}_s$ forcing for descent (Fig. 4.20c). The positioning of the region of $\mathbf{Q}_n$ forcing for descent over and to the southeast of the surface anticyclone suggests that the surface anticyclone may strengthen and expand southeastward. In addition, the orientation of

the Q_n vectors from cold to warm air in the entrance region of the jet streak (Figs. 4.20a,b) suggests that the geostrophic flow may be contributing to upper-level frontogenesis.

By 0000 UTC 19 January 1985, while the surface anticyclone has not strengthened, it has expanded southeastward over western Canada in the left entrance region of the jet streak since 1200 UTC 18 January 1985 (compare Figs. 4.20a,d). Also, the jet streak over western North America has intensified, likely due to TPV–jet interaction (compare Figs. 4.20a,d). Furthermore, the magnitude of the 600–400-hPa potential temperature gradient associated with the jet streak has strengthened between 1200 UTC 18 January and 0000 UTC 19 January 1985 (not shown), indicating that upper-level frontogenesis may be occurring as previously suggested. In addition, as the jet streak has strengthened, confluence in the entrance region of the jet streak has increased as indicated by the increase in the along-stream variation in the 600–400-hPa wind speed in the entrance region of the jet streak (compare Figs. 4.20a,d). The increased confluence in the entrance region of the jet streak suggests that the thermally direct ageostrophic circulation in the entrance region of the jet streak may have strengthened, which would support increased forcing for descent in the left entrance region of the jet streak. As anticipated, in the left entrance region of the jet streak, the magnitude of $\mathbf{Q}_n$ has increased between 1200 UTC 18 January and 0000 UTC 19 January 1985, and although the magnitude of $\mathbf{Q}_n$ forcing for descent has not increased, the region of $\mathbf{Q}_n$ forcing for descent has expanded in areal coverage (compare Figs. 4.20d,e to Figs. 4.20a,b). The region of $\mathbf{Q}_n$ forcing for descent in the left entrance region of the jet streak, over and to the south and east of the surface anticyclone, at 0000 UTC 19 January 1985 suggests that the surface anticyclone may strengthen and expand southeastward. Also, there is now a small, but relatively and weak and disorganized region of $\mathbf{Q}_s$ forcing for descent positioned upstream of the TPV and to the south and east of the surface anticyclone (Fig. 4.20f),

which would at least suggest that the surface anticyclone may build southeastward. This region of $\mathbf{Q}_s$ forcing for descent may be related to a subtle short-wave trough over southern Manitoba associated with the TPV (Fig. 4.20f). The location of the maximum of $\mathbf{Q}_s$ forcing for descent upstream of the short-wave trough is anticipated from Sanders and Hoskins (1990).

As anticipated, between 0000 UTC and 1200 UTC 19 January 1985, the surface anticyclone strengthens from ~1046 hPa to ~1051 hPa, or by ~5 hPa in 12 h, and expands southeastward, while the jet streak continue to intensify, likely in response to TPV–jet interaction (compare Figs. 4.20d,g). There continues to be a broad region of $\mathbf{Q}_n$ forcing for descent in the left entrance region of the jet streak, just west of the TPV, over and to the southeast of the surface anticyclone (Figs. 4.20g,h), as well as a smaller and weaker area of $\mathbf{Q}_s$ forcing for descent in the left entrance region of the jet streak, over and to the south and east of the surface anticyclone (Figs. 4.20g,i), suggesting that the surface anticyclone may strengthen further and build southeastward. As anticipated, the surface anticyclone strengthens between 1200 UTC 19 January and 0000 UTC 20 January 1985 from ~1051 hPa to ~1054 hPa, or by about 3 hPa in 12 h, and continues to build southeastward as TPV jet–interaction continues (compare Figs. 4.20g,j). There continues to be a similar pattern of $\mathbf{Q}_n$ and $\mathbf{Q}_n$ forcing for descent near the TPV at 0000 UTC 20 January 1985 as 12 h earlier (compare Fig. 4.20k,h). Although $\mathbf{Q}_s$ forcing for descent has increased in magnitude as the short-wave trough associated with the TPV has sharpened between 1200 UTC 19 January and 0000 UTC 20 January 1985 (compare Figs. 4.20i,l), the $\mathbf{Q}_s$ forcing for descent remains weaker in magnitude and smaller in areal coverage compared to that of $\mathbf{Q}_n$ (compare Fig. 4.20l,k). In general, as the jet streak strengthens during TPV–jet interaction, there is an increase in magnitude of $\mathbf{Q}_n$ and an increase in areal coverage of the $\mathbf{Q}_n$ forcing for descent in the left entrance region of the jet streak. The concomitant

strengthening and expansion of the surface anticyclone in the left entrance region of the jet streak, corresponding to the region of $\mathbf{Q}_n$ forcing for descent, suggests that TPV–jet interaction may play an important role in the strengthening and expansion of the surface anticyclone. Given the important role that this surface anticyclone plays in the development of the January 1985 CAO, TPV–jet interaction may play an important role in CAO development.

4.3 Summary

Both the January 1982 CAO and January 1985 CAO are linked to a cold pool associated with a TPV. Ridge amplification, related to ECs and their associated poleward fluxes of warm, moist air from lower to higher latitudes and diabatically driven upper-tropospheric outflow, plays an important role in the equatorward transport of the TPV and cold pool in each case. The large spatial overlap and temporal coincidence of the TPV and cold pool throughout much of their lifetimes in each case suggest that the TPV and cold pool are dynamically linked and demonstrates that the influence of TPVs can extend throughout the depth of the troposphere and over a widespread geographical area. In each case, cross sections show that as the TPV becomes better defined and stronger, the upward bowing of the isentropes within and beneath the TPV becomes more pronounced and the cold pool becomes better defined and stronger, illustrating a dynamical linkage between the TPV and cold pool and demonstrating that the TPV has a tropospheric-deep impact. Also, the cross sections in each case show that near the surface, the cold air from the cold pool associated with the TPV spreads far away from the core of the cold pool, illustrating that the TPV has a geographically widespread impact and plays an important role in CAO development. In addition, the Q-vector analysis in each case suggests that TPV–jet

interaction may play an important role in the strengthening and expansion of the surface anticyclone in the left entrance region of the associated jet streak. The surface anticyclone in turn helps allow cold air from the cold pool associated with the TPV to spread far away from the core of the cold pool in each case, further illustrating that the TPV has a geographically widespread impact and plays an important role in CAO development.

Previous studies have examined cold pools and strong surface anticyclones linked to CAO development (e.g. Boyle and Bosart 1983; Shapiro et al. 1987; Konrad and Colluci 1989; Colle and Mass 1995; Walsh et al. 2001). Additionally, Boyle and Bosart (1983) show that strong surface anticyclones linked to CAO development may move along with a jet streak. The case studies in this chapter complement and expand upon these aforementioned studies by illustrating a dynamical linkage between TPVs and cold pools and by suggesting that TPV–jet interaction may play an important role in the development of strong surface anticyclones. Short-wave troughs and midlevel cyclones discussed as being important to CAO development in previous studies (e.g., Shapiro et al. 1987; Konrad and Colucci 1989) may, in some cases, be related to TPVs, as is the case with the midlevel cyclone or "polar vortex" feature studied by Shapiro et al. (1987) for the January 1985 CAO.

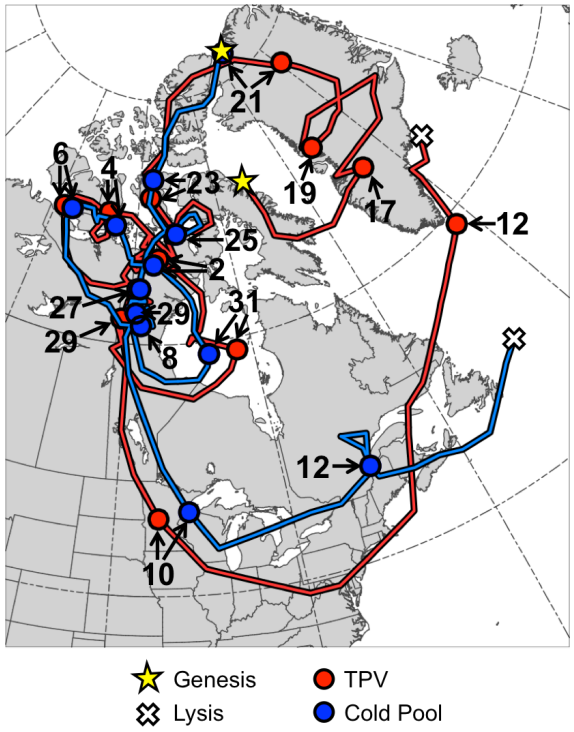

Fig. 4.1. Tracks of TPV (red) from 0600 UTC 15 December 1981 to 0000 UTC 13 January 1982 and cold pool (blue) from 1800 UTC 20 December 1981 to 1800 UTC 13 January 1982 for January 1982 CAO case. Stars denote locations of genesis, crosses denote locations of lysis, and red and blue dots represent 0000 UTC positions of TPV and cold pool, respectively, every 48 h. Numbers pointing toward dots represent dates of the 0000 UTC positions of the TPV and cold pool, such that numbers ≥17 correspond to dates in December 1981 and numbers ≤12 correspond to dates in January 1982.

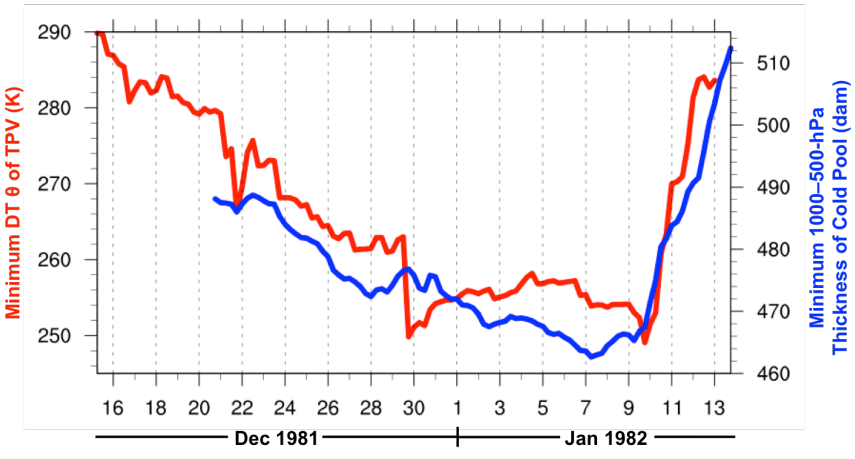

Fig. 4.2. Time series of minimum DT potential temperature (θ) of TPV (K, red) every 6 h from 0600 UTC 15 December 1981 to 0000 UTC 13 January 1982 and minimum 1000–500-hPa thickness of cold pool (dam, blue) every 6 h from 1800 UTC 20 December 1981 to 1800 UTC 13 January 1982 for January 1982 CAO case.

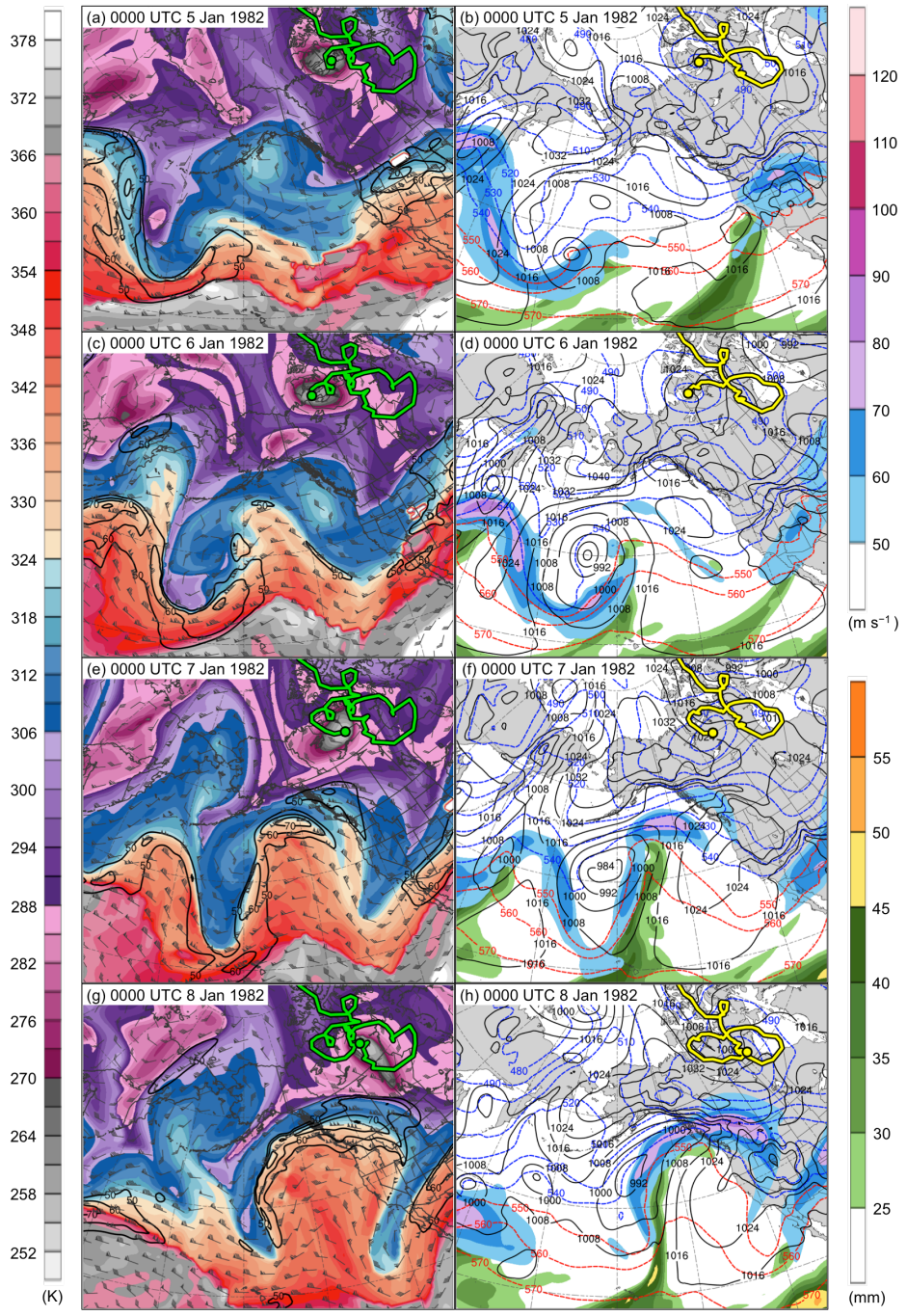

Fig. 4.3. DT (2-PVU surface) potential temperature (K, shaded), wind speed (black contours every 10 m s^{-1}, beginning at 50 m s^{-1}), and wind (m s^{-1}, flags and barbs) at (a) 0000 UTC 5 January, (c) 0000 UTC 6 January, (e) 0000 UTC 7 January, and (g) 0000 UTC 8 January 1982; 250-hPa wind speed (m s^{-1}, shaded), 1000–500-hPa thickness (dashed red and blue contours every 10 dam, contoured red for values >540 dam and blue otherwise), SLP (black contours every 8 hPa), and precipitable water (mm, shaded) at (b) 0000 UTC 5 January, (d) 0000 UTC 6 January, (f) 0000 UTC 7 January, and (h) 0000 UTC 8 January 1982. Green line and dot represent track and position of TPV, respectively, and yellow line and dot represent track and position of cold pool, respectively.

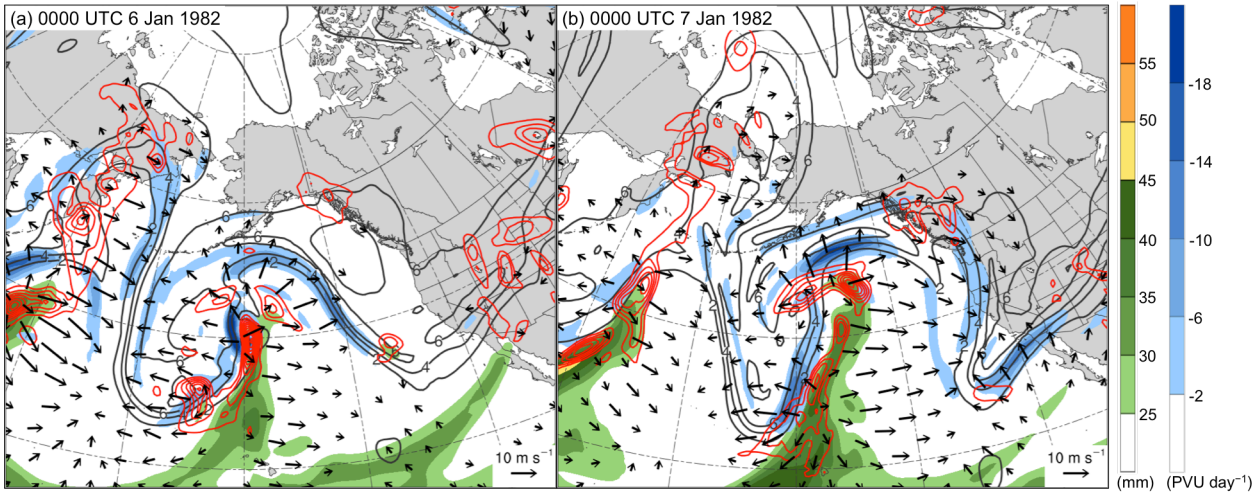

Fig. 4.4. Precipitable water (mm, shaded), 600–400-hPa ascent (red contours every 2.5×10^{-3} hPa s^{-1}), and 300–200-hPa PV (PVU, gray), irrotational wind (vectors, starting at 3 m s^{-1}), and negative PV advection by the irrotational wind (PVU day^{-1}, shaded) at (a) 0000 UTC 6 January and (b) 0000 UTC 7 January 1982.

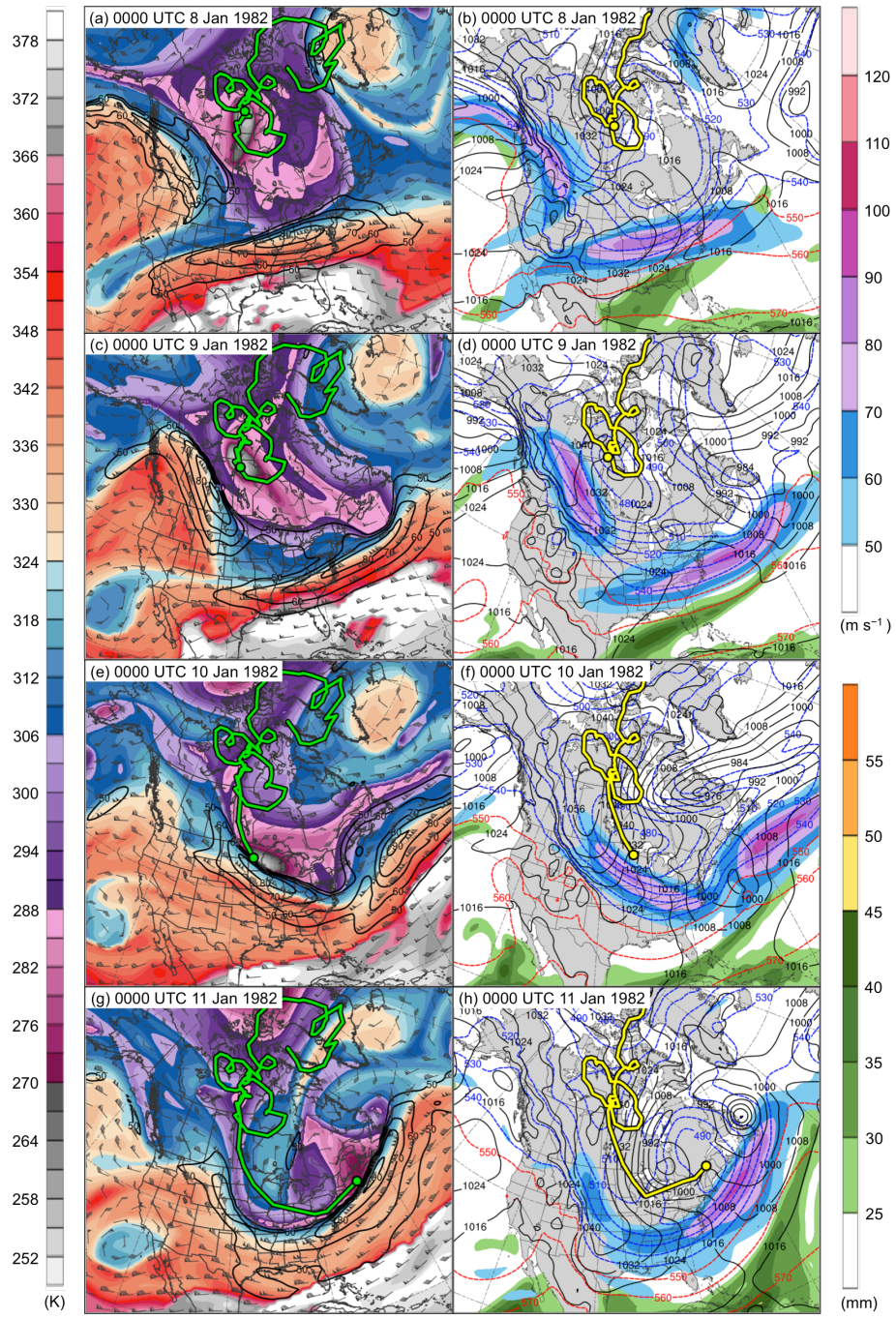

Fig. 4.5. DT (2-PVU surface) potential temperature (K, shaded), wind speed (black contours every 10 m s^{-1}, beginning at 50 m s^{-1}), and wind (m s^{-1}, flags and barbs) at (a) 0000 UTC 8 January, (c) 0000 UTC 9 January, (e) 0000 UTC 10 January, and (g) 0000 UTC 11 January 1982; 250-hPa wind speed (m s^{-1}, shaded), 1000–500-hPa thickness (dashed red and blue contours every 10 dam, contoured red for values >540 dam and blue otherwise), SLP (black contours every 8 hPa), and precipitable water (mm, shaded) at (b) 0000 UTC 8 January, (d) 0000 UTC 9 January, (f) 0000 UTC 10 January, and (h) 0000 UTC 11 January 1982. Green line and dot represent track and position of TPV, respectively, and yellow line and dot represent track and position of cold pool, respectively.

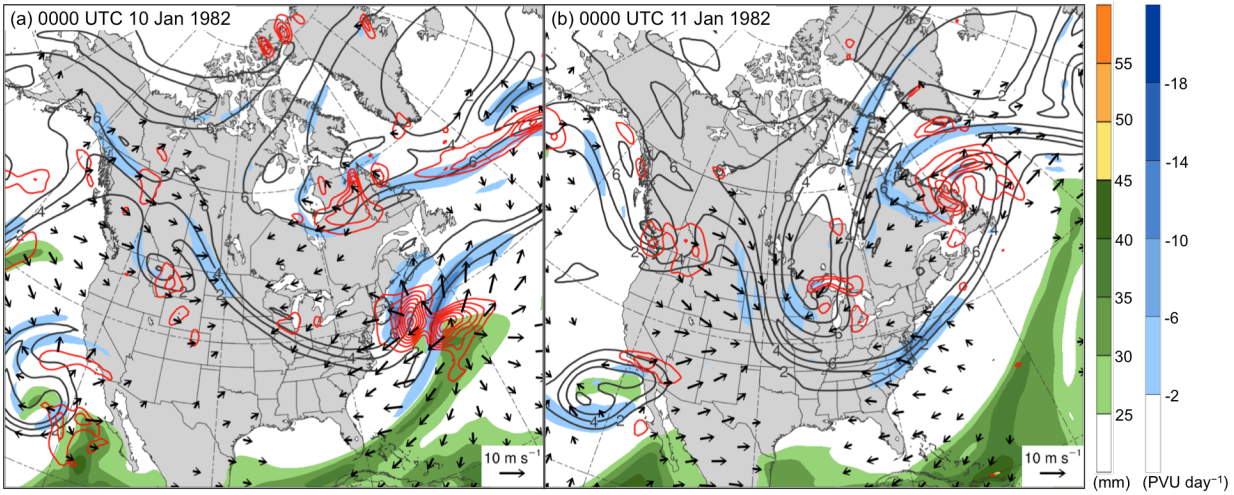

Fig. 4.6. Precipitable water (mm, shaded), 600–400-hPa ascent (red contours every 2.5×10^{-3} hPa s^{-1}), and 300–200-hPa PV (PVU, gray), irrotational wind (vectors, starting at 3 m s^{-1}), and negative PV advection by the irrotational wind (PVU day^{-1}, shaded) at (a) 0000 UTC 10 January and (b) 0000 UTC 11 January 1982.

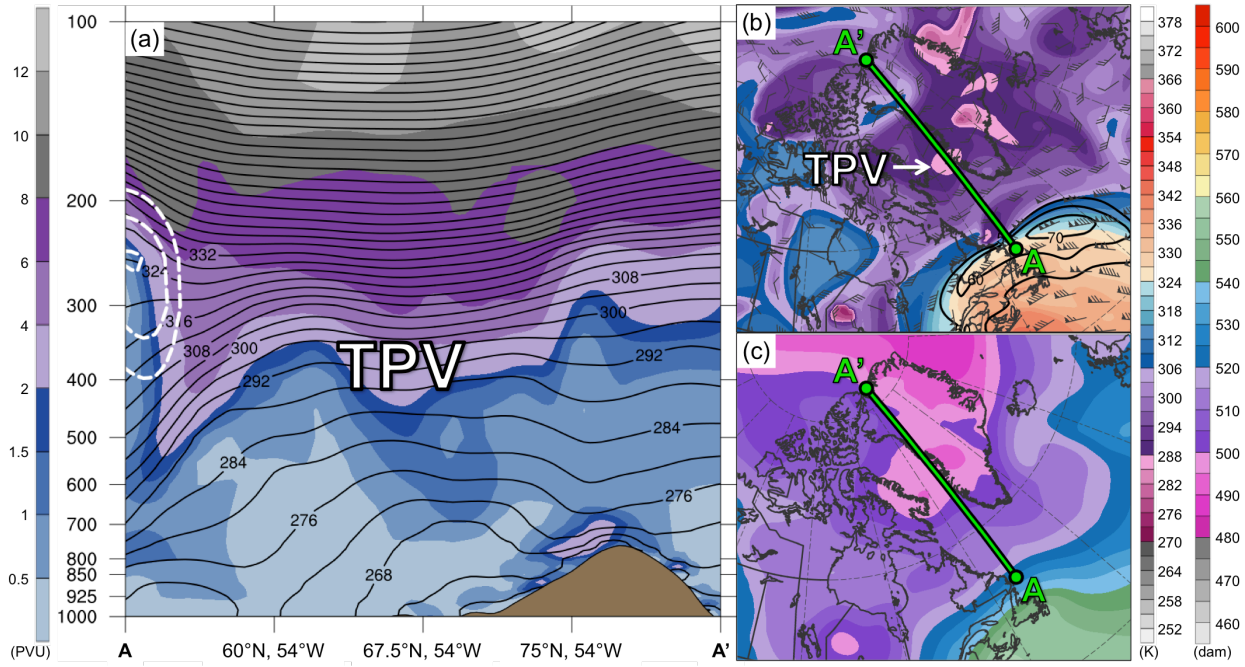

Fig. 4.7. (a) Cross section along line AA' of PV (PVU, shading), potential temperature (K, black), and wind speed (dashed white contours every 10 m s^{-1}, beginning at 50 m s^{-1}); (b) DT (2-PVU surface) potential temperature (K, shaded), wind speed (black contours every 10 m s^{-1}, beginning at 50 m s^{-1}), and wind (m s^{-1}, flags and barbs); and (c) 1000–500-hPa thickness (dam, shading) at 1200 UTC 16 December 1981. Green line in (b) and (c) represents transect of cross section AA'. Label "TPV" represents location of TPV.

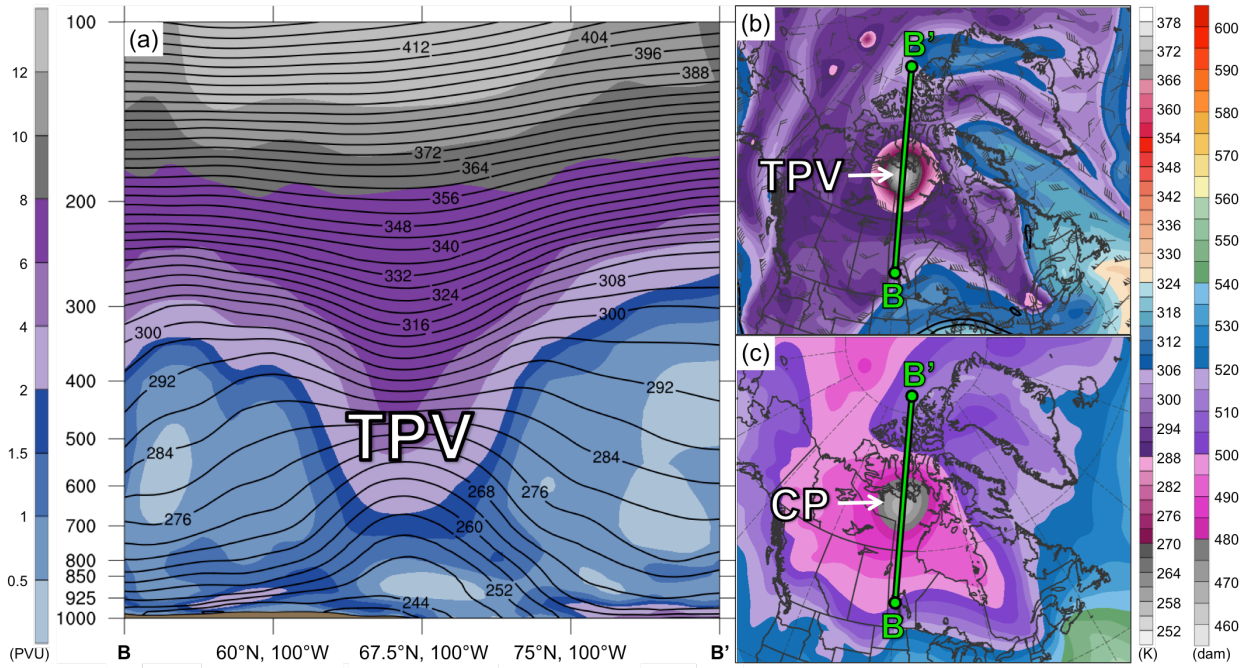

Fig. 4.8. As in Fig. 4.7, but for cross section along line BB' at 1200 UTC 2 January 1982. Label "CP" represents location of cold pool.

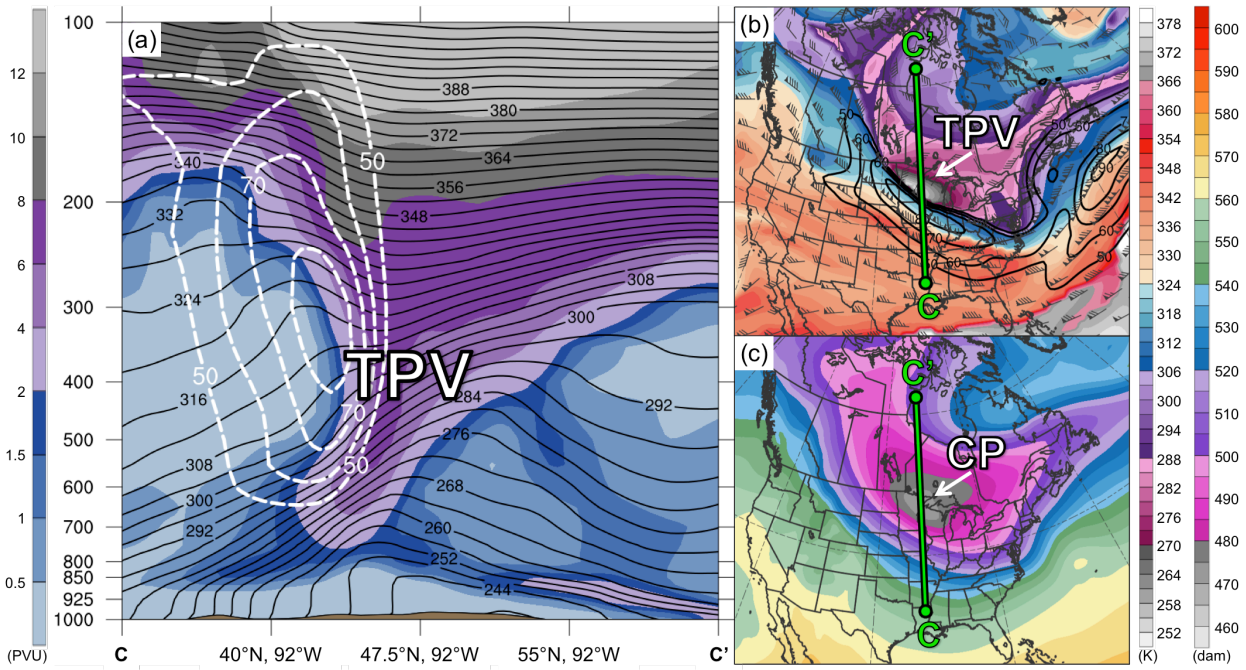

Fig. 4.9. As in Figs. 4.7 and 4.8, but for cross section along line CC' at 0000 UTC 10 January 1982.

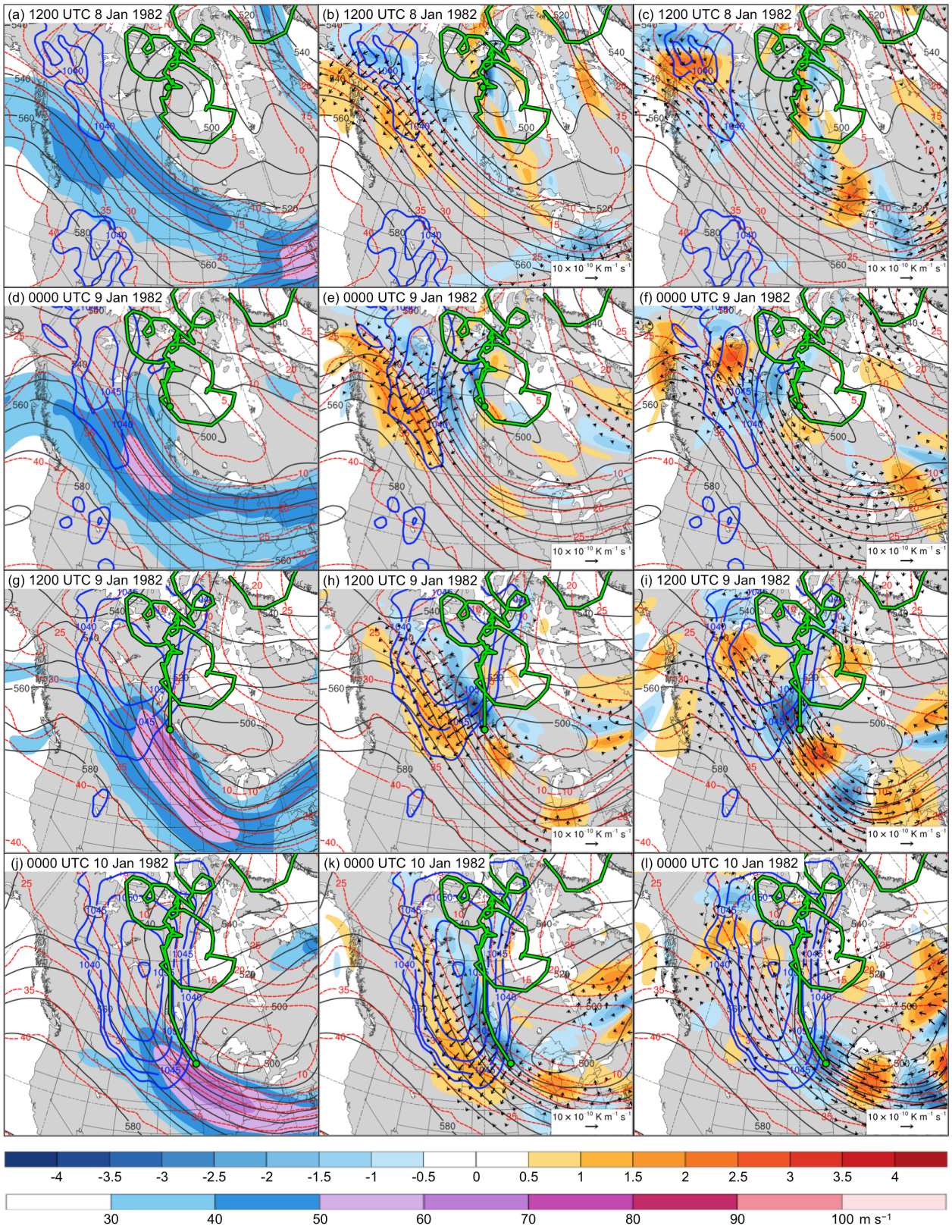

Fig. 4.10. In all panels are SLP (thick blue contours every 5 hPa, beginning at 1040 hPa), and 600–400-hPa geopotential height (dark gray contours every 10 dam) and potential temperature

(dashed red contours every 5°C). Also, 600–400-hPa wind speed (m s^{-1}, shaded) at (a) 1200 UTC 8 January, (d) 0000 UTC 9 January, (g) 1200 UTC 9 January, and (j) 0000 UTC 10 January 1982; 600–400-hPa $\mathbf{Q}_n$ (K m^{-1} s^{-1}, vectors) and $\mathbf{Q}_n$ forcing for vertical motion (10^{-17} Pa^{-1} s^{-3}, shaded) at (b) 1200 UTC 8 January, (e) 0000 UTC 9 January, (h) 1200 UTC 9 January, and (k) 0000 UTC 10 January 1982; and 600–400-hPa $\mathbf{Q}_s$ (K m^{-1} s^{-1}, vectors) and $\mathbf{Q}_s$ forcing for vertical motion (10^{-17} Pa^{-1} s^{-3}, shaded) at (c) 1200 UTC 8 January, (f) 0000 UTC 9 January, (i) 1200 UTC 9 January, and (l) 0000 UTC 10 January 1982. Green line and dot represent track and position of TPV, respectively.

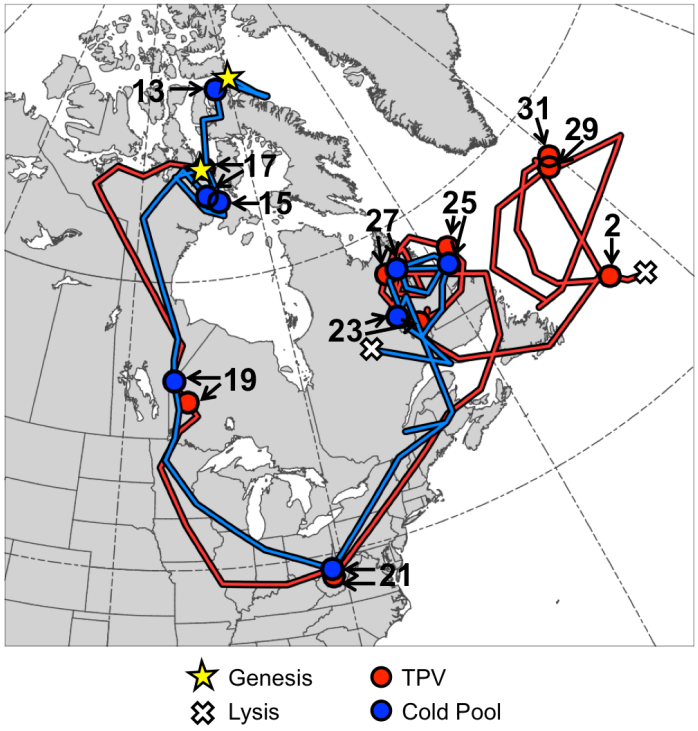

Fig. 4.11. Tracks of TPV (red) from 1800 UTC 16 January to 1200 UTC 2 February 1985 and cold pool (blue) from 1800 UTC 11 January to 0600 UTC 28 January 1985 for January 1985 CAO case. Stars denote locations of genesis, crosses denote locations of lysis, and red and blue dots represent 0000 UTC positions of TPV and cold pool, respectively, every 48 h. Numbers pointing toward dots represent dates of the 0000 UTC positions of the TPV and cold pool, such that numbers ≥13 correspond to dates in January 1985 and the number "2" corresponds to 2 February 1985.

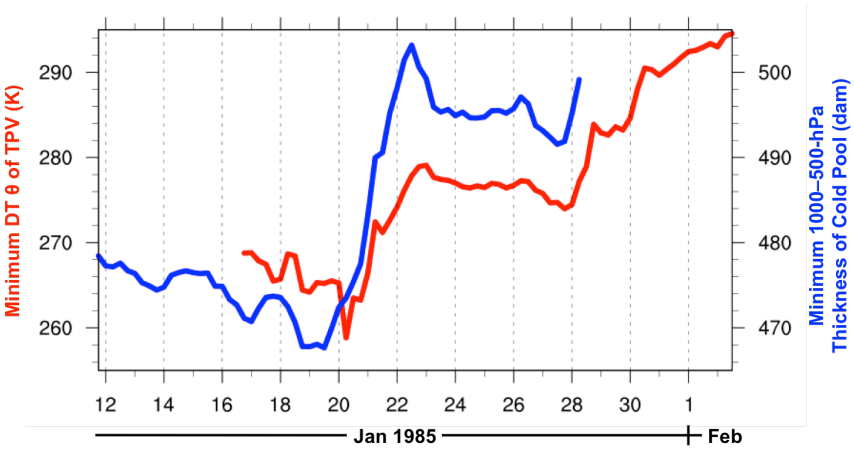

Fig. 4.12. Time series of minimum DT potential temperature (θ) of TPV (K, red) every 6 h from 1800 UTC 16 January to 1200 UTC 2 February 1985 and minimum 1000–500-hPa thickness of cold pool (dam, blue) every 6 h from 1800 UTC 11 January to 0600 UTC 28 January 1985 for January 1985 CAO case.

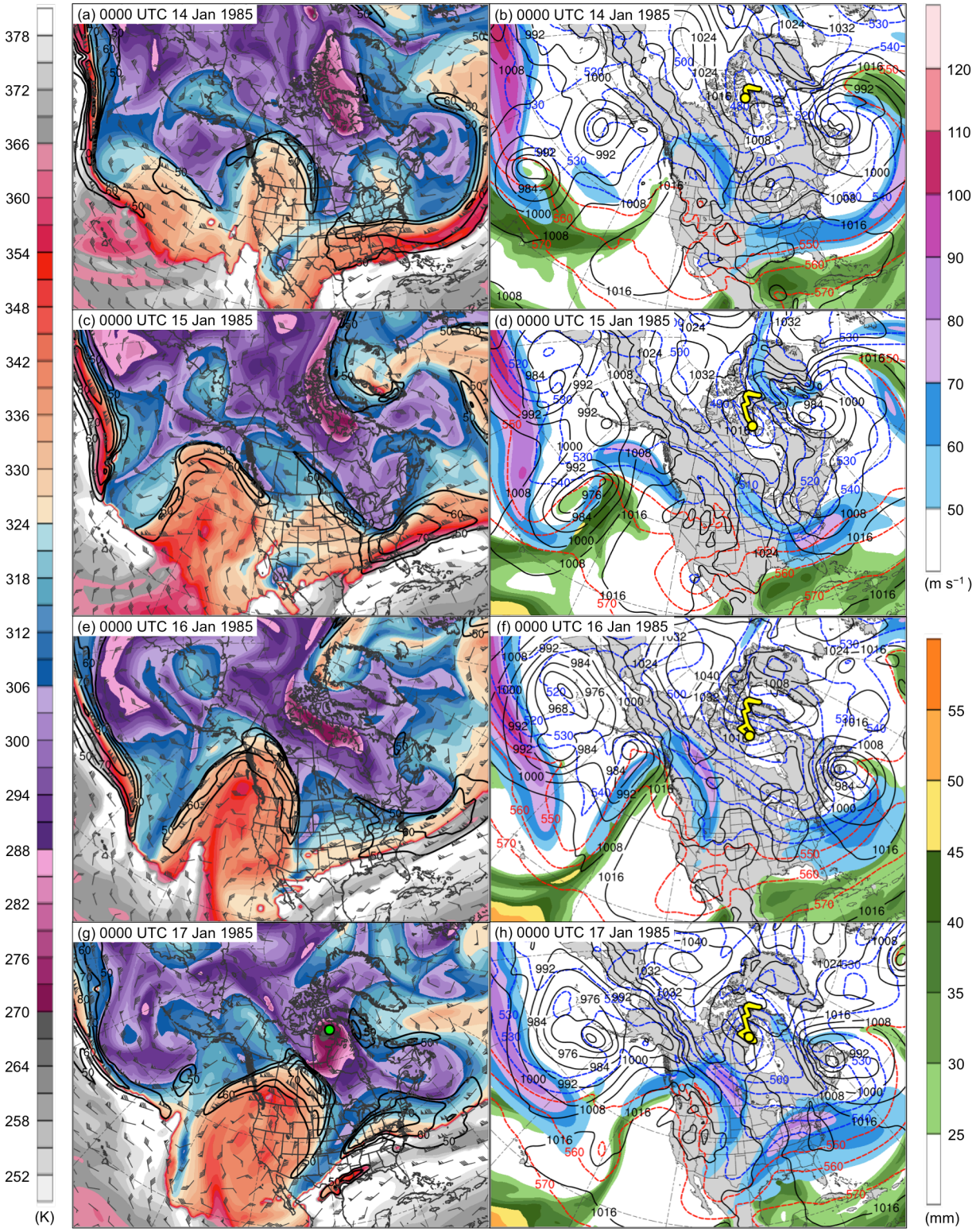

Fig. 4.13. DT (2-PVU surface) potential temperature (K, shaded), wind speed (black contours every 10 m s^{-1}, beginning at 50 m s^{-1}), and wind (m s^{-1}, flags and barbs) at (a) 0000 UTC 14 January, (c) 0000 UTC 15 January, (e) 0000 UTC 16 January, and (g) 0000 UTC 17 January

1985; 250-hPa wind speed (m s^{-1}, shaded), 1000–500-hPa thickness (dashed red and blue contours every 10 dam, contoured red for values >540 dam and blue otherwise), SLP (black contours every 8 hPa), and precipitable water (mm, shaded) at (b) 0000 UTC 14 January, (d) 0000 UTC 15 January, (f) 0000 UTC 16 January, and (h) 0000 UTC 17 January 1985. Green line and dot represent track and position of TPV, respectively, and yellow line and dot represent track and position of cold pool, respectively.

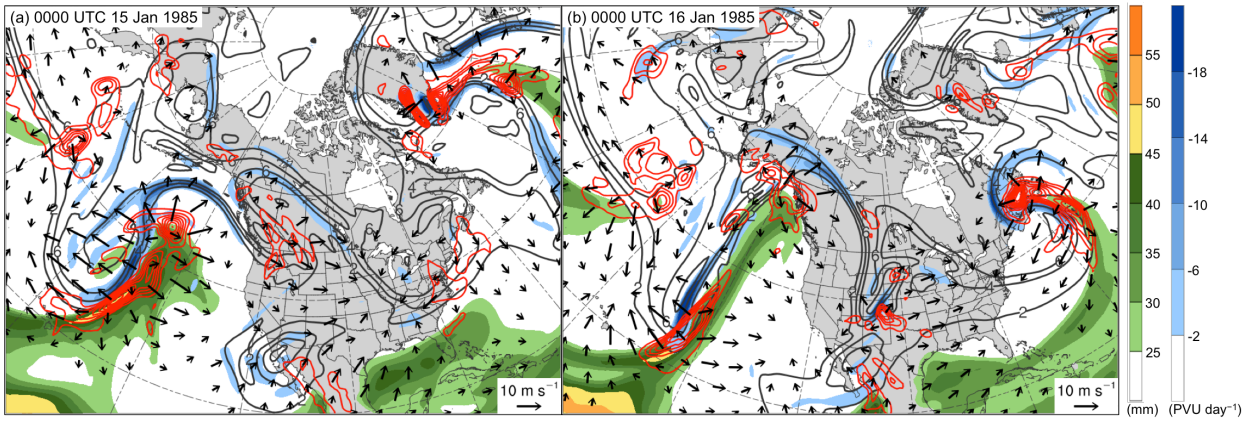

Fig. 4.14. Precipitable water (mm, shaded), 600–400-hPa ascent (red contours every 2.5 × 10^{-3} hPa s^{-1}), and 300–200-hPa PV (PVU, gray), irrotational wind (vectors, starting at 3 m s^{-1}), and negative PV advection by the irrotational wind (PVU day^{-1}, shaded) at (a) 0000 UTC 15 January and (b) 0000 UTC 16 January 1985.

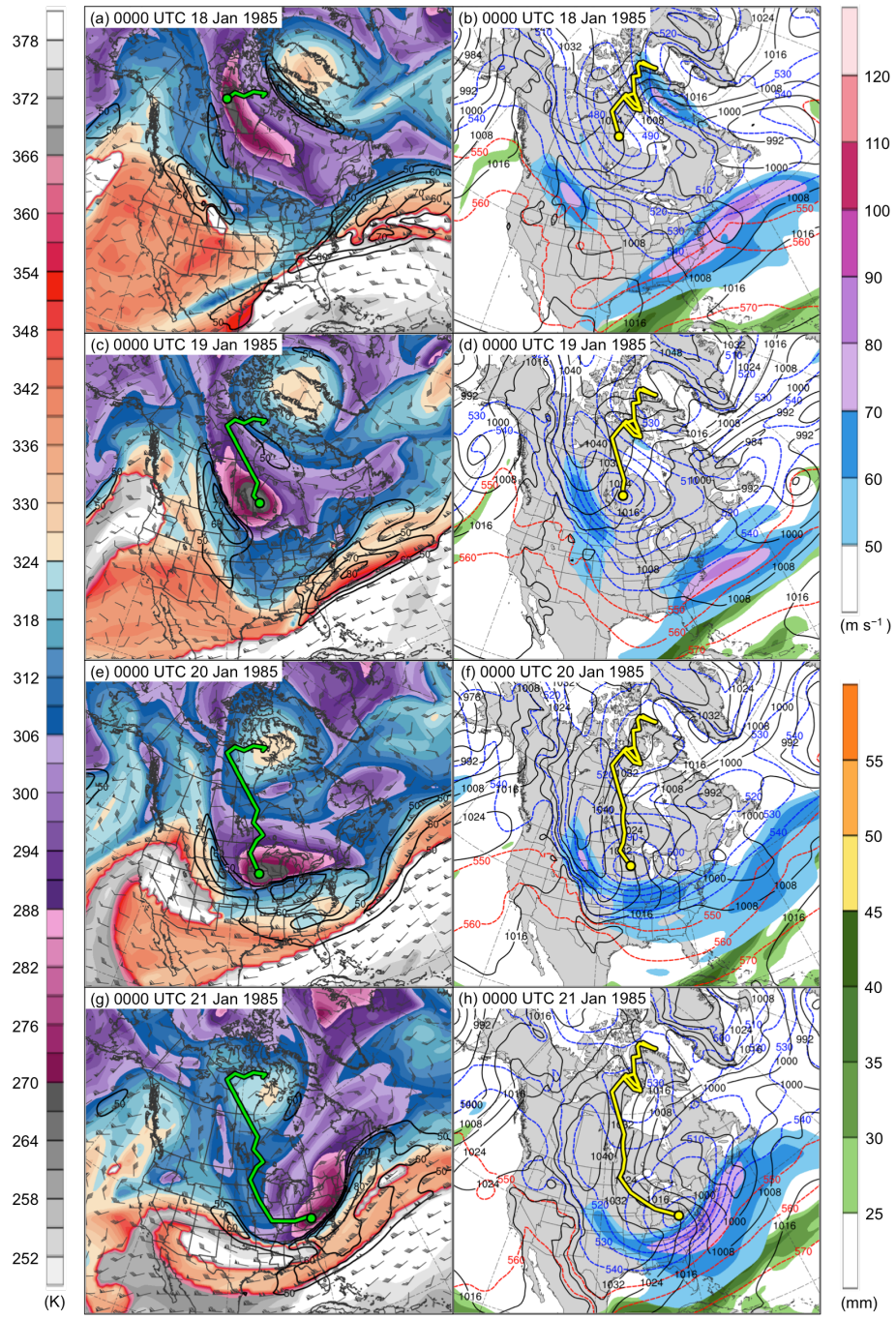

Fig. 4.15. DT (2-PVU surface) potential temperature (K, shaded), wind speed (black contours every 10 m s^{-1}, beginning at 50 m s^{-1}), and wind (m s^{-1}, flags and barbs) at (a) 0000 UTC 18 January, (c) 0000 UTC 19 January, (e) 0000 UTC 20 January, and (g) 0000 UTC 21 January 1985; 250-hPa wind speed (m s^{-1}, shaded), 1000–500-hPa thickness (dashed red and blue contours every 10 dam, contoured red for values >540 dam and blue otherwise), SLP (black contours every 8 hPa), and precipitable water (mm, shaded) at (b) 0000 UTC 18 January, (d) 0000 UTC 19 January, (f) 0000 UTC 20 January, and (h) 0000 UTC 21 January 1985. Green line and dot represent track and position of TPV, respectively, and yellow line and dot represent track and position of cold pool, respectively.

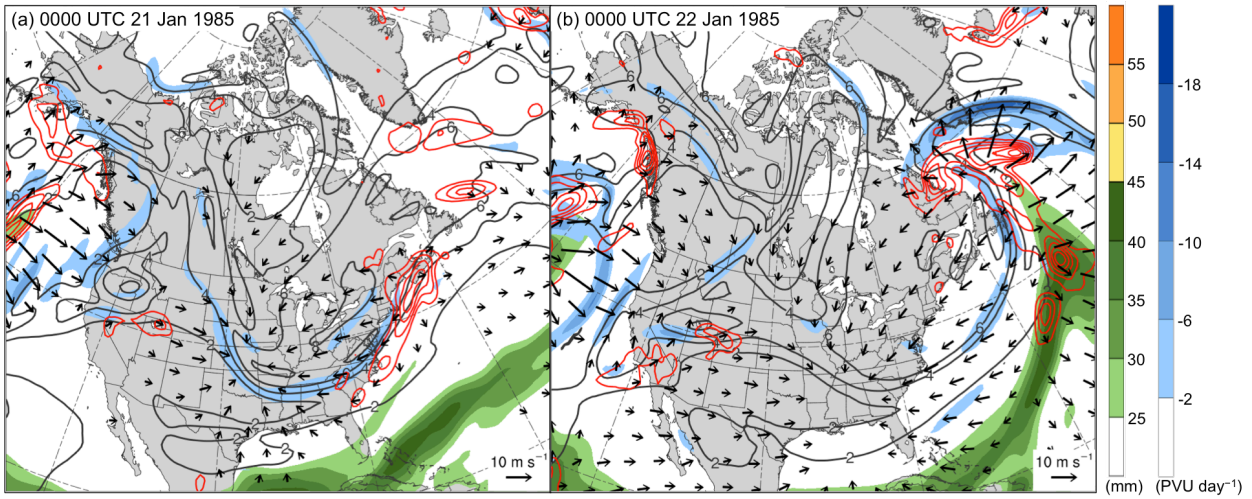

Fig. 4.16. Precipitable water (mm, shaded), 600–400-hPa ascent (red contours every 2.5 × 10^{-3} hPa s^{-1}), and 300–200-hPa PV (PVU, gray), irrotational wind (vectors, starting at 3 m s^{-1}), and negative PV advection by the irrotational wind (PVU day^{-1}, shaded) at (a) 0000 UTC 21 January and (b) 0000 UTC 22 January 1985.

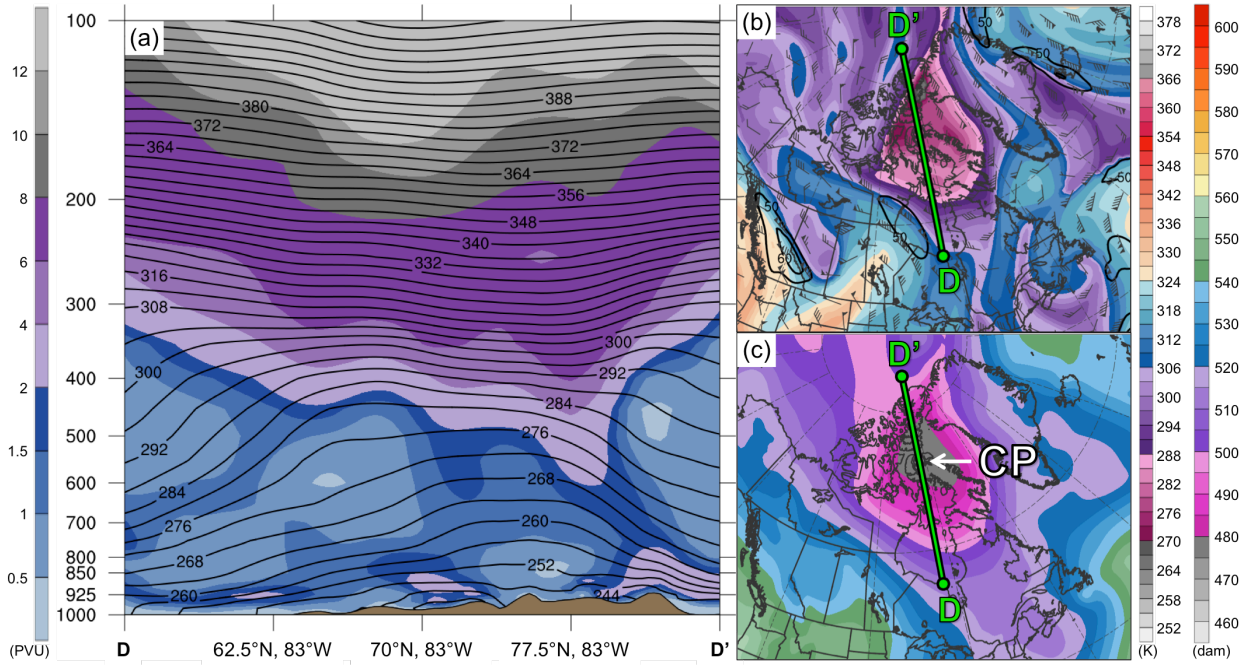

Fig. 4.17. As in Fig. 4.7, but for cross section along line DD' at 0000 UTC 13 January 1985.

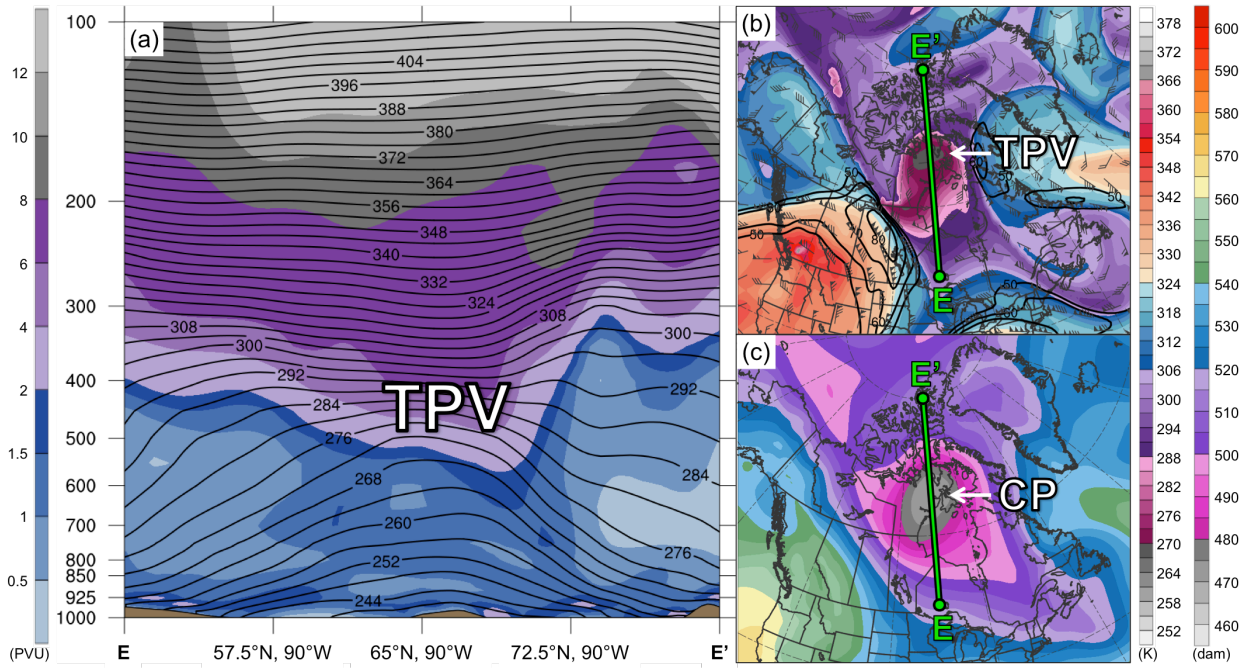

Fig. 4.18. As in Fig. 4.7, but for cross section along line EE' at 0000 UTC 17 January 1985.

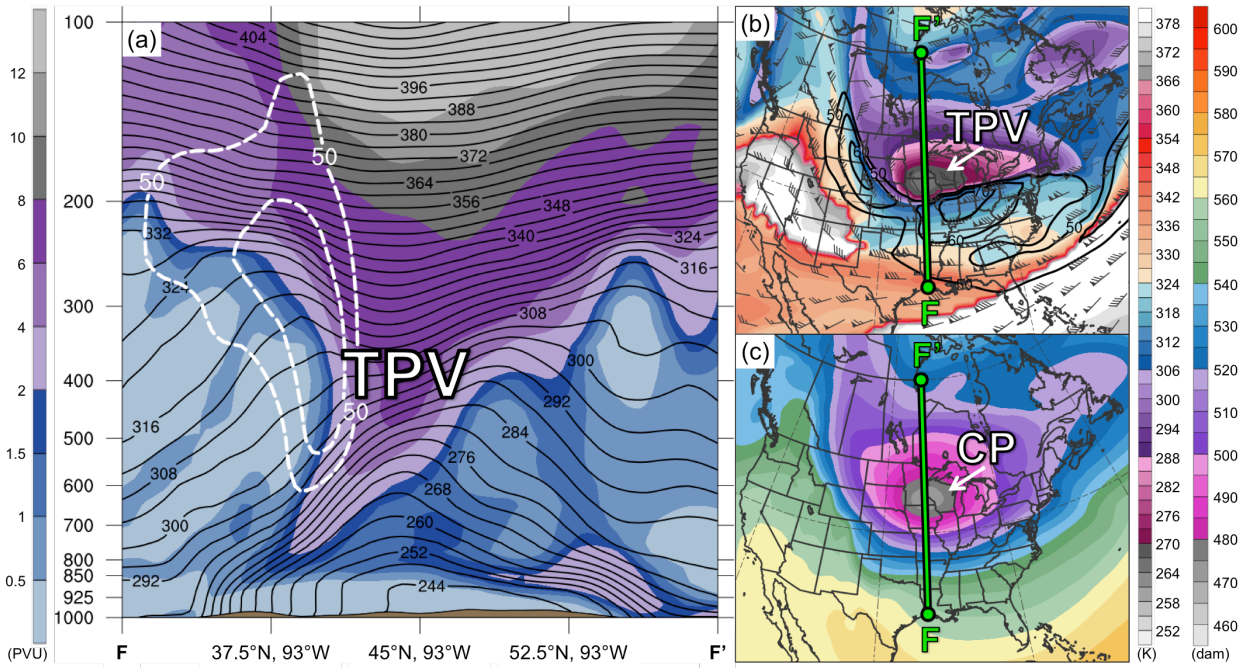

Fig. 4.19. As in Fig. 4.7, but for cross section along line FF' at 0000 UTC 20 January 1985.

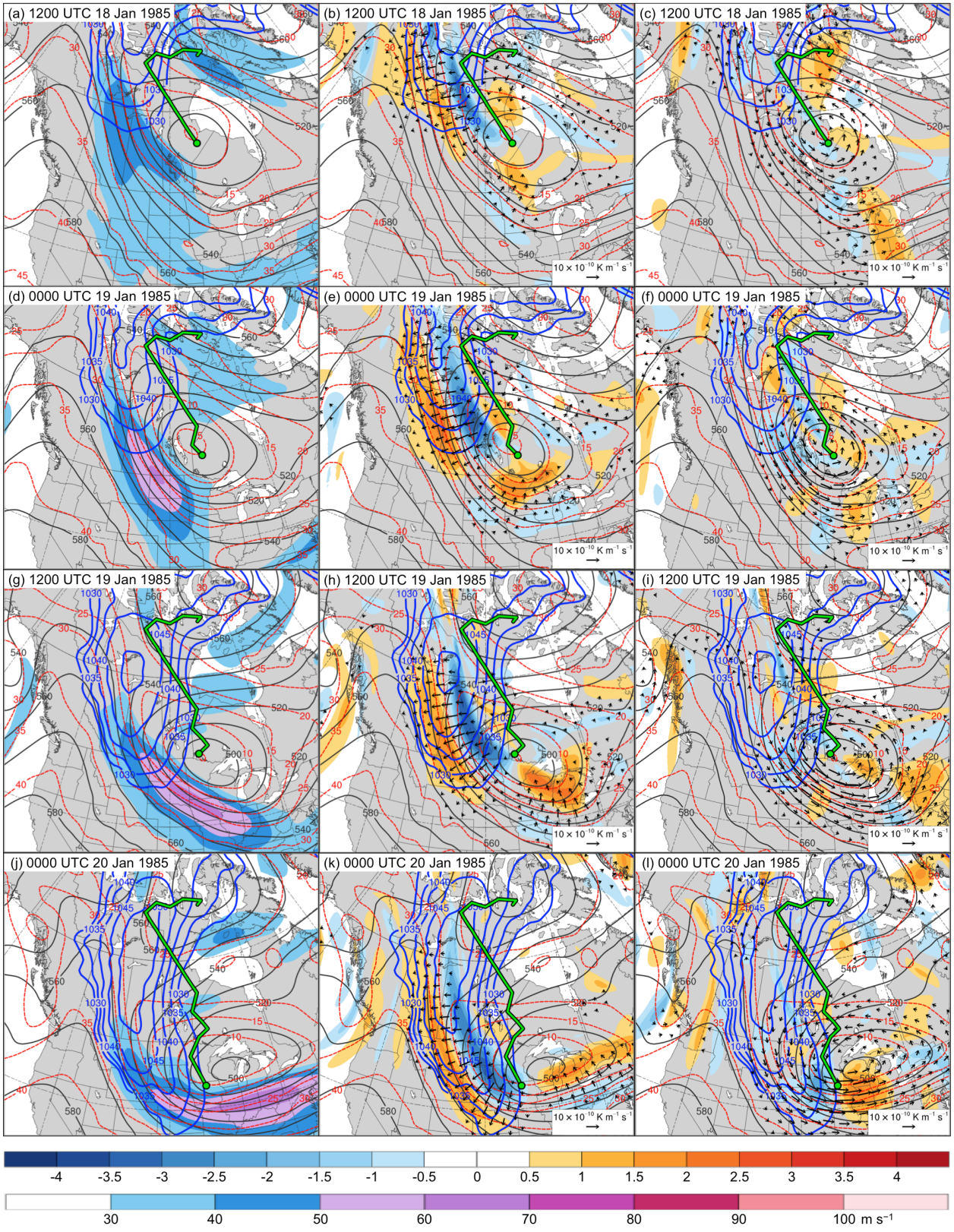

Fig. 4.20. In all panels are SLP (thick blue contours every 5 hPa, beginning at 1030 hPa), and 600–400-hPa geopotential height (dark gray contours every 10 dam) and potential temperature

(dashed red contours every 5°C). Also, 600–400-hPa wind speed (m s^{-1}, shaded) at (a) 1200 UTC 18 January, (d) 0000 UTC 19 January, (g) 1200 UTC 19 January, and (j) 0000 UTC 20 January 1985; 600–400-hPa $\mathbf{Q}_n$ (K m^{-1} s^{-1}, vectors) and $\mathbf{Q}_n$ forcing for vertical motion (10^{-17} Pa^{-1} s^{-3}, shaded) at (b) 1200 UTC 18 January, (e) 0000 UTC 19 January, (h) 1200 UTC 19 January, and (k) 0000 UTC 20 January 1985; and 600–400-hPa $\mathbf{Q}_s$ (K m^{-1} s^{-1}, vectors) and $\mathbf{Q}_s$ forcing for vertical motion (10^{-17} Pa^{-1} s^{-3}, shaded) at (c) 1200 UTC 18 January, (f) 0000 UTC 19 January, (i) 1200 UTC 19 January, and (l) 0000 UTC 20 January 1985. Green line and dot represent track and position of TPV, respectively.

5. Discussion, Conclusions, and Suggestions for Future Work

5.1 Discussion and Conclusions

The goals of this research were to improve understanding of 1) the equatorward transport of TPVs and cold pools to middle latitudes and 2) the dynamical linkages between TPVs, cold pools, and CAOs. Although previous studies have examined CAOs linked to cold pools and have discussed upper-level features that may play a role in CAOs, no previous study has examined the dynamical linkages between TPVs, cold pools, and CAOs from a climatological perspective. Climatologies of TPVs and cold pools were constructed to gain insight on regions favorable for the equatorward transport of TPVs and cold pools. A climatology of CAOs over the central and eastern U.S. that are linked to cold pools associated with TPVs was then constructed to gain understanding of the dynamical linkages between TPVs, cold pools, and CAOs. Case study investigations of two CAOs that are linked to cold pools associated with TPVs were performed to gain further understanding of the equatorward transport of TPVs and cold pools to middle latitudes and the dynamical linkages between TPVs, cold pools, and CAOs.

5.1.1 Climatologies

5.1.1.1 TPVs and Cold Pools

Many of the results of the TPV climatology are in agreement with past studies of TPVs. TPV track density is highest over the high latitudes, especially over the Canadian Archipelago and northern Siberia, in agreement with the results of Cavallo and Hakim (2009, 2012). Cavallo and Hakim (2009, 2010, 2012, 2013) have shown that TPVs are common over high latitudes

because longwave radiative cooling, which may maintain and intensify TPVs, dominates latent heating, which may act to weaken or destroy TPVs. In addition, as shown by Cavallo and Hakim (2012), the regions of high TPV track density over the Canadian Archipelago and northern Siberia coincide with climatological 500-hPa troughs. TPVs meandering around within these troughs may contribute to high TPV track density in these regions. Similar to TPVs, regions of high cold pool track density are found over the high latitudes, especially over the Canadian Archipelago and northern Siberia and the adjacent Arctic Ocean. Longwave radiative cooling over these regions from surface snow and ice cover, as well as from ice crystals, condensate, and low-level clouds often found in the cold air over the Arctic (e.g., Curry 1983; Emanuel 2008), may support the maintenance and intensification of cold pools (e.g., Turner and Gyakum 2011; Turner et al. 2013).

The climatologies of TPVs and cold pools transported to middle latitudes indicate that central and eastern North America and Siberia and eastern Asia are favorable corridors for the equatorward transport of TPVs and cold pools to middle latitudes. Ridge amplification over the eastern North Pacific and western North America may lead to the downstream equatorward transport of TPVs and cold pools over central and eastern North America, as illustrated in the case studies in chapter 4 as well as in past studies including those of Hakim et al. (1995, 1996) and Bosart et al. (1996). Since central and eastern North America is a favored region for CAOs (e.g., Konrad and Colucci 1989; Colle and Mass 1995; Walsh et al. 2001), TPVs and cold pools transported equatorward over central and eastern North America may play important roles in the development of CAOs. The TPVs and cold pools that frequently track over Siberia and eastern Asia may be involved in cold surges over eastern Asia (e.g., Chang and Lau 1980; Boyle 1986; Chen et al. 2002). For example, Boyle (1986) showed that cold air ushered in by synoptic-scale

short waves passing through the long-wave trough over eastern Asia may result in cold surges over eastern Asia. TPVs and associated cold pools over Siberia and eastern Asia may similarly result in cold surges over eastern Asia.

In addition, a high track density of TPVs and cold pools transported to middle latitudes was found near the entrance regions and along the poleward sides of the North Atlantic and North Pacific jet streams. TPVs and cold pools tracking near these jet streams may contribute to the development and intensification of jet streaks. TPVs may contribute to the development and intensification of jet streaks via TPV–jet interaction (e.g., Pyle et al. 2004), and cold pools may contribute to the development and intensification of jet streaks by contributing to increases in lower-tropospheric baroclinicity (e.g., Sanders and Davis 1988). The development and intensification of jet streaks may support the development of strong ECs (e.g., Uccellini et al. 1985; Uccellini and Kocin 1987). Furthermore, TPVs themselves can be precursors to the development of strong ECs (e.g., Hakim et al. 1995, 1996; Bosart et al. 1996), and the movement of cold pools over strong SST gradients associated with the Gulf Stream and the Kuroshio current may support strong sensible and latent heat fluxes and a reduction in static stability, which may provide favorable conditions for the development of strong ECs (e.g., Sanders and Gyakum 1980).

5.1.1.2 CAOs that are Linked to Cold Pools Associated with TPVs

As discussed in section 3.3, there is a much larger percentage of CAOs that are linked to cold pools in northern regions of the U.S., comprising the WNC, ENC, and Northeast regions (~85–90%), compared to the southern regions of the U.S., comprising the South and Southeast

regions (~28–36%), which is likely related to the large meridional gradient of track density of cold pools transported to middle latitudes over southern Canada and the northern U.S. Thus, there is likely more opportunity for northern regions of the U.S to be impacted by cold pools compared to the southern regions of the U.S. For example, a cold pool that moves across southern Canada may only impact northern regions of the U.S., especially if the flow pattern over the U.S. is relatively zonal and cold air cannot penetrate far equatorward. For cold pools that impact both the northern and southern regions of the U.S., although the core of the cold pool may only move over the northern regions of the U.S., the cold air associated with the cold pool may still spread far away and impact southern regions of the U.S. For example, as shown in the case studies in chapter 4 and in previous studies (e.g., Boyle and Bosart 1983; Colle and Mass 1995), a cold pool may be accompanied by a strong surface anticyclone on the eastern side of the Rocky Mountains. The strong SLP gradient associated with the surface anticyclone and a terrain-tied northerly component of low-level motion east of the Rocky Mountains (e.g., Dunn 1987, 1992; Colle and Mass 1995) may allow cold air from the cold pool to advect equatorward.

Previous studies have shown that upper-level features may be associated with cold pools. For example, Boyle and Bosart (1983) showed that a PV maximum was found above a cold pool leading to a CAO over North America during November 1969, and Shapiro et al. (1987) showed that a midlevel cyclone or "polar vortex" feature was associated with a cold pool that played an important role in the development of the January 1985 CAO. As shown in chapter 4, this "polar vortex" feature corresponds to a TPV. This thesis expands upon these prior studies by offering a climatological explanation of the relationship between TPVs and cold pools. As discussed in section 3.3, it has been found that 6,288 out of the total 8,395 cold pools transported to middle latitudes, or 74.9%, match with at least one TPV transported to middle latitudes. Also, 6,510 out

of the total 25,085 TPVs transported to middle latitudes, or 26.0%, match with at least one cold pool transported to middle latitudes. Although a large percentage of cold pools transported to middle latitudes (74.9%) are associated with TPVs, an equally large percentage of TPVs (74.0%) are not associated with cold pools. In many instances, TPVs may be too small or weak to be associated with a cold pool. For example, when the TPV in the January 1982 CAO case is relatively small and weak early in its life cycle, it is not associated with an identifiable cold pool. Regardless, when this TPV is small and weak, it is still associated with cold air throughout the depth of the troposphere, suggesting that small and weak TPVs not associated with cold pools may still be associated with cold air throughout the depth of the troposphere. Furthermore, a TPV may be strong, but may be associated with a 1000–500-hPa thickness trough that is not trackable if, for example, a region of cold air characterized by relatively low values of 1000–500-hPa thickness associated with the TPV is embedded in a strong horizontal thickness gradient.

After comparing the climatologies of TPVs, cold pools, and CAOs, it was found that ~74–88% of CAOs are linked to cold pools associated with TPVs over northern regions of the U.S., while only ~24–28% of CAOs are linked to cold pools associated with TPVs over southern regions of the U.S. Thus, while cold pools associated with TPVs may contribute to CAO development over the entire central and eastern U.S., they are more likely to cause CAO development over northern regions of the U.S. The large percentage of CAOs over northern regions of the U.S. that are linked to cold pools associated with TPVs suggests that TPVs may play an important role in CAO development and that improved understanding of TPVs may lead to improved understanding of CAOs. The climatology of CAOs that are linked to cold pools associated with TPVs complements and extends existing studies of CAOs linked to cold pools

and upper-level features (e.g., Shapiro et al. 1987) by providing climatological context for the linkages between TPVs, cold pools, and CAOs.

5.1.2 Case Studies

Similar to previous studies showing the equatorward transport of TPVs (e.g., Hakim et al. 1995, 1996; Bosart et al. 1996) and cold pools (e.g., Namias 1978), ridge amplification over the eastern North Pacific and western North America appears to play an important role in the equatorward transport of the TPV and cold pool in both the January 1982 CAO case and the January 1985 CAO case, with ridge amplification over the northwestern North Atlantic also playing an important role in the equatorward transport of the TPV and cold pool in the January 1985 CAO case. Poleward fluxes of warm, moist air and diabatically driven upper-tropospheric divergent outflow associated with ECs appear to play important roles in ridge amplification in both cases.

In both case studies presented in chapter 4, the large spatial overlap and temporal coincidence of the TPV and cold pool throughout much of their lifetimes suggests that the TPV and cold pool are dynamically linked. The composite cross section of TPVs from Cavallo and Hakim (2010), which shows anomalously cold air throughout the troposphere within and beneath the TPV, also suggests that there may be a dynamical linkage between TPVs and cold pools. Cross sections of the TPV and cold pool in each case were examined to better understand the linkages between TPVs and cold pools. In the January 1982 CAO case, as the TPV becomes stronger and deeper, the upward bowing of the isentropes within and beneath the TPV becomes more pronounced, and the cold pool concomitantly becomes stronger. In the January 1985 CAO

case, the formation of the cold pool precedes the formation of the TPV. After the TPV forms and strengthens, the upward bowing of the isentropes throughout the troposphere is more pronounced compared to prior to the formation of the TPV, and the cold pool is stronger after the formation of the TPV compared to prior to the formation of the TPV. Thus there appears to be a dynamical linkage between the TPV and cold pool in both cases, demonstrating that the influence of TPVs can extend throughout the depth of the troposphere and cover a widespread geographical area. In addition, in both cases, when the TPV interacts with a jet streak, a classic tropopause fold structure (e.g., Reed and Danielsen 1959; Danielsen 1968; Keyser and Shapiro 1986) is evident, illustrating an important connection between tropopause folds and TPVs. Tropopause folds have been shown to play a key role in the development of strong ECs (e.g., Uccellini et al. 1985), further illustrating that TPVs can be important precursors to EC development.

In the January 1982 and January 1985 CAO cases, a jet streak over western North America strengthens as TPV–jet interaction occurs, and a strong surface anticyclone over western North America concomitantly strengthens and expands equatorward in the left entrance region of the jet streak. A composite analysis of strong surface anticyclones occurring over western North America performed by Jones and Cohen (2011) suggests that the composite surface anticyclone also strengthens in the left entrance region of a jet streak, where there is Q-vector divergence and thus QG forcing for descent over and to the south and east of the composite surface anticyclone. In both cases examined in chapter 4, there is an enhancement of $\mathbf{Q}_n$ forcing for descent in the left entrance region of the jet streak as the jet streak strengthens during TPV–jet interaction. In addition, the TPV in each case is associated with a short-wave trough, with $\mathbf{Q}_s$ forcing for descent found upstream of the short-wave trough, as anticipated from Sanders and Hoskins (1990). As the TPV interacts with the jet streak in each case, the $\mathbf{Q}_s$ forcing

for descent is found in the left entrance region of the jet streak, coinciding with the region of $\mathbf{Q}_n$ forcing for descent. The $\mathbf{Q}_s$ forcing for descent is larger in magnitude and better organized in the January 1982 CAO case compared to the January 1985 CAO case, possibly due in part to the short-wave trough associated with the TPV in the January 1982 CAO case being sharper compared to that in the January 1985 CAO case. In both cases, the enhanced patterns of $\mathbf{Q}_n$ and $\mathbf{Q}_s$ forcings for descent in the left entrance region of the jet streak related to the TPV and TPV–jet interaction likely support the strengthening and expansion of the surface anticyclone in the left entrance region of the jet streak. Therefore, TPV–jet interaction may play an important role in the strengthening and expansion of strong surface anticyclones related to CAO development.

As the TPV and cold pool move into the U.S., and the surface anticyclone expands equatorward on the eastern side of the Rocky Mountains, an expected terrain-tied northerly component of strong low-level flow (e.g., Dunn 1987, 1992; Colle and Mass 1995) in the vicinity of the strong SLP gradient associated with the surface anticyclone likely helps allow cold air from the cold pool associated with the TPV to be rapidly transported equatorward. The strong surface anticyclone thus likely plays an important role in CAO development in each case, consistent with previous studies on CAO development including Dallavalle and Bosart (1975), Boyle and Bosart (1983), Colucci and Davenport (1987), Konrad and Colucci (1989), Colle and Mass (1995), Walsh et al. (2001), and Jones and Cohen (2011).

The cases studies in chapter 4 illustrate that TPVs may play a central role in CAO development given that 1) the TPV is associated with a cold pool that moves in tandem with the TPV into the U.S. during the time of the occurrence of the CAO and 2) the TPV via TPV–jet interaction may help to strengthen a strong surface anticyclone that helps transport cold air from the cold pool associated with the TPV far away from the core of the cold pool. Therefore, the

case studies in chapter 4 complement and extend existing studies of cold pools and strong surface anticyclones linked to CAO development by illustrating linkages to TPVs. Also, as previously discussed, this thesis shows that the midlevel cyclone or "polar vortex" feature illustrated by Shapiro et al. (1987) to play an important role in the development of the January 1985 CAO is related to a TPV, suggesting that short-wave troughs and midlevel cyclones identified to play important roles in CAO development in prior studies may be related to TPVs. For example, it may be possible that there are linkages between the cold pool discussed by Boyle and Bosart (1983) and a TPV, especially given that Boyle and Bosart (1983) describe the existence of an upper-level PV maximum collocated with the 1000–500-hPa thickness minimum of the cold pool. If there is a TPV linkage, the degree to which TPV–jet interaction plays a role in the evolution of the surface anticyclone discussed by Boyle and Bosart (1983) could be examined, especially given that the surface anticyclone in their case moves equatorward along with a jet streak.

5.2 Suggestions for Future Work

A remaining research issue is whether and how CAOs that are linked to cold pools associated with TPVs may differ from CAOs that are not linked to cold pools associated with TPVs. To address this research issue, composites of CAOs that are linked to cold pools associated with TPVs for different regions comprising the central and eastern U.S. could be constructed and compared to corresponding composites of CAOs that are not linked to cold pools associated with TPVs. In addition, idealized modeling could be used to further investigate the dynamical linkage between TPVs and cold pools. For example, the strength and structure of an

idealized TPV could be modified in order to better understand how changes in the strength and structure of the TPV impact a cold pool associated with the TPV. Furthermore, in both cases in chapter 4, processes hypothesized to play a role in intensity changes of the TPV and cold pool, such as longwave radiative cooling, latent heating, and sensible heating, could be quantified in order to better understand the impact of these processes on TPV and cold pool intensity in each case. For example, a thermodynamic budget similar to that used by Turner et al. (2013) could be used to quantify the influence of radiative cooling on the intensity of each cold pool.

The TPV and cold pool climatologies presented in this thesis indicate that Siberia and eastern Asia are favored regions for the equatorward transport of TPVs and cold pools. A climatology of CAOs that are linked to cold pools associated with TPVs could be constructed for Siberia and eastern Asia, and the role of TPVs and cold pools on the development of cold surges over eastern Asia (e.g., Chang and Lau 1980; Boyle 1986) could be examined. Furthermore, it has been shown that cold surges over eastern Asia may potentially impact the state and structure of the North Pacific jet stream (e.g., Chang and Lau 1982; Handlos and Martin 2016), which may impact the downstream synoptic-scale flow (e.g., Griffin and Martin 2017). Therefore, it is possible that changes in the state and structure of the North Pacific jet stream occurring in response to upstream precursor disturbances such as TPVs, cold pools, and associated cold surges over eastern Asia may impact the synoptic-scale flow over the eastern North Pacific and western North America, which in turn may influence whether TPVs and cold pools are transported to middle latitudes over North America. Climatological, composite, case, and predictability studies of the impact of TPVs, cold pools, and associated cold surges over eastern Asia on the state and structure of the North Pacific jet stream could be carried out. In addition, the subsequent impact of the state and structure of the North Pacific jet stream on the structure of

the downstream synoptic-scale flow and equatorward transport of TPVs and cold pools over North America could be examined.

REFERENCES

Bosart, L. F., B. J. Moore, J. M. Cordeira, and H. M. Archambault, 2017: Interactions of North Pacific tropical, midlatitude, and polar disturbances resulting in linked extreme weather events over North America in October 2007. *Mon. Wea. Rev.,* **145,** 1245–1273.

——, G. J. Hakim, K. R. Tyle, M. A. Bedrick, W. E. Bracken, M. J. Dickinson, and D. M. Schultz, 1996: Large-scale antecedent conditions associated with the 12–14 March 1993 cyclone ("superstorm '93") over eastern North America. *Mon. Wea. Rev.,* **124,** 1865–1891.

Boyle, J. S., 1986: Comparison of the synoptic conditions in midlatitude accompanying cold surges over eastern Asia for the months of December 1974 and 1978. Part I: Monthly mean fields and individual events. *Mon. Wea. Rev.,* **114,** 903–918.

——, and L. F. Bosart, 1983: A cyclone/anticyclone couplet over North America: An example of anticyclone evolution. *Mon. Wea. Rev.,* **111,** 1025–1045.

Cavallo, S. M., and G. J. Hakim, 2009: Potential vorticity diagnosis of a tropopause polar cyclone. *Mon. Wea. Rev.,* **137,** 1358–1371.

——, and ——, 2010: Composite structure of tropopause polar cyclones. *Mon. Wea. Rev.,* **138,** 3840–3857.

——, and ——, 2012: Radiative impact on tropopause polar vortices over the Arctic. *Mon. Wea. Rev.,* **140,** 1683–1702.

——, and ——, 2013: Physical mechanisms of tropopause polar vortex intensity change. *J. Atmos. Sci.,* **70,** 3359–3373.

Chang, C.-P., and K. M. Lau, 1980: Northeasterly cold surges and near-equatorial disturbances over the winter MONEX area during December 1974. Part II: Planetary-scale aspects. *Mon. Wea. Rev.,* **108,** 298–312.

——, and ——, 1982: Short-term planetary-scale interactions over the tropics and midlatitudes during northern winter. Part I: Contrasts between active and inactive periods. *Mon. Wea. Rev.,* **110,** 933–946.

Chang, E. K. M., and I. Orlanski, 1993: On the dynamics of a storm track. *J. Atmos. Sci.,* **50,** 999–1015.

Chen, T.-C., M.-C. Yen, W.-R. Huang, and W. A. Gallus Jr., 2002: An East Asian cold surge: Case study. *Mon. Wea. Rev.,* **130,** 2271–2290.

Colle, B. A., and C. F. Mass, 1995: The structure and evolution of cold surges east of the Rocky Mountains. *Mon. Wea. Rev.,* **123,** 2577– 2610.

Colucci, S. J., and J. C. Davenport, 1987: Rapid surface anticyclogenesis: Synoptic climatology and attendant large-scale circulation changes. *Mon. Wea. Rev.,* **115,** 822–836.

Cunningham, P., and D. Keyser, 2000: Analytical and numerical modelling of jet streaks: Barotropic dynamics. *Quart. J. Roy. Meteor. Soc.,* **126,** 3187–3217.

Curry, J., 1983: On the formation of continental polar air. *J. Atmos. Sci.,* **40,** 2278–2292.

Dallavalle, J. P., and L. F. Bosart, 1975: A synoptic investigation of anticyclogenesis accompanying North American polar air outbreaks. *Mon. Wea. Rev.,* **103,** 941–957.

Danielsen, E. F., 1968: Stratospheric–tropospheric exchange based on radioactivity, ozone and potential vorticity. *J. Atmos. Sci.,* **25,** 502–518.

Dee, D. P., and Coauthors, 2011: The ERA-Interim reanalysis: Configuration and performance of the data assimilation system. *Quart. J. Roy. Meteor. Soc.,* **137,** 553–597.

Defant, F., and H. Taba, 1957: The threefold structure of the atmosphere and the characteristics of the tropopause. *Tellus,* **9,** 259–275.

Dickinson, M. J., L. F. Bosart, W. E. Bracken, G. J. Hakim, D. M. Schultz, M. A. Bedrick, and K. R. Tyle, 1997: The March 1993 Superstorm cyclogenesis: Incipient phase synoptic- and convective-scale flow interaction and model performance. *Mon. Wea. Rev.,* **125,** 3041–3072.

Donnadille, J., J.-P. Cammas, P. Mascart, and D. Lambert, 2001a: FASTEX IOP 18: A very deep tropopause fold. II: Quasi-geostrophic omega diagnoses. *Quart. J. Roy. Meteor. Soc.,* **127,** 2269 –2286.

——, ——, ——, ——, and R. Gall, 2001b: FASTEX IOP 18: A very deep tropopause fold. I: Synoptic description and modelling. *Quart. J. Roy. Meteor. Soc.,* **127,** 2247–2268.

Dunn, L., 1987: Cold air damming by the Front Range of the Colorado Rockies and its relationship to locally heavy snows. *Wea. Forecasting,* **2,** 177–189.

——, 1992: Evidence of ascent in a sloped barrier jet and an associated heavy-snow band. *Mon. Wea. Rev.,* **120,** 914–924.

Emanuel, K. A., 2008: Back to Norway: An essay. *Meteorological Monographs,* **33,** 87–96.

Griffin, K. S., and J. E. Martin, 2017: Synoptic features associated with temporally coherent modes of variability of the North Pacific jet stream. *J. Climate,* **30,** 39–54.

Hakim, G. J., 2000: Climatology of coherent structures on the extratropical tropopause. *Mon. Wea. Rev.,* **128,** 385–406.

——, and A. K. Canavan, 2005: Observed cyclone-anticyclone tropopause asymmetries. *J. Atmos. Sci.,* **62,** 231–240.

——, L. F. Bosart, and D. Keyser, 1995: The Ohio Valley wave-merger cyclogenesis event of 25–26 January 1978. Part I: Multiscale case study. *Mon. Wea. Rev.,* **123,** 2663–2692.

——, D. Keyser, and L. F. Bosart, 1996: The Ohio Valley wave-merger cyclogenesis event of 25–26 January 1978. Part II: Diagnosis using quasigeostrophic potential vorticity inversion. *Mon. Wea. Rev.,* **124,** 2176–2205.

Handlos, Z. J., and J. E. Martin, 2016: Composite analysis of large-scale environments conducive to west Pacific polar/subtropical jet superposition. *J. Climate,* **29,** 7145–7165.

Hoskins, B. J., and M. A. Pedder, 1980: The diagnosis of middle latitude synoptic development. *Quart. J. Roy. Meteor. Soc.,* **106,** 707–719.

——, M. E. McIntyre, and A. W. Robertson, 1985: On the use and significance of isentropic potential vorticity maps. *Quart. J. Roy. Meteor. Soc.,* **111,** 877–956.

Jones, J. E. and J. Cohen, 2011: A diagnostic comparison of Alaskan and Siberian strong anticyclones. *J. Climate,* **24,** 2599–2611.

Kalnay, E., and Coauthors, 1996: The NCEP/NCAR 40-Year Reanalysis Project. *Bull. Amer. Meteor. Soc.,* **77,** 437–472.

Keyser, D., and M. A. Shapiro, 1986: A review of the structure and dynamics of upper-level frontal zones. *Mon. Wea. Rev.,* **114,** 452–499.

——, B. D. Schmidt, and D. G. Duffy, 1992: Quasigeostrophic vertical motions diagnosed from along- and cross-isentrope components of the Q vector. *Mon. Wea. Rev.,* **120,** 731–741.

Konrad, C. E., and S. J. Colucci, 1989: An examination of extreme cold air outbreaks over eastern North America. *Mon. Wea. Rev.,* **117,** 2687–2700.

Kravitz, J. R., 2007: A study of coherent tropopause disturbances from a climatological perspective. M.S. thesis, Department of Earth and Atmospheric Sciences, University at Albany/SUNY, Albany, NY, 191 pp.

Lackmann, G. M., D. Keyser, and L. F. Bosart, 1997: A characteristic life cycle of upper-tropospheric cyclogenetic precursors during the Experiment on Rapidly Intensifying Cyclones over the Atlantic (ERICA). *Mon. Wea. Rev.,* **125,** 2729–2758.

Lang, A. A., and J. E. Martin, 2010: The influence of rotational frontogenesis and its associated shearwise vertical motions on the development of an upper-level front. *Quart. J. Roy. Meteor. Soc.,* **136,** 239–252.

Menne, M. J., I. Durre, R. S. Vose, B. E. Gleason, and T. G. Houston, 2012: An overview of the Global Historical Climatology Network-Daily database. *J. Atmos. Oceanic Technol.,* **29,** 897–910.

Murphy, Z. B., 2017: A climatological and multiscale analysis of cold air outbreaks in the northeast United States. M.S. thesis, Department of Earth and Atmospheric Sciences, University at Albany/SUNY, Albany, NY, 91 pp.

Namias, J., 1978: Multiple causes of the North American abnormal winter of 1976–77. *Mon. Wea. Rev.,* **106,** 279–295.

Nielsen-Gammon, J. W., and R. J. Lefevre, 1996: Piecewise tendency diagnosis of dynamical processes governing the development of an upper-tropospheric mobile trough. *J. Atmos. Sci.,* **53,** 3120–3142.

Orlanski, I., and E. K. M. Chang, 1993: Ageostrophic geopotential fluxes in downstream and upstream development of baroclinic waves. *J. Atmos. Sci.,* **50,** 212–225.

——, and J. P. Sheldon, 1995: Stages in the energetics of baroclinic systems. *Tellus,* **47A,** 605–628.

Pyle, M. E., D. Keyser, and L. F. Bosart, 2004: A diagnostic study of jet streaks: Kinematic signatures and relationship to coherent tropopause disturbances. *Mon. Wea. Rev.,* **132,** 297–319.

Reed, R. J., and E. F. Danielsen, 1959: Fronts in the vicinity of the tropopause. *Arch. Meteor. Geophys. Bioklim.,* **A11**, 1–17.

Rogers, J. C. and R. V. Rohli, 1991: Florida citrus freezes and polar anticyclones in the Great Plains. *J. Climate,* **4,** 1103–1113.

Sanders, F., and J. R. Gyakum, 1980: Synoptic-dynamic climatology of the ‘‘bomb.’’ *Mon. Wea. Rev.,* **108,** 1589–1606.

——, and C. A. Davis, 1988: Patterns of thickness anomaly for explosive cyclogenesis over the west-central North Atlantic Ocean. *Mon. Wea. Rev.,* **116,** 2725–2730.

——, and B. J. Hoskins, 1990: An easy method for estimation of Q-vectors from weather maps. *Wea. Forecasting,* **5,** 346–353.

Shapiro, M. A., T. Hampel, and A. J. Krueger, 1987: The Arctic tropopause fold. *Mon. Wea. Rev.,* **115,** 444–454.

Takayabu, I., 1991: ‘‘Coupling development’’: An efficient mechanism for the development of extratropical cyclones. *J. Meteor. Soc. Japan,* **69,** 837–841.

Turner, J. K., and J. R. Gyakum, 2011: The development of Arctic air masses in Northwest Canada and their behavior in a warming climate. *J. Climate,* **24,** 4618–4633.

——, ——, and S. M. Milrad, 2013: A thermodynamic analysis of an intense North American arctic air mass. *Mon. Wea. Rev.,* **141,** 166–181.

Uccellini, L. W., and P. J. Kocin, 1987: The interaction of jet streak circulations during heavy snow events along the East Coast of the United States. *Wea. Forecasting,* **2,** 289–308.

——, D. Keyser, K. F. Brill, and C. H. Walsh, 1985: The Presidents’ Day cyclone of 18–19 February 1979: Influence of upstream trough amplification and associated tropopause folding on rapid cyclogenesis. *Mon. Wea. Rev.,* **113,** 962–988.

Wagner, A.J., 1982: Weather and circulation of January 1982: A stormy month with two record cold waves. *Mon. Wea. Rev.,* **110,** 310–317.

Wallace, J. M., and D. S. Gutzler, 1981: Teleconnections in the geopotential height field during the Northern Hemisphere winter. *Mon. Wea. Rev.,* **109,** 784–812.

Walsh, J. E., A. S. Phillips, D. H. Portis, and W. L. Chapman, 2001: Extreme cold outbreaks in the United States and Europe, 1948–99. *J. Climate,* **14,** 2642–2658.

Waugh, D. W., A. H. Sobel, and L. M. Polvani, 2017: What is the polar vortex and how does it influence weather?. *Bull. Amer. M eteor. Soc.,* **98,** 37–44.